



**Michigan
Technological
University**

Michigan Technological University
Digital Commons @ Michigan Tech

Dissertations, Master's Theses and Master's Reports

2020

OPTIMIZATION OF SHAPE AND CONTROL OF LINEAR AND NONLINEAR WAVE ENERGY CONVERTERS

Jiajun Song

Copyright 2020 Jiajun Song

Follow this and additional works at: <https://digitalcommons.mtu.edu/etdr>



Part of the [Ocean Engineering Commons](#)

OPTIMIZATION OF SHAPE AND CONTROL OF LINEAR AND NONLINEAR
WAVE ENERGY CONVERTERS

By

Jiajun Song

A DISSERTATION

Submitted in partial fulfillment of the requirements for the degree of

DOCTOR OF PHILOSOPHY

In Mechanical Engineering-Engineering Mechanics

MICHIGAN TECHNOLOGICAL UNIVERSITY

2020

© 2020 Jiajun Song

This dissertation has been approved in partial fulfillment of the requirements for the Degree of DOCTOR OF PHILOSOPHY in Mechanical Engineering-Engineering Mechanics.

Department of Mechanical Engineering-Engineering Mechanics

Dissertation Co-advisor: *Dr. Ossama Abdelkhalik*

Dissertation Co-advisor: *Dr. Jeffrey Allen*

Committee Member: *Dr. Bo Chen*

Committee Member: *Dr. Fernando Ponta*

Committee Member: *Dr. Yang Yang*

Department Chair: *Dr. William Predebon*

Dedication

To my mother and father

Without your love and support, I would neither be who I am nor would this work be what it is today.

To my advisor and committee

Who guide, support and encourage me with your knowledge and patience.

To my colleagues and friends

Who enrich my life.

Contents

List of Figures	xi
List of Tables	xxiii
Preface	xxv
Acknowledgments	xxvii
Abstract	xxix
1 Introduction	1
1.1 Overview	1
1.2 Optimal Control of a Heaving Point Absorber	3
1.3 Hydrodynamic Consideration of a Small WEC	6
1.4 Nonlinear Dynamic Model	8
1.5 Motivation of This Study	13
2 Modeling of the Wave Energy Converters	15
2.1 Hydrodynamic Models of WECs	15
2.1.1 Linear Hydrodynamic model	15

2.1.2	Control Based on Linear Model	18
2.1.3	Non-Linear Hydrodynamic Model	19
3	Multi resonant Feedback Control of Heave Wave Energy Converters	25
3.1	Decomposition of the WEC Control Problem	26
3.2	Proportional Derivative Approximation for C3	31
3.2.1	Stability of the Proposed Proportional Derivative Control	36
3.3	Feedback Signal Processing	37
3.4	Implementation of the PDC3	40
3.5	Numerical Results	42
3.6	Discussion	51
4	Hydrodynamic Design and Near-Optimal Control of a Small Wave Energy Converter for Ocean Measurement Applications	61
4.1	Deterministic Wave Prediction	62
4.2	Geometry Optimization	66
4.3	Dynamic Model	68
4.4	Calculations	74
4.5	Discussion	77
4.6	Conclusions	79

5 Optimization of Shape and Control of non-linear Wave Energy	
Converters Using Genetic Algorithms	91
5.1 Optimization of the Buoy Shape	92
5.2 Optimization of the Control	98
5.3 Numerical results	99
5.3.1 Test Case Without Control Force Constraint	100
5.3.2 Test Case With Control Force Constraint	102
6 Conclusion	107
References	111
A Letters of Permission	149

List of Figures

2.1	A axisymmetric heaving device with generic profile $f(\sigma)$, 2.1(a) shows the equilibrium position with the center of gravity at the still water level (SWL) and the draft h_0 ; 2.1(b) shows the free elevation η and the device displacement z_d after a time t^* . The pressure is integrated over the surface between σ_1 and σ_2	23
	(a)	23
	(b)	23
3.1	Block diagram of a WEC control system of a single frequency regular wave	28
3.2	Block diagram of the decomposed WEC control system	29
3.3	Block diagram of the WEC multi resonant control system	30
3.4	Block diagram of the proposed feedback WEC control system	31
3.5	Simulation for both actual and Theoretical PDC3 control: Control and Energy	43
	(a) Control Force	43
	(b) Extracted Energy	43

3.6	Simulation for both actual and theoretical PDC3 control: Position and Velocity	44
	(a) Position of The Buoy	44
	(b) Velocity of The Buoy	44
3.7	Simulation for both PDC3, Theoretical PDC3, analytical PDC3, and C3 for a 3-frequency excitation force	46
	(a) Full history of simulation	46
	(b) Steady state part only	46
3.8	Bretshneider spectrum	47
3.9	Simulation of Bretshneider wave for PDC3, C3 for a 4 Dominant frequencies, C3 for All frequencies	48
	(a) Full history of simulation	48
	(b) Steady state part only	48
3.10	Ochi-Hubble spectrum	49
3.11	Simulation of Ochi-Hubble wave for PDC3, C3 for a 7 Dominant frequencies, C3 for All frequencies	50
	(a) Full history of simulation	50
	(b) Steady state part only	50
3.12	Control and Energy: as the time step gets smaller the difference between the PDC3 and the C3 gets smaller	53
	(a) Control Force	53

(b)	Extracted Energy	53
3.13	Position and Velocity: as the time step gets smaller the difference between the PDC3 and the C3 gets smaller	54
(a)	Velocity of The Buoy	54
(b)	Position of The Buoy	54
3.14	Reactive power for both the C3 and the PDC3	56
4.1	Space-time diagram for real-ocean waves. This is used along with the re- quired prediction time to determine the distance and duration of the up- wave measurement.	64
4.2	Comparison of computed wave elevation time domain history at x_B and predicted wave elevation history at x_f	64
4.3	81
(a)	A standard oceanographic buoy with original two-discs shape design of reaction frame, this figure shows input mesh file of WAMIT. A rigid connect is added between two discs to help WAMIT recognize two parts of WEC system: buoy and reaction frame. Radius of buoy and discs are $1.2m$. Thickness of discs are $0.1m$. Equivalent draft of buoy is $1m$. Spacing between bottom surface of buoy and top surface of discs is $2m$	81

(b)	Buoy with original buoy and two-spheres shape design of reaction frame, this figure shows input mesh file of WAMIT. Radius of spheres are $1.2m$. Distance between buoy and top sphere is $2m$. Distance between two spheres is $1m$	81
(c)	Buoy with original buoy and two-hemispheres shape design of reaction frame, this figure shows input mesh file of WAMIT. Radius of hemispheres is $1.2m$, distance between top hemisphere and buoy is $2m$, distance between two hemispheres is $1m$. . .	81
4.4	82
(a)	Dashed line is Total exciting force, solid line is Relative exciting force. Relative exciting force larger than total exciting force leads to total movement less than relative movement.	82
(b)	Dashed line is Total exciting force, solid line is Relative exciting force. Two spheres design provide large exciting force for reaction frame. Peak of solid line means largest difference between relative and total exciting force at low frequency.	82
(c)	Hemispheres design for reaction frame provide highest average difference between relative and total exciting force, through peak difference value is less than spheres design.	82
4.5	Effective Radiation Damping calculated with $H_{s1} = 0.3m, H_{s2} = 0.2m, T_{e1} = 9s, T_{e2} = 4.5s$, with out motion constraint.	83

(a)	Reaction frame with a flat top surface shows a second peak at low frequency.	83
(b)	Reaction Frame with deeper submerged design shows lower value in radiation damping then original design.	83
(c)	Larger design of reaction frame give higher value of effective radiation damping, flat top surface of reaction frame give high second peak value at low frequency.	83

4.6	Figure 4.6(a) shows converted power by Buoy-Discs design, Buoy-Spheres design and Buoy-Hemispheres design constraint $\alpha_r = 2.5$. Dashed line is Buoy-Discs, Solid line is Buoy-Spheres, Dash-Dot line is Buoy-Hemispheres. This figure use Significant Wave height $H_s = 0.2m$	84
-----	--	----

(a)	84
(b)	84
(c)	84

4.7	This figure shows converted power result (4.7(a)) form $H_{s1} = 0.3m, H_{s2} = 0.2m$, constraint $\alpha_r = 2.5$, Buoy-Hemispheres design have higher converted power over T_{e1}, T_{e2} spacing.	85
-----	--	----

(a)	85
(b)	85
(c)	85

4.8	The heaving axisymmetric 2-body device used in this work. Relative oscillation is used for energy conversion using a linear generator or hydraulic cylinder type power take-off mechanism/actuator, which is assumed to be linear and ideal (i.e. lossless). The figure shows the ‘starting/baseline’ geometry for the submerged instrument frame comprised of two circular discs held together by a central strut (not shown). The power take-off also applies the required control force in this work, though in practice it may be advantageous to use two actuators, one for power take-off, and one for reactive forcing.	86
4.9	Calculation based on yearly data from [1], constraint $\alpha_r = 1$, is applied to maintain in feasible relative displacement range. Dashed line is Buoy-Discs, Solid line is Buoy-Spheres. Best wave climate data of each month is collected to run this calculation. 2-spheres design of reaction frame shows slightly smaller control force.	87
(a)	87
(b)	87
(c)	87
(d)	87

4.10 Calculation based on yearly data from [1], constraint $\alpha_r = 1$, is applied to maintain in feasible relative displacement range. Dashed line is Buoy-Discs, Solid line is Buoy-Hemispheres. Best wave climate data of each month is collected to run this calculation. 2-hemispheres design of reaction frame shows greater energy conversion, meanwhile control force increase significantly. Simulation results of Buoy-Discs design consistent with Figure 4.9. 88

(a) 88

(b) 88

(c) 88

(d) 88

4.11 Calculation based on yearly data from [1], constraint $\alpha_r = 2.5$, is applied to keep energy capture level. Dashed line is Buoy-Discs, Solid line is Buoy-Spheres. Worst wave climate data of each month is collected to run this calculation. 2-spheres design of reaction frame shows smaller Maximum value of reactive power. Contribute to easy energy storage design. 89

(a) 89

(b) 89

(c) 89

(d) 89

4.12 Calculation based on yearly data from [1], constraint $\alpha_r = 2.5$, is applied to maintain in feasible relative displacement range. Dashed line is Buoy-Discs, Solid line is Buoy-Hemispheres. Worst wave climate data of each month is collected to run this calculation. 2-hemispheres design of reaction frame still shows greater energy conversion, control force with smaller constraint α_r shows lower value compared to original design. Simulation results of Buoy-Discs design consistent with Figure 4.11.	90
(a)	90
(b)	90
(c)	90
(d)	90
5.1 The surface of an axisymmetric heaving device with generic profile $f(\sigma)$. 2.1(a) shows the equilibrium position at the still water level (SWL) and the draft h_0 ; 2.1(b) shows the free elevation η and the device displacement z_d after a time t^* . The pressure is integrated over the wetted surface between σ_1 (the bottom point of the buoy) and σ_2 (the wave elevation at time t).	93
(a)	93
(b)	93

5.2	Each section i of decomposed shape can be described by two variables α_i and h_i or less.	96
	(a)	96
	(b)	96
	(c)	96
	(d)	96
5.3	Bertschneider spectrum used in the time domain simulation. The spectrum is with $H_s = 0.8m$ and $T_p = 10s$	100
5.4	Shape comparison between the optimal solution without control constraint and the baseline cylindrical WEC. And motion comparison between both cases in time domain simulation.	102
	(a)	102
	(b)	102
5.5	Time domain simulation results of the optimal solution without control constraint and the baseline cylindrical WEC using the complex wave profile as input, in terms of instantaneous power, mean power, maximum power, and total converted energy. Solid horizontal lines in Fig.5.5(a) represent the maximum power and the average power of the optimal non-linear shape design, dashed horizontal lines in Fig.5.5(a) represent the maximum power and the average power of the baseline shape.	103

(a)	103
(b)	103
5.6	Different hydrodynamic force history for the optimal solution without control constraint and the baseline WEC in the time domain simulation.	103
(a)	103
(b)	103
5.7	Different control force history for the optimal solution without control constraint and the baseline WEC in the time domain simulation. . .	104
5.8	Different velocity history for the optimal solution without control constraint and the baseline WEC in the time domain simulation. . . .	104
5.9	Shape comparison between the optimal solution with control constraint and the baseline cylindrical WEC. And motion comparison between both cases in time domain simulation.	105
(a)	105
(b)	105

5.10	Time domain simulation results of the optimal solution with control constraint and the baseline cylindrical WEC using the complex wave profile as input, in terms of instantaneous power, mean power, maximum power, and total converted energy. Solid horizontal lines in Fig.5.5(a) represent the maximum power and the average power of the optimal non-linear shape design, dashed horizontal lines in Fig.5.5(a) represent the maximum power and the average power of the baseline shape.	105
(a)	105
(b)	105
5.11	Different hydrodynamic force history for the optimal solution with control constraint and the baseline WEC in the time domain simulation.	106
(a)	106
(b)	106
5.12	Different control force history for the optimal solution with control constraint and the baseline WEC in the time domain simulation.	106
5.13	Different velocity history for the optimal solution with control constraint and the baseline WEC in the time domain simulation.	106
A.1	The permission letter of reusing the paper [2]	150
A.2	The permission letter of reusing the paper [3]	150

List of Tables

Preface

Chapter 1 presents the introduction of this dissertation, including the motivation of this research, the wave energy research background and the contribution of this dissertation. Chapter 2 provides a detailed literature review of wave energy conversion, including model of wave energy converters, the control strategies of wave energy converters, and the Power-take-off mechanisms. Chapter 3 presents a time-domain feedback control algorithm that approximates the complex conjugate control. The proposed control algorithm targets both amplitude and phase feedback, and is constructed from individual frequency components that comes from the spectral decomposition of the measurements signal. The material of Chapter 3 is published in reference [2] and reference [4]. Chapter 4 examines the impact of reaction-frame geometries on overall power capture. Performance is evaluated in a range of realistic wave conditions. The material of Chapter 4 is published as reference [3]. Chapter 5 presents a novel implementation on genetic optimization of both the design of WEC buoy shapes, and controls, leveraging non-linear hydrodynamics, to improve energy conversion. The material of Chapter 5 is published as reference [5].

Acknowledgments

I would like to express my deepest gratitude to all those who have supported me, helped me, and inspired me during my doctoral program at Michigan Technological University. Thanks to everyone, this journey towards PhD is truly wonderful!

I would like to thank my advisor, Dr. Ossama Abdelkhalik. Thank you for giving me the opportunity to join your research group and pursue a PhD degree. This work won't be done without your guidance, support, and encouragement. I learned not only knowledge but also personal qualities from you.

Also, I am grateful to Dr. Jeffery Allen, Dr. Bo chen, Dr Rush Robinett, Dr. Giorgio Bacelli and all the instructors and professors who provided advises and supported me while working on my research. Dr. Umesh Korde helped me in developing 4 of this dissertation.

I would like to thank my parents. Thank you for supporting me through this important period of my life.

Finally, I would like to thank all my colleagues and friends. You made my life in Michigan such a wonderful journey.

Abstract

In this dissertation, we address the optimal control and shape optimization of Wave Energy Converters. The wave energy converters considered in this study are the single-body heaving wave energy converters, and the two-body heaving wave energy converters. Different types of wave energy converters are modeled mathematically, and different optimal controls are developed for them. The concept of shape optimization is introduced in this dissertation; the goal is to leverage nonlinear hydrodynamic forces which are dependant on the buoy shape. In this dissertation, shape optimization is carried out and its impact on energy extraction is investigated. In all the studies conducted in this dissertation the objective is set to maximize the harvested energy, in various wave climates. The development of a multi-resonant feedback controller is first introduced which targets both amplitude and phase through feedback that is constructed from individual frequency components that comes from the spectral of the measurements signal. Each individual frequency uses a Proportional-Derivative control to provide both optimal resistive and reactive elements.

Two-body heaving pointer absorbers are also investigated. Power conversion is from the relative heave oscillation between the two bodies. The oscillation is controlled on a wave-by-wave basis using near-optimal feed-forward control. Chapter 4 presents the dynamic formulation used to evaluate the near-optimal, wave-by-wave control forces

in the time domain. Also examined are the reaction-frame geometries for their impact on overall power capture through favorable hydrodynamic inter-actions. Performance is evaluated in a range of wave conditions sampled over a year at a chosen site of deployment. It is found that control may be able to provide the required amounts of power to sustain instrument operation at the chosen site, but also that energy storage options be worth pursuing.

Chapter 5 presents an optimization approach to design axisymmetric wave energy converters (WECs) based on a non-linear hydrodynamic model. The time domain non-linear Froude-Krylov force can be computed for a complex buoy shape, by adopting analytical formulas of its basic shape components. The time domain Froude-Krylov force is decomposed into its dynamic and static components, and then contribute to the calculation of the excitation force and the hydrostatic force. A non-linear control is assumed in the form of the combination of linear and non-linear damping terms. A variable size genetic algorithm (GA) optimization tool is developed to search for the optimal buoy shape along with the optimal control coefficients simultaneously. Chromosome of the GA tool is designed to improve computational efficiency and to leverage variable size genes to search for the optimal non-linear buoy shape. Different criteria of wave energy conversion can be implemented by the variable size GA tool. Simulation results presented in this thesis show that it is possible to find non-linear buoy shapes and non-linear controllers that take advantage of non-linear hydrodynamics to improve energy harvesting efficiency with out adding reactive terms to the

system.

Chapter 1

Introduction

1.1 Overview

Ocean wave energy is a very attractive source of renewable energy in today's energy market. Energy can be extracted from oceans which cover around 3/4 of the earth surface. As ocean water absorbs swell motion energy, solar energy and wind energy, then transfer mechanical energy in the format of waves. The capacity of global wave power resource has been estimated to be at least 8 GW. The annual energy production potential is comparable to the energy production from hydro-power[6]. But by the end of 2016, the global ocean energy production was only 536 MW[7].

Ocean wave energy also has the benefit of higher power density than other renewable

energy sources. Usage of wave energy converters (WECs) has less negative impact of the environment [8], however, it is a challenge to overcome both the difficulty of designing a working WEC device and the commercial competitiveness of energy extraction.

Wave energy conversion concepts are investigated based on the different mechanism of energy absorbing, different deploy location of the device (offshore, near-shore, shoreline) and different wave climates [9]. Three main wave energy conversion concepts are [10]: oscillating body system [11, 12], oscillating water column devices [13], and over-topping converters (on-shore, off-shore) [8]. Oscillating body system has different working principles as well, most studied mechanism are: the single-body heaving buoys [14] (single-body point absorber), the two-body heaving systems [15, 16], fully submerged heaving bodies [17, 18], and pitching devices [19].

In a typical heaving body (point absorber) system, the energy conversion results from the heaving motion of a floating body reacting against a frame of reference (the seabottom or the second body of the point absorber system) [20]. A hydraulic cylinder or an electric direct-drive motor is connected to the floating buoy of a typical point absorber. The heave motion of the floating buoy drives the hydraulic cylinder or the electric direct-drive motor, to drive a generator or to connect with a power conversion device [21, 22, 23]. This type of WECs converts the heave wave energy. There are other types of WECs extract energy from the pitching motion [24], for example, the

WaveStar Buoy. The mechanical device that translate the motion of the oscillating bodies into useful electrical energy are called Power take-off (PTO) device.

1.2 Optimal Control of a Heaving Point Absorber

Several algorithms have been developed in the literature that search for the optimal solution to the control of wave energy converters (WEC) problem. The optimization goal is to maximize the energy conversion. The frequency domain analysis of a WEC heaving buoy system leads to the criterion for maximum energy conversion - known as the Complex Conjugate Control (C3) that provides a means to compute the optimal float velocity [25], regardless of the spectral distribution of the excitation force. This C3, however, is not causal which means a prediction for the wave elevation or the excitation force is needed for real time implementation. One implementation uses a feed forward control assuming the availability of the excitation force (wave) model [26]. Another feedback implementation computes the control force using both the measurements and the wave prediction data [27, 28]. A velocity-tracking approach can also be used to implement the C3 where the estimates of the excitation force is used to compute the optimal float velocity (through the feed forward loop) which is imposed on the WEC through a feedback loop [29]. In all these C3 implementations, a prediction for the wave elevation and/or the wave excitation force is necessary.

Constraints on motions and forces, however, motivated researchers to look for solutions in the time domain. In general, the solution of the constraint optimization problem is different from that of the unconstrained C3. The basic latching and declutching control strategies are attractive in that they do not require reactive power [30]. In latching, the optimum oscillation phase is achieved by holding the absorber fixed during parts of the cycle. In clutching, it is achieved via coupling and decoupling the machinery at intervals [31, 32]. Reference [33] shows that clutching is theoretically better than pseudo-continuous control that has a linear damping effect. Reference [34] investigates the use of discrete control over continuous control, for latching control, declutching control and the combination of both. The latter gives better results than each one individually; and the discrete control is always better when it is absolute, switching instantaneously from one model to the other [34]. Reference [35] applies a direct transcription approach to maximize the energy extraction. The results show that the direct transcription method generates a latching behavior for the cases with power constraints, while the declutching behavior only results when tether goes slack.

Reference [30] compares between various control strategies including velocity-proportional control, approximate C3, approximate optimal velocity tracking, and model predictive control, for a point absorber. The Model Predictive Control (MPC) methods use a discrete-time model for predicting the states in the future to form the objective function for energy optimization. Reference [36] compares several control strategies experimentally, including Proportional-Integral (PI) control and MPC. The

authors have found that MPC can significantly improve energy absorption when compared to the PI control; however MPC needs a reliable estimation of the incoming incident wave, and the performance improvement is sensitive to the quality of the wave estimation. A PID control is used in [37] in which the controller gains are optimized for certain wave environments using information about the excitation force. A variety of feedback control laws were developed using the C3 optimality conditions in [38]. For example, the optimal velocity trajectory can be estimated, via wave estimation, and used along with the actual velocity in a feedback control system that aims at tracking the estimated optimal velocity. A linear quadratic Gaussian optimal control can be used to track optimal velocity as in reference [39]. One of the relatively recent WEC control optimization methods that can accommodate constraints on the control and the states is the dynamic programming [40]. A prediction for the wave is needed when using the dynamic programming, and a discretization for the time and space domains makes the computational cost of the method feasible for real time implementation [40]. Another time domain strategy that can also handle constraints on both the control and the states is the pseudo spectral method. In pseudo spectral methods the system states and control are assumed as series of basis functions, and the search for the solution is conducted using the assumed approximate functions [41]. A shape-based approach is recently developed for WECs control [42, 43] where a series expansion is used to approximate only the buoy velocity; this method can also accommodate motion constraints. A key optimality criterion is to make the buoy

oscillation in phase with the excitation force. Reference [44] presents a time domain control that meets this criteria and maintains the amplitude of the oscillation within given constraints. In [44], a non-stationary harmonic approximation for the wave excitation force is used. The controller tunes the ratio between the excitation force and the velocity in real-time for performance and constraints handling. A performance close to C3 and to MPC is achieved. Recently, an adaptive wave-by-wave control was developed such that the oscillation velocity closely matches the hydrodynamically optimum velocity for best power absorption [45]. Such control requires prediction of the wave profile using up-wave measurements [45]. In a more recent feedforward implementation, reference [46] investigates wave-by-wave control of a wave energy converter using deterministic incident wave prediction based on up-wave surface measurement.

1.3 Hydrodynamic Consideration of a Small WEC

Many wave energy devices convert power using the relative oscillation of floating bodies with respect to a reference body that is stationary or nearly stationary [47]. Typically, the floating bodies are designed so that their natural periods approximately match a chosen range of energy periods in the wave scatter diagram for a deployment site. As wave conditions change over seasons, power conversion performance drops. Wave energy devices thus often tend to be bulky and uneconomical in terms of annual power generation and the overall costs. Smaller devices are of interest because they

experience smaller structural loads [48] and thus require smaller investments. Based on the practice of Froude-scaling, where the scaling factor s is the ratio between a length measurement of a full scale WEC and the reduced scale WEC, power scales as $s^{3.5}$ with buoy radius, while wave period scales as $s^{0.5}$ (see e.g. [49]). Thus, for a given set of wave periods as determined by a given site of deployment, converted power scales as s^3 . For this reason, smaller devices also convert considerably smaller power amounts in the same wave climates. Further, most small devices have narrow response bandwidths, which makes them highly sensitive to wave periods. However, they can be made more cost effective if their dynamic response can be actively controlled to match incoming wave conditions.

Such control was first attempted by Salter for the Edinburgh duck and Budal for a heaving buoy [50], [51]. Recent years have seen a large number of control applications, as reviewed in [47] and [52]. Control can involve a combination of reactive and resistive loading (applied by the power take-off) (e.g. [53], [46], [54], etc) or resistive loading alone together with switching control of the device oscillation (e.g. [55], [56], [29], etc.). The former approach is referred to as complex conjugate control for impedance matching, while the latter is termed ‘latching’ when used to slow down the response of a small buoy to bring about force-velocity phase match in longer waves.

The few control approaches that have been attempted in practice have shown 2-3 fold improvements in energy capture [54] through the addition of reactive tuning to

the baseline approaches based on resistive loading alone. Further improvements require wave-by-wave control, which is difficult to apply because wave-by-wave reactive cancellation and resistive match (i.e. wave-by-wave impedance matching) requires knowledge of the future oscillations/wave elevations [57], [58]. Operation close to optimum velocity frequently results in excessive velocities and very large displacements. Practical limitations require oscillation constraints. An intuitively natural constraint is based on the device swept volume, which limits the oscillation amplitude to buoy draft (or freeboard if smaller) [59], [60]. Operation under oscillation constraints limits power conversion, especially, for small buoys.

1.4 Nonlinear Dynamic Model

Ocean waves can be a reliable source of renewable energy if wave energy converters (WEC) can be operated in an economic way under various sea conditions. Once the deploy location of a WEC device is determined, the shape of the buoy and the control can be optimized to maximize the converted wave energy. Time domain motion simulation of the WEC device and the statistic wave climate data can be used to evaluate such optimization. Alternatively, a specific shape of buoy and a specific control can be computed through optimization using the statistic wave spectrum data of the selected deploy location as the input. Shape optimization of WECs based on linear hydrodynamic theory was investigated by Korde and Jiajun [3]. Limited cases

of shape designs were evaluated based on the exciting force and the radiation damping. Results shows that non-cylindrical buoy could lead to better energy extraction.

The dynamic modeling of WEC has been a topic for marine energy study for a long time. According to Falnes [25], a linear dynamic model provides enough accuracy to study the energy conversion and the body motion within a small wave amplitude environment. However, a large motion of the buoy due to high wave amplitudes and a complex realistic wave spectrum input would be outside the boundary conditions of the linear model. A non-linear hydrodynamic model of WEC device can result in significant improvement in accuracy of the time domain simulation of wave energy extraction with complex wave input.

In the 1970s Budal [51] and Salter [50] start the research topic of wave energy conversion. In recent years there have seen a large amount of applications, as reviewed in Falnes's [47] and Ringwood's review paper [52]. A basic linear model for a heaving-floater of mass m single-input-single-output system can be described as an equation of motion as shown in Eqn.(1.1) according to Falnes's book [25].

$$m\ddot{Z} = f_e + f_r + f_s + u \quad (1.1)$$

Where, \ddot{Z} is the acceleration of the buoy along the vertical axis. f_e is the excitation

force given from the incoming wave around the immersed surface. In time domain simulation, input is defined as an complex waves profile. Such wave profile can be defined from finite frequency components captured from a wave spectrum. For a complex incoming wave profile with n different frequencies, each frequency components of the input wave profile contains the wave amplitude coefficient A_i and the wave frequency ω_i . The total complex excitation force at a time step can be computed as the summation of the excitation forces generated from all frequency components of the input wave profile.

The radiation force, f_r , is due to the radiated wave from motion of the floater. f_r can be computed from the radiation impulse response function h_r as shown in Eqn.(1.2), where m_∞ is the added-mass at infinite frequency.

$$f_r(t) = - \int_0^\infty h_r(\tau) \dot{Z}(t - \tau) d\tau - m_\infty \ddot{Z}(t) \quad (1.2)$$

The hydrostatic force f_s represent the spring-like characteristic of the interaction motion between floater and water as shown in Eqn.(1.3), where k is the hydrostatic stiffness due to buoyancy.

$$f_s(t) = -kZ(t) \quad (1.3)$$

And u in Eqn.(1.1) is the external power-take-off force or the control force.

The three methods to generate non-linear mode of WECs are the CFD approach, the potential flow theory approach and the analytical approach [61]. The CFD approach, which uses continues meshing method [62], is one of the non-linear WEC mathematical models. Similar simulations have been tested by Penalba and Ringwood [63]. Implementing the CFD approach in GA requires large amount of computation time, such as using Aqua to compute the forces acting on the buoy. Because every propagation step needs a updated mesh of the immersed surface, and GA requires an numerous size of propagation steps. A computational efficient hydrodynamic model method was chosen to be implemented in this chapter.

The analytical approach requires less computational time cost. Giorgi and Ringwood [64] developed such non-linear hydrodynamic model as shown below:

$$(m + m_{\infty})\ddot{Z} = F_{FK_{st}} + (F_{FK_{dy}} + F_D) + F_R + F_{PTO} \quad (1.4)$$

And the analytical solution of the non-linear FK force was developed by Ringwood [65] for WECs of simple geometries. Compare Eqn.(1.1) with Eqn.(1.4), terms in the linear model can be replaced with non-linear term from the Froude-Krylov force: $f_s = F_{FK_{st}}$, $f_e = F_{FK_{dy}} + F_D$. The hydrodynamic model can be expressed as Eqn.(1.4). Where $F_{FK_{st}}$ is the static Froude-Krylov force, given as the difference between the gravity force and the Archimed force, $F_{FK_{dy}}$ is the dynamic Froude-Krylov force, F_D is the diffraction force from the undisturbed incoming wave. Airy's wave theory for

deep water waves is used to compute the pressure along the immersed surface. The non-linear Froude-Krylov force is the integration of the pressure along the immersed surface. $F_{PTO} = u$ is the force of the power-take-off (PTO) device. F_R is the radiation force computed from the time domain steady-state-representation of the radiation impulse response function h_r .

Falnes [25], Clement and Ferrant [66] showed that when the dimension of the device is considerably smaller than the wave length, the non-linearities of the diffraction force are negligible. This assumption holds true as the diameter of the buoy discussed in this chapter is less than 1/5 of the wave length. Mériçaud et al. [67] showed that the response of a heaving point absorber is mainly affected by the non-linear FK forces, while the non-linear radiation and diffraction force have minor effects on system dynamics. Validation of a non-linear Froude-Krylov model with linear radiation and diffraction term was tested using a real wave tank by Gilloteaux [68] and Guerinel et al. [67]. The non-linear model shows a significant improvement of accuracy with respect to a full-linear model and good agreement with experimental measurements. Similar results were obtained by Giorgi and Ringwood [69].

1.5 Motivation of This Study

Considering the linear hydrodynamic model of a WEC, the complex conjugate criterion predicts the maximum energy that can be harvested. Yet, most existing control strategies are either not achieving this maximum energy level, or are require complex computations to achieve this level of harvested energy. This dissertation presents an intuitive and simple approach that approximates the complex conjugate control, and results in energy levels that are very close to that predicted by the complex conjugate criterion.

In the context on nonlinear hydrodynamic modeling of WECs, most existing studies present the nonlinear hydrodynamics as a higher level fidelity model, compared to the linear model, and suggest using these nonlinear models for better prediction of harvested energy of a given WEC and control system. Yet, it was not found in the literature any work that leverages these nonlinearities to improve the harvested energy. The nonlinear forces depend on the shape of the buoy, and hence the shape can be optimised to leverage the nonlinear hydrodynamic forces and improve the harvested energy. This topic is investigated in this dissertation.

Chapter 2

Modeling of the Wave Energy

Converters

2.1 Hydrodynamic Models of WECs

2.1.1 Linear Hydrodynamic model

The research about the extraction of wave energy starts from mid of 1970s by Budal [51] and Salter [50]. In recent years there have seen a large amount of applications, as reviewed in Falnes's [47] and Ringwood's review paper [52]. The typical linear dynamic equations of motion for a floater of mass m can be described as equation 2.1

according to Falnes's book [25], Ringwood and Korde's control theory [70].

$$m\ddot{x} = f_e + f_r + f_s + u \quad (2.1)$$

Where, f_e is the excitation force given from the incoming wave around the immersed surface. For a spectrum of incoming waves with n different frequencies, each frequency components of the wave spectrum contains the wave amplitude A_i and the wave frequency ω_i . The excitation force coefficient F_{ei} and the phase shift from incoming wave to excitation force ϕ_i , where F_{ei} and ϕ_i can be calculated using Nemoh from the input of a wetted surface mesh. The total excitation force f_e can be expressed by the following Fourier series:

$$f_e(t) = \sum_{i=1}^n F_{ei} A_i \sin(\omega_i t + \phi_i) \quad (2.2)$$

The radiation force, f_r , is due to the radiated wave from motion of the floater. Which can be expressed as in [71] and [70]:

$$f_r(t) = - \int_0^{\text{inf}} h_r(\tau) \dot{x}_i(t - \tau) d\tau - \mu_{\text{inf}} \ddot{x} \quad (2.3)$$

where h_r is the radiation impulse response function, μ_{inf} is the added mass at infinity frequency.

The hydrostatic force f_s represent the spring-like characteristic of the interaction motion between floater and water.

$$f_s = f_g - f_b \approx -kx \quad (2.4)$$

where f_g is the gravity force and f_b present the buoyancy force. For a linear model, the hydrostatic force can be approximately expressed as a spring term in the equation of motion.

The radiation force f_r can be described as a state space model, in which \vec{x}_r is a state vector subject to [71].

$$\begin{aligned} \dot{\vec{x}}_r &= A_r \vec{x}_r + B_r \dot{x} \\ f_r &= C_r \vec{x}_r \end{aligned} \quad (2.5)$$

The radiation matrices A_r, B_r and C_r in 2.5 can be calculated by approximating the impulse response function in the Laplace domain $H_r(s)$ as following equation 2.6 [72],

$$H_r(S) = \frac{p_n s^n + P_{n-1} s^{n-1} + \dots + p_1 s + p_0}{q_m s^m + q_{m-1} s^{m-1} + \dots + q_1 s + q_0} \quad (2.6)$$

Where $n < m$.

2.1.2 Control Based on Linear Model

Several control algorithms have been developed in the literature that search for optimal/sub-optimal solution of the control of WECs. The frequency domain analysis of a heaving WEC device leads to the Complex Conjugate Control (C3) [25]. C3 provides a means to compute the optimal floating velocity, which will lead to the optimal energy conversion. This C3, however, is not causal which means a prediction for excitation force is needed for real time implementation. One implementation uses a feed forward control assuming knowledge of the excitation force (wave) [73]. Another feedback implementation uses both the measurements and the wave prediction data [28]. In all these C3 implementations, a prediction for future wave information is necessary.

Constraints on the motion and the control force motivates researchers to look for control algorithms in the time domain. In general, the solution of the constraint optimization WEC problem is different from that from the unconstrained C3 case. Multiple methods have been developed for the constrained problems. An adaptive wave-by-wave control of a wave energy converter was developed, such that, the oscillating velocity closely matches the hydro-dynamically optimum for best energy extraction [45]. This control requires the wave profile prediction using up-wave measurements.

A time-domain control algorithm that tracks both amplitude and phase from individual frequency components of the wave spectrum was developed in MTU by Abdelkhalik, Robinett III and Jiajun [2]. The concept is essentially the same as the complex conjugate control, yet it is a time domain feedback implementation. However, this multi-resonant wide band controller, which decomposes the WEC control problem into sub-problems, could result in high control force or unrealistic large motion in a realistic wave environment. Large control force is needed when the resonant frequency has a high amplitude in ocean wave spectrum due to its resonant concept.

2.1.3 Non-Linear Hydrodynamic Model

Mathematical models for WECs are an essential tool for device design, optimization, control and management. The choice of an appropriate model depends on the specific requirements demanded by the intended research project [61]. In particular, for the design of a WEC device working in a realistic ocean wave environment with extreme events and load studies, a non-linear hydrodynamic model is required to simulate the motion and the energy extraction with expected accuracy [74].

One of the mathematical models of non-linear WEC problems is the CFD approach using the continuous meshing method [62]. Similar simulations have been tested by Penalba and Ringwood [63]. This CFD approach requires a large amount of computation time,

because a new mesh is needed for every update of the propagation step.

A computational hydrodynamic model method was chosen to be implemented in the proposed research. A typical non-linear computational hydrodynamic model of a floater in inviscid flow can be expressed as 2.7

$$m\ddot{\xi}(t) = F_g - \iint_{S(t)} P(t)ndS + F_{PTO}(t) \quad (2.7)$$

In 2.7, m is the mass of the floater, $\xi = (x, y, z)$ is the general displacement of the floater from its equilibrium position, F_g is the gravity force, P is the pressure, n is the normal vector to the surface, $S(t)$ is the submerged surface, The pressure P is obtained by applying Bernoulli's equation [49]:

$$P(t) = -\rho gz(t) - \rho \frac{\partial \phi(t)}{\partial t} - \rho \frac{|\nabla \phi(t)|^2}{2} \quad (2.8)$$

Where, ρ is the water density, g the gravity acceleration, $P_{st} = -\rho gz$ is the hydrostatic pressure and ϕ is the potential flow.

However, above format of non-linear hydrodynamic model 2.7 is not in a computation efficient format. Giorgi and Ringwood [64] came up with a simplified format:

$$m\ddot{\xi} = F_{FK_{st}} + (F_{FK_{dy}} + F_D) + F_R + F_{PTO} \quad (2.9)$$

Compare 2.1 with Eq. 2.9, terms in the linear model can be replaced with non-linear term from the Froude-Krylov force: $f_s = F_{FK_{st}}$, $f_e = F_{FK_{dy}} + F_D$. Regarding the radiation force term $f_r = F_R$. Falnes [25], Clement and Ferrant [66] showed that the nonlinearities of radiation and diffraction force are assumed to be negligible when the device dimension is considerably smaller than the wave length. Meriguad et al. [67] showed that the response of a heaving point absorber is mainly affected by the nonlinear FK forces, while the nonlinear radiation and diffraction force have minor effects on system dynamics. Validation of a nonlinear Froude-Krylov model with linear radiation and diffraction term was tested using a real wave tank by Gilloteaux [68] and Guerinel et al. [67]. The nonlinear model shows a significant improvement of accuracy with respect to a full-linear model and good agreement with experimental measurements. Similar results were obtained by Giorgi and Ringwood [75]

An analytical solution of the nonlinear FK force was developed by Ringwood [65] for WECs of simple geometries. The hydrodynamic model can be expressed as Eq. 2.9. Where $F_{FK_{st}}$ is the static Froude-Krylov force, given as the difference between the gravity force and the Archimed force:

$$F_{FK_{st}} = F_g - \iint_{S(t)} P_{st}(t) \vec{n} dS \quad (2.10)$$

$F_{FK_{dy}}$ is the dynamic Froude-Krylov force:

$$F_{FK_{dy}} = - \iint_{S(t)} P_{dy}(t) \vec{n} dS \quad (2.11)$$

To solve for $F_{FK_{st}}$ and $F_{FK_{dy}}$, the pressure P is required. Which can be obtained using Airy's wave theory for deep water waves:

$$P(x, z, t) = \rho g a e^{\chi z} \cos(\omega t - \chi x) - \rho g z \quad (2.12)$$

where x is the direction of wave propagation, z is the vertical direction (positive upwards), a is the wave amplitude, $\chi = \frac{2\pi}{\lambda}$ (λ the wave length) is the wave number and ω is the wave frequency.

Giorgi developed a format to describe an axisymmetric geometry Fig. 2.1 with a fixed vertical axis 2.13 [19]:

As shown in Fig. 2.1, the surface of an axisymmetric body can be described in

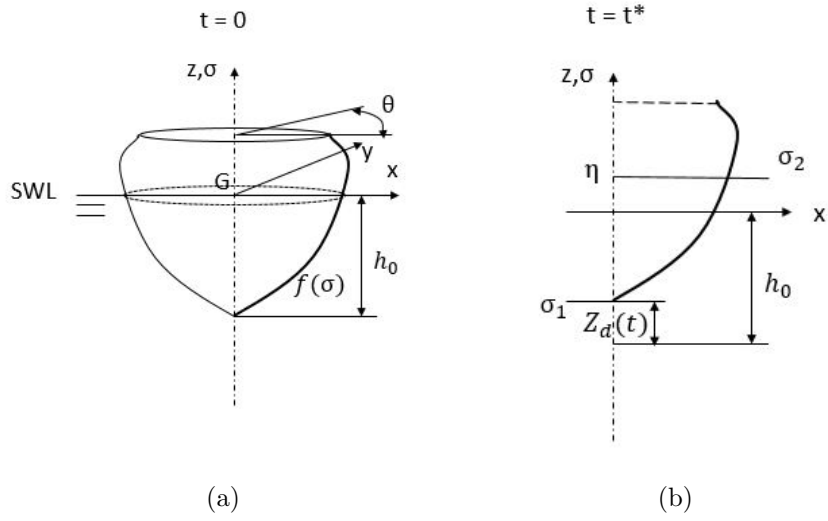


Figure 2.1: A axisymmetric heaving device with generic profile $f(\sigma)$, 2.1(a) shows the equilibrium position with the center of gravity at the still water level (SWL) and the draft h_0 ; 2.1(b) shows the free elevation η and the device displacement z_d after a time t^* . The pressure is integrated over the surface between σ_1 and σ_2

parametric cylindrical coordinates:

$$\begin{aligned}
 x(\sigma, \theta) &= f(\sigma) \cos \theta \\
 y(\sigma, \theta) &= f(\sigma) \sin \theta \\
 z(\sigma, \theta) &= \sigma \\
 \theta &\in [0, 2\pi) \cap \sigma \in [\sigma_1, \sigma_2]
 \end{aligned}
 \tag{2.13}$$

Where,

$$\begin{aligned}
 \sigma_1 &= z_d(t) - h_0 \\
 \sigma_2 &= \eta(t)
 \end{aligned}
 \tag{2.14}$$

The magnitude of the Froude-Krylov force in the vertical direction becomes:

$$F_{FK} = \int_0^{2\pi} \int_{\sigma_1}^{\sigma_2} P(x(\sigma, \theta), z(\sigma, \theta), t) f'(\sigma) f(\sigma) d\sigma d\theta \quad (2.15)$$

Substitute Eq. 2.8 into Eq. 2.15, a numerical equation of the nonlinear FK force is expressed as:

$$F_{FK} = \int_0^{2\pi} \int_{\sigma_1}^{\sigma_2} (\rho g a e^{\chi\sigma} \cos(\omega t - \chi f(\sigma) \cos\theta) - \rho g \sigma) \times f'(\sigma) f(\sigma) d\sigma d\theta \quad (2.16)$$

Chapter 3

Multi resonant Feedback Control of Heave Wave Energy Converters

This chapter presents a time-domain control algorithm that targets both amplitude and phase through feedback that is constructed from individual frequency components that comes from the spectral decomposition of the measurements signal. This intuitive concept is essentially the same as the complex conjugate control (C3); yet it is a time domain feedback implementation. The focus in this chapter is to show, analytically and numerically, that the proposed control may provide a time-domain implementation that approaches pure complex conjugate control. This chapter is organized as follows. Section 3.1 describes the concept of the proposed multi resonant feedback control. Section 3 describes a proportional derivative version of the

multi resonant feedback control. Section 4 details the implementation of the spectral decomposition step using fast Fourier transform, and Section 5 describes the implementation of the feedback control system. Section 6 presents the results of numerical simulations and Section 7 is a discussion and insight on the obtained results.

3.1 Decomposition of the WEC Control Problem

This chapter 3 assumes a linear hydrodynamic model for the WEC. The simulator used for testing also assumes a linear hydrodynamic model. For a heaving buoy, the Cummins' equation of motion is [76]:

$$(m + \tilde{a}(\infty))\ddot{z} + \int_0^\infty h_r(\tau)\dot{z}(t - \tau)d\tau + kz = f_e + u \quad (3.1)$$

where m is the buoy mass, $\tilde{a}(\infty)$ is the added mass at infinite frequency, z is the heave position of the buoy's center of mass with respect to the mean water level, k is the hydrostatic stiffness due to buoyancy, u is the control force, f_e is the excitation force, and h_r is the radiation force term (radiation kernel). The second term in equation 3.1 is affected by the present as well as past oscillations.

Consider the simple case of a regular wave where the excitation force has only one frequency (ω_i); in such case it is possible to show that the radiation term can be

quantified using an added mass and a radiation damping term, each being considered constant at frequency ω_i only [49]. The equation of motion for this simple case becomes:

$$(m + \tilde{a}_i)\ddot{z} + c_i\dot{z}_i + kz_i = f_{ei} + u_i \quad (3.2)$$

Where \tilde{a}_i and c_i are constants for a given exciting frequency. The excitation force in this case is:

$$f_{ei} = A_{ei} \sin(\omega_i t + \phi_i) \quad (3.3)$$

If we assume no control, the system input-output transfer function in the Laplace domain becomes:

$$G_i(s) \equiv \frac{Z_i(s)}{F_{ei}(s)} = \frac{1}{(m + \tilde{a}_i)s^2 + c_i s + k} \quad (3.4)$$

Where $Z_i(s)$ and $F_{ei}(s)$ are the Laplace transforms of $z_i(t)$ and $f_{ei}(t)$ respectively. Using this transfer function we can add a feedback control that uses measurements of the buoy's position and velocity. Let the controller transfer function in the Laplace domain be $D_i(s)$, the the block diagram for this WEC control system can be constructed as shown in Figure 3.1.

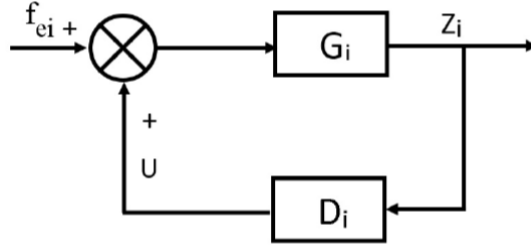


Figure 3.1: Block diagram of a WEC control system of a single frequency regular wave

Let $H_i(s)$ be the closed loop system transfer function in the Laplace domain; hence

$$H_i(s) \equiv \frac{Z_i(s)}{F_{ei}(s)} = \frac{G_i(s)}{1 - D_i(s)G_i(s)} \quad (3.5)$$

The exciting force f_e for a practical converter in a realistic wave is band-limited (approaching zero at high frequencies) [49], and can be assumed as a linear superposition of N different exciting forces at different frequencies [77], that is:

$$f_e = \sum_{i=1}^N f_{ei} = \sum_{i=1}^N A_{ei} \sin(\omega_i t + \phi_i) \quad (3.6)$$

In the case of a real wave, then, there will be N transfer functions $G_i(s)$ because each frequency has its own value of c_i and \tilde{a}_i . In other words, the system reacts differently to different input frequencies, and hence a different transfer function is needed for each input frequency. This can be represented by the block diagram shown in Figure 3.2. The resultant buoy motion will be the combined motion of the individually computed motions; that is the buoy position $z(t)$ is the summation of all individually

computed positions $z_i(t)$.

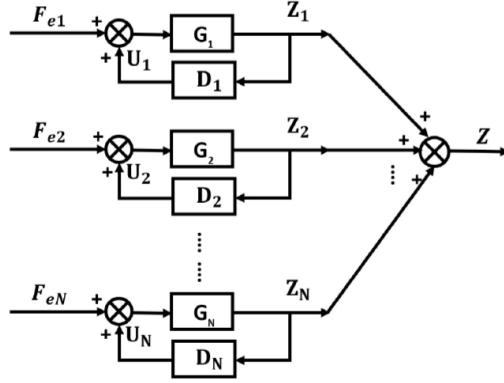


Figure 3.2: Block diagram of the decomposed WEC control system

Implicit in this treatment is the assumption that each block G_i - D_i responds to the particular frequency ω_i only. That is, the overall converter response is modeled as a linear superposition of multiple blocks $G_i(s)\delta(s_i\omega_i)$, where $\delta(s_i\omega_i)$ represents the Dirac delta function centered at ω_i . In the limit as $N \rightarrow \infty$, one expects that such a superposition would provide a close approximation to the true converter response [77].

Figure 3.2 shows a control strategy that designs a separate controller for each frequency in the spectrum. This strategy can be implemented if it is possible to measure (or estimate) the position and velocity components associated with each frequency. This can be achieved using a Fast Fourier Transform (FFT) approach, and it will be discussed in detail in Sections 3.3 and 3.4. For now, let us assume that it is possible to extract the individual positions $z_i(t)$ given the buoy position $z(t)$ and the individual

velocities $\dot{z}_i(t)$ given the buoy velocity $\dot{z}(t)$. Then the system block diagram can be presented as shown in Figure 3.3. In Figure 3.3 the individual transfer functions G_i represent the system's hydrodynamics and are all gathered in one dotted box labeled "Hydrodynamic Model"; similarly all the individual controllers D_i are gathered in a dotted box called "Controller".

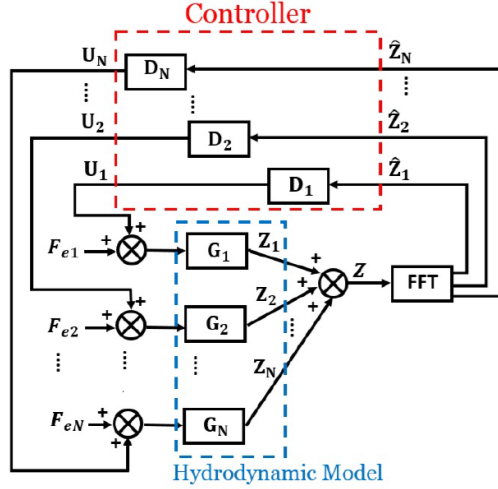


Figure 3.3: Block diagram of the WEC multi resonant control system

In implementing this controller, the summation of all the individual controllers is computed and it is the control that gets applied to the system. Hence:

$$U(s) = \sum_{i=1}^N U_i(s) = \sum_{i=1}^N D_i(s) Z_i(s) \quad (3.7)$$

We can also combine all the individual excitation forces F_{ei} in the total excitation force F_e , and the resulting block diagram for the system becomes as shown in Figure 3.4. In Figure 3.4 the system hydrodynamic transfer functions G_i are gathered in

block called "Model". The WEC control problem is to design the controller $D(s)$;

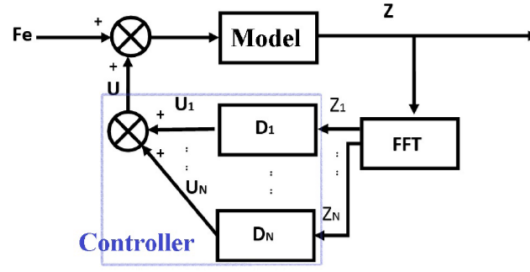


Figure 3.4: Block diagram of the proposed feedback WEC control system

the design criteria considered in this chapter 3 is to maximize the energy extraction. In summary, the WEC control problem is decomposed into N control sub-problems, as illustrated in Figure 3.2. In this case, N different controls, $D_i(s)$, are designed. Using a proportional derivative control, two control gains are to be designed for each individual controller D_i . One advantage of this approach is that the input is a single-frequency for each sub-problem and hence eliminating the need to evaluate a convolution integral. The other advantage is that each controller D_i can be optimized independently from other controllers to its input frequency.

3.2 Proportional Derivative Approximation for C3

The control approach presented in Section 3.1 can be used to approximate the well known complex conjugate control (C3) [78]. In the C3, the WEC velocity is in phase with the excitation force and the control impedance is equal to the complex conjugate

of the mechanical impedance. This section considers an implementation based on N Proportional-Derivative controllers, where each of them is tuned according to its individual exciting force frequency. Proportional-Integral-Derivative (PID) control has been used for WEC control as in [39, 79]. Note that in practice this implementation will be achieved using a combination of actuators and power amplifiers. The gains k_{pi} and k_{di} are representative of the combined effect of the hardware and the software settings.

For each of the control sub-problems described in Section 3.1, the PD controller has the form:

$$D_i(s) = -k_{pi} - k_{di}s \quad (3.8)$$

The dynamic system for this sub-problem can then be written as:

$$(m + \tilde{a}_i)\ddot{z}_i + c_i\dot{z}_i + kz_i = f_e - k_{pi}z_i - k_{di}\dot{z}_i \quad (3.9)$$

$$\therefore (m + \tilde{a}_i)\ddot{z}_i + (c_i + k_{di})\dot{z}_i + (k + k_{pi})z_i = f_e \equiv A_{ei}\sin(\omega_i t + \phi_i) \quad (3.10)$$

For the system described in Equation 3.10, the velocity \dot{z}_i will be in resonance with the excitation force f_{ei} if the following condition is satisfied:

$$\omega_{ni} \equiv \sqrt{\frac{k + k_{pi}}{m + \tilde{a}_i}} = \omega_i \quad (3.11)$$

Let $\bar{m}_i = m + \tilde{a}_i$, then the proportional gain is:

$$k_{pi} = \omega_i^2 * \bar{m}_i - k \quad (3.12)$$

For maximum useful energy, the complex conjugate control implies that the real part of the control impedance is equal to the real part of the mechanical impedance [80]; hence the derivative control gain is selected to be:

$$k_{di} = c_i \quad (3.13)$$

The above control is here referred to as PD Complex Conjugate Control (PDC3). It is possible to show analytically that the PDC3 is equivalent to the C3 as follows. Consider a regular wave with a single frequency, for which the buoy equation of motion is given in equation 3.2. The C3, u_{c3} , is defined as:

$$u_{c3i} = (m + \tilde{a}_i)\ddot{z}_i + kz_i - c_i\dot{z}_i \quad (3.14)$$

Substituting the excitation force ($f_{ei} = A_{ei} \sin(\omega_i t)$) and the control u_{c3i} into the equation of motion (equation 3.2), then the solution of equation 3.2 becomes:

$$\dot{z}_i = \frac{A_{ei}}{2c_i} \sin(\omega_i t) \quad (3.15)$$

$$\therefore z_i = \frac{-A_{ei}}{2c_i\omega_i} \cos(\omega_i t) \quad (3.16)$$

Substituting equation 3.15 and 3.16 into equation 3.14, we get:

$$\begin{aligned}
u_{c3i} &= (m + \tilde{a}_i) \frac{A_{ei}\omega}{2c_i} \cos(\omega t) + k \frac{-A_{ei}}{2c_i\omega_i} \cos(\omega t) - c_i \frac{A_{ei}}{2c_i} \sin(\omega_i t) \\
&= \frac{A_{ei}}{2c_i} \cos(\omega_i t) \left(\omega_i(m + \tilde{a}_i) - \frac{k}{\omega_i} \right) - \frac{A_{ei}}{2} \sin(\omega_i t)
\end{aligned} \tag{3.17}$$

The PDC3 control, u_{PDC3} , is defined in equation 3.8. Substituting equation 3.15 and equation 3.16 into equation 3.8, we get:

$$u_{PDC3i} = k_{pi} \frac{A_{ei}}{2c_i\omega_i} \cos(\omega_i t) - k_{di} \frac{A_{ei}}{2c_i} \sin(\omega_i t) \tag{3.18}$$

Comparing the terms in both u_{PDC3i} and u_{c3i} (equation 3.17 and 3.18). We get:

$$\frac{k_{pi}}{\omega_i} = \left(\omega_i(m + \tilde{a}_i) - \frac{k}{\omega_i} \right) \Rightarrow k_{pi} = \omega_i^2(m + \tilde{a}_i) - k \tag{3.19}$$

$$k_{di} = c_i \tag{3.20}$$

Equation 3.19 and 3.20 are identical to the k_{pi} and k_{di} expressions computed in equation 3.12 and 3.13, which confirms that both controllers would generate the same motion described by equation 3.15 and 3.16 and hence both controllers are equivalent. Generalizing this analysis from a single frequency case to a multi-frequency case is straightforward.

To completely design this PDC3 control, it is required to know the stiffness coefficient

k , the added mass \tilde{a}_i , the damping coefficient c_i , and the frequencies of the excitation force ω_i, \forall_i . The frequencies of the excitation force are unknown. However, the steady state response of a system to a sinusoidal input has the same frequency as the input frequency [81]. Hence, both z_i in the steady state and f_{ei} have the same frequency. In the proposed feedback control system, the device response $z(t)$ is measured. By extracting the frequencies in $z(t)$, one can determine the frequencies of the excitation force and use them to update the controller gains in near-real time (Fourier transformation uses data from the past and has no predictive element. It can be assumed that the frequency-phase-amplitude combination is slowly varying, hence the near-real time.)

In this study, the Matlab Fast Fourier Transform (FFT) function is used to extract the frequencies of $z(t)$. The accuracy of the obtained frequencies, amplitudes, and phases need to be controlled to guarantee good performance for the proposed PDC3 control. The following section describes the FFT implementation used to generate the results in this chapter. Any other signal processing approach can be used for the same purpose.

3.2.1 Stability of the Proposed Proportional Derivative Control

This section addresses the stability of the PDC3 control proposed in 3.1. Consider the block diagram in Figure 3.3. There are N controls $D_i, i = 1 \dots N$. Each controller D_i is basically a feedback control for the system G_i . From the block diagram in Figure 3.3, it can be seen that if all the subsystems (G_i and $D_i, \forall i = 1 \dots N$) are stable then the overall system is stable. In other words, if the output from each subsystem is bounded then the linear summation of all the outputs is also bounded. Hence, the stability problem of the system reduces to finding the stability conditions for the subsystem (G_i and D_i) for arbitrary i . The subsystem open loop transfer function $G_{i\text{math}}$ is a second order transfer function as shown in equation 3.2. The PD controller is defined in equation 3.8. The closed loop system equation of motion is given in equation 3.10, for which the characteristic equations is:

$$((m + \tilde{a}_i)s^2 + (c_i + k_{di})s + (k + k_{pi}))Z_i(s) = 0 \quad (3.21)$$

A Routh stability analysis for the system given in equation 3.21 yields that this system is stable if $k + k_{pi} > 0$ and $c_i + k_{di} > 0$. From equation 3.12, we can write:

$$k + k_{pi} = \omega_i^2 \tilde{m}_i > 0 \quad (3.22)$$

Also, equation 3.13 shows that $k_{di} = c_i$, which is always a positive damping coefficient. We can conclude that for the proposed PDC3, any arbitrary subsystem is stable and hence the overall system is stable. The above stability analysis does not take into consideration model uncertainties.

Consider a continuous disturbance force on the buoy. In Figure 3.1, a disturbance on the buoy would not be different from the wave excitation force, from the buoy prospective. In other words, the proposed PDC3 controller would take advantage of any external force to further increase the energy absorption in the same way the controller reacts to the excitation force. A disturbance force affects the buoy motion z and the frequencies of the buoy motion are extracted whether they are caused by wave excitation force or disturbance force or both. The PDC3 controller will then try to resonate with these frequencies to maximize the energy absorption.

3.3 Feedback Signal Processing

The Matlab FFT function when tested on a numerical WEC case study for a regular wave did not produce accurate predictions for the amplitudes and phases that comprise the buoy position signal, even when assuming perfect measurements for the buoy position. One reason for this inaccuracy is the leakage error which is the error in amplitude and frequency that occurs due to the non-periodicity of the measured signal in

the sample interval. Leakage is probably the most common and most serious digital signal processing error. Time weighting functions, called windows, are usually used to better satisfy the periodicity requirement of FFT [82, 83]. These windows weight heavily the beginning and end of the sample to zero, while the middle of the sample is heavily weighted towards unity. There is a variety of windows; in this chapter the Hanning window is used. The Hanning window is a cosine bell shaped weighting; this window type can have amplitude errors but it is most useful for searching operations where good frequency resolution is needed [84]. The sample data period size should be selected so as to reduce the errors. There is a trade-off between a smaller sample data period size, which may result in only frequencies of the window function, and a larger sample data period size, which may not track the change of buoy's oscillation [85]. An important step is to find a good size for the sample period. In section 3.6 a period of a $6T$ to $8T$ (T is the period of incoming wave) is selected as suggested in [86] and also based on several simulations. The sampling rate used in FFT is 100 Hz. To further reduce the error in the obtained amplitudes and phases, an optimization step is carried out before applying the control. The optimization objective is to minimize the error between the measured position and velocity signals and the predicted position and velocity signals from the FFT. The optimization variables are the amplitudes and phases. Let $\hat{\omega}_i$, $\hat{\phi}_i$, and $\hat{\zeta}_i$ be the estimated frequencies, phases,

and amplitudes, $\forall_i = 1 \dots N$, then:

$$\hat{z} = \sum_{i=1}^N \hat{\zeta}_i \cos(\hat{\omega}_i t + \hat{\phi}_i) \quad (3.23)$$

and

$$\hat{\dot{z}} = \sum_{i=1}^N -\hat{\omega}_i \hat{\zeta}_i \sin(\hat{\omega}_i t + \hat{\phi}_i) \quad (3.24)$$

The optimization objective function can be written as:

$$J = \frac{w_1}{w_1 + w_2} (z - \hat{z})^2 + \frac{w_2}{w_1 + w_2} (\dot{z} - \hat{\dot{z}})^2 \quad (3.25)$$

where w_1 and w_2 are weight factors. In this chapter, the ranges for the amplitudes is assumed as:

$$0.98 \leq \frac{\zeta_{opt}}{\hat{\zeta}_i} \leq 1.1 \quad (3.26)$$

where ζ_{opt} is the optimal amplitude. Also a range is assumed for the phase as:

$$-\frac{\pi}{8} \leq \phi_{iopt} - \hat{\phi}_i \leq \frac{\pi}{8} \quad (3.27)$$

where ϕ_{iopt} is the optimal phase. So, for estimated values of $\hat{\zeta}_i$ and $\hat{\phi}_i$, ranges for these two variables are set according to Equations 3.26 and 3.27.

3.4 Implementation of the PDC3

Section 3.1 explained the concept of decomposing the WEC control problem and section 3.2 explained how to use that concept in developing a feedback control strategy that produces a complex conjugate control. This section describes how this feedback control strategy is implemented. The proposed control strategy is an adaptive feedback controller which utilizes only the measured buoy position and velocity; there is no data required about the excitation force or the waves. Hence, we are not decomposing the excitation force into its components as might be inferred from Figure 3.2. Figure 3.2 only explains the concept of exploiting the linearity (and principle of superposition) of the system to generate the proposed control. The PDC3 control implementation block diagram is shown in Figure 3.4. As shown in Figure 3.4, the system output is decomposed into its components and the individual controls are computed. These individual components are then added up to get the control force that is actually applied to the system. This system is simulated in Matlab and the results are detailed in section 3.5.

In fact the block diagram shown in Figure 3.2 can be implemented if the excitation force is well known. This can be used in simulations - as another implementation - to verify the accuracy of the FFT processing used in the PDC3. When assuming that the excitation force is well known, the proposed control will be referred to as

"PDC3 Theoretical". In this "PDC3 Theoretical" implementation, the excitation force frequencies are known; each component of the excitation force is propagated using its own $G_i(s)$; no FFT step is needed since the frequencies are known and the amplitudes of the position and velocities are directly read from the individual propagators. This implementation is also simulated and the results are presented in section 3.5. The "PDC3 Theoretical" is considered as an upper limit for the PDC3.

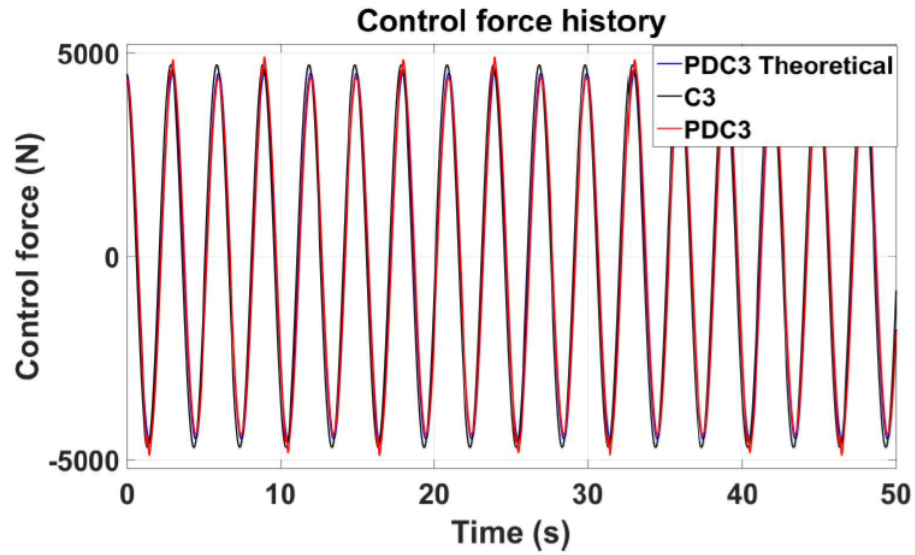
In implementing the PDC3, it is assumed that we have only four frequencies for the controller; that is $N = 4$ in the controller. This number is chosen as some studies have shown that three to four frequencies usually capture most of the energy in most wave spectra [87]. The number of controller frequencies, however, is a parameter that is selected at the beginning of the simulation; it can be tuned. In the simpler simulation cases presented in this chapter where it is assumed that the input excitation force has only three frequencies, we assumed that the controller has only three frequencies; for the Bretshneider wave we assumed the controller has four frequencies. As the wave conditions change, the controller will always look for the four frequencies with highest amplitudes (most significant). Hence if a frequency is added and it is among the top four frequencies in terms of the amplitudes then it will be captured. Similarly if a frequency disappears, the next frequency will be captured instead of the disappeared one. Once the frequencies are captured, the controller gains are updated based on the new captured frequencies.

3.5 Numerical Results

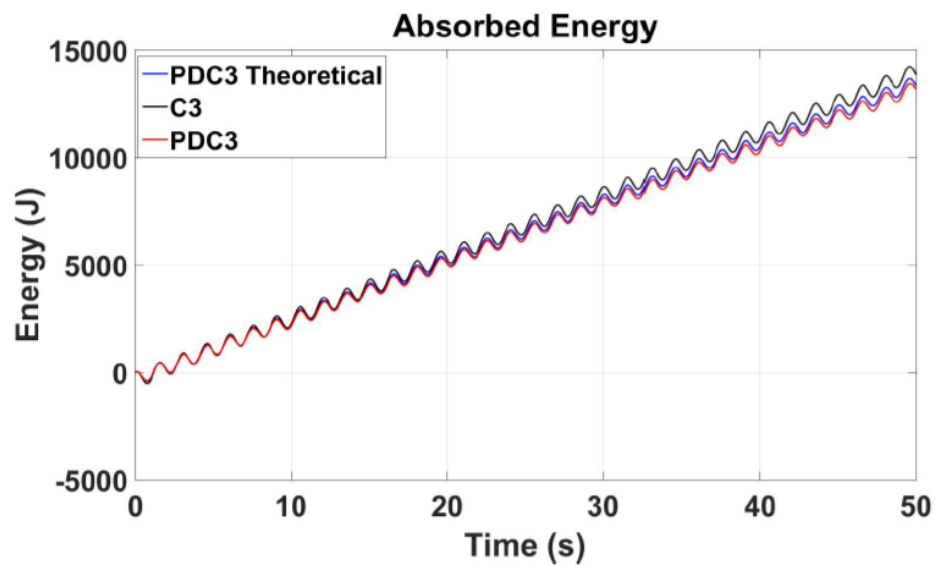
A spherical buoy is assumed of radius of 1 m. The equilibrium level is such that half of the sphere is submerged. The mass of the sphere in this case is $2.0944 \times 10^3 kg$. The corresponding added mass at infinite frequency is $1.1253 \times 10^3 kg$. A regular excitation force is assumed with a frequency of $\frac{2\pi}{3}$.

Two implementations for the PDC3 are presented in this section. The first implementation assumes perfect knowledge of the excitation force and its frequencies, amplitudes and phases (here referred to as PDC3 Theoretical). The second implements FFT with window and optimization as detailed in Section 3.3 to extract the frequencies, amplitudes and phases of the measured buoy position, assuming no knowledge is available about the excitation force nor the wave (this implementation is referred to as PDC3). Both implementations are compared to the complex conjugate control.

Figure 3.5(a) shows the simulated control for both the PDC3 and the PDC3 Theoretical as well as the C3. Both PDC3 and PDC3 Theoretical are almost identical which indicates that the FFT processing resulted in an accurate estimation for the frequencies, amplitudes, and phases. Both controls are also very close to the C3. The corresponding extracted energy is shown in Figure 3.5(b), for the PDC3, the PDC3 Theoretical, and the C3. The energy from PDC3 is almost identical to the energy



(a) Control Force

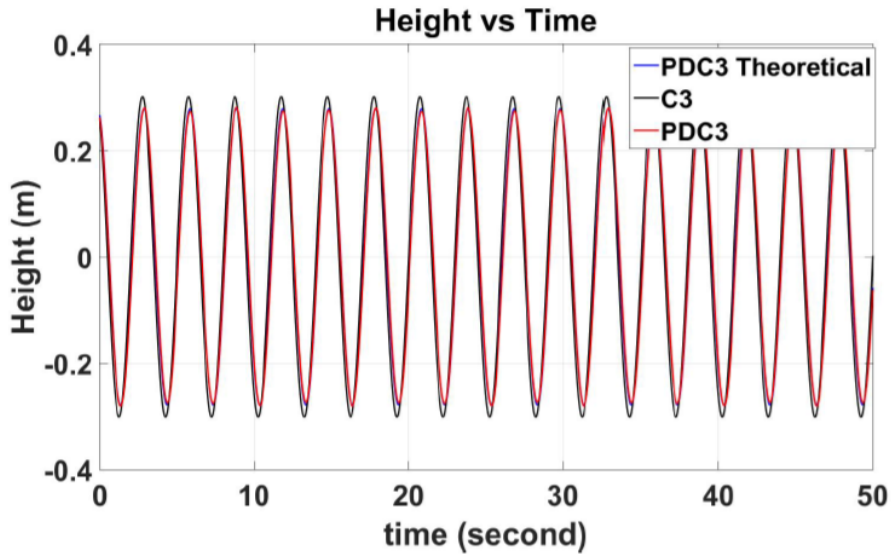


(b) Extracted Energy

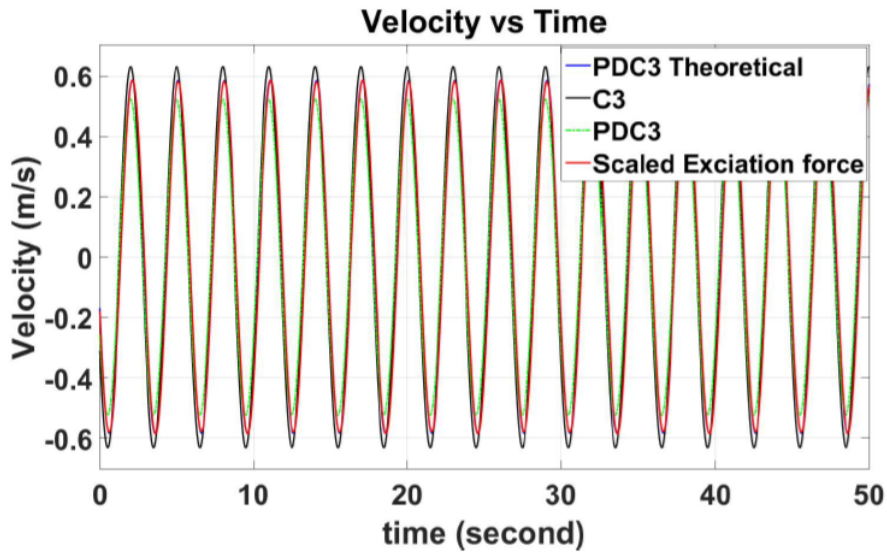
Figure 3.5: Simulation for both actual and Theoretical PDC3 control: Control and Energy

from the PDC3 Theoretical, while both are slightly off from the C3 energy. The position and velocity of the buoy for this case are shown in Figure 3.6. Shown also in Figure 3.6(b) is the scaled excitation force to emphasize that the resulting control

puts the buoy velocity in phase with the excitation force as predicted by the C3.



(a) Position of The Buoy



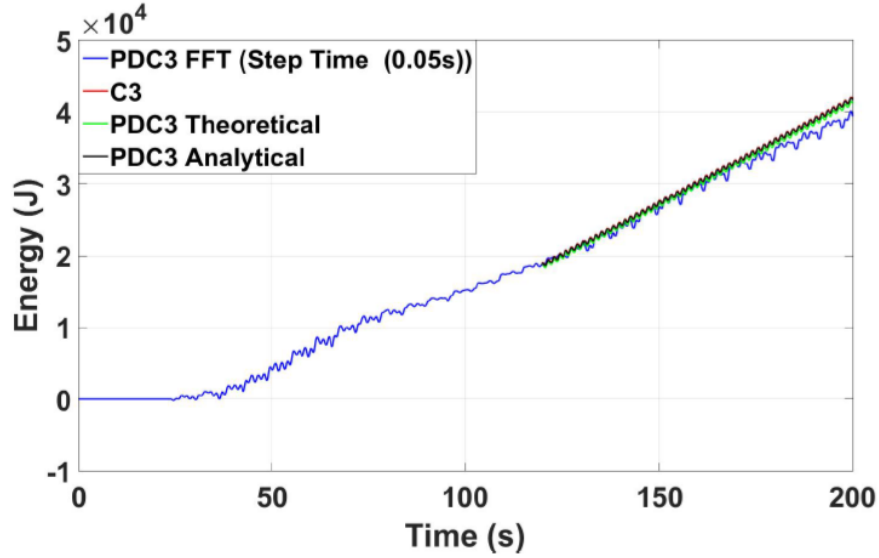
(b) Velocity of The Buoy

Figure 3.6: Simulation for both actual and theoretical PDC3 control: Position and Velocity

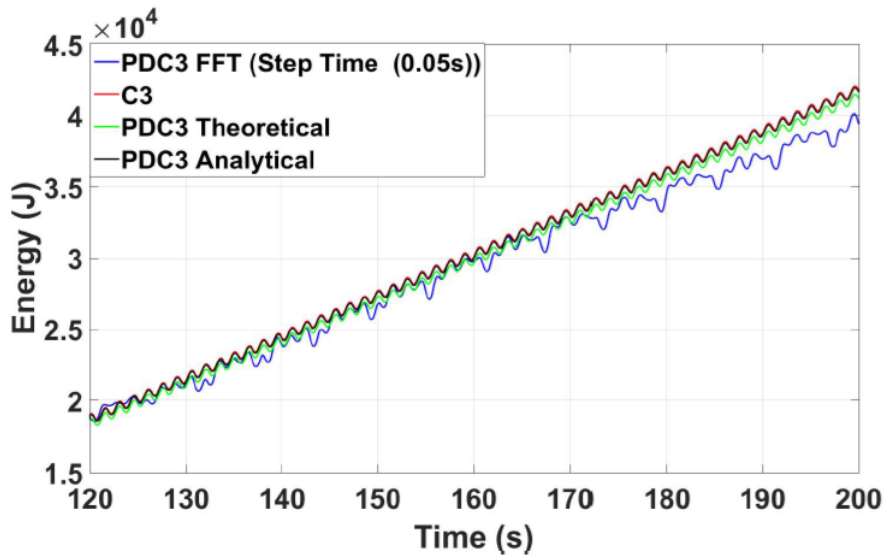
The same device was simulated assuming an incident wave with three frequencies. The

wave periods are 1.5, 2, and 3 seconds. The corresponding amplitudes of these wave are 0.05, 0.05, and 0.1 m, respectively. These values generate a small motion for which the linear model remains valid. Figure 3.7 shows the energy using the PDC3 and the Theoretical PDC3 compared to the C3. To emphasize the optimality of the PDC3 approach, a fourth curve is plotted to represent the analytical PDC3. The analytical PDC3 energy is computed based on the analytic formulae for the control and velocity given in equation 3.18 and 3.15, respectively. Figure 3.7(a) shows the full history of simulation and Figure 3.7(b) zooms on the steady state part only. Note that the C3 curve is valid only in the steady state part. Hence, for the sake of comparison with the PDC3, the C3 calculations started only in the steady state part and it is initialized with an energy level equal to that computed using the PDC3 FFT at time $t = 120$ seconds (beginning of the C3 calculations). More about this point is discussed in Section 3.6. It can be seen from Figure 3.7 that the analytic PDC3 line almost coincides with the C3 line. The PDC3 theoretical assumes perfect decomposition of the output signal yet using numerical integrator for the system differential equations is slightly off. The PDC3 FFT adds another source of error due to the efficiency of the signal decomposition.

The same device was simulated on a more realistic case where the wave is assumed to have a Bretshneider spectrum, with a significant wave height of 0.035 m and peak period of 6.28319 seconds. The Bretshneider spectrum wave is sampled at 257 frequencies for simulation, as shown in Figure 3.8.



(a) Full history of simulation



(b) Steady state part only

Figure 3.7: Simulation for both PDC3, Theoretical PDC3, analytical PDC3, and C3 for a 3-frequency excitation force

NEMOH, a boundary element numerical software tool [88, 89], was used to generate the excitation force coefficients for the given buoy shape. The excitation force is then

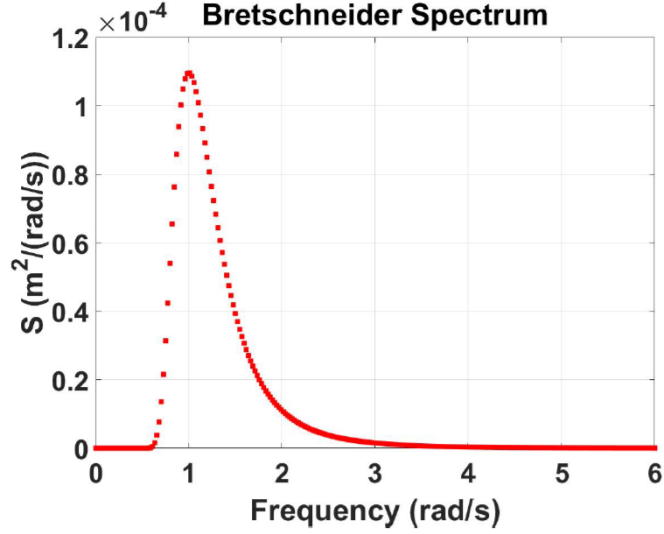


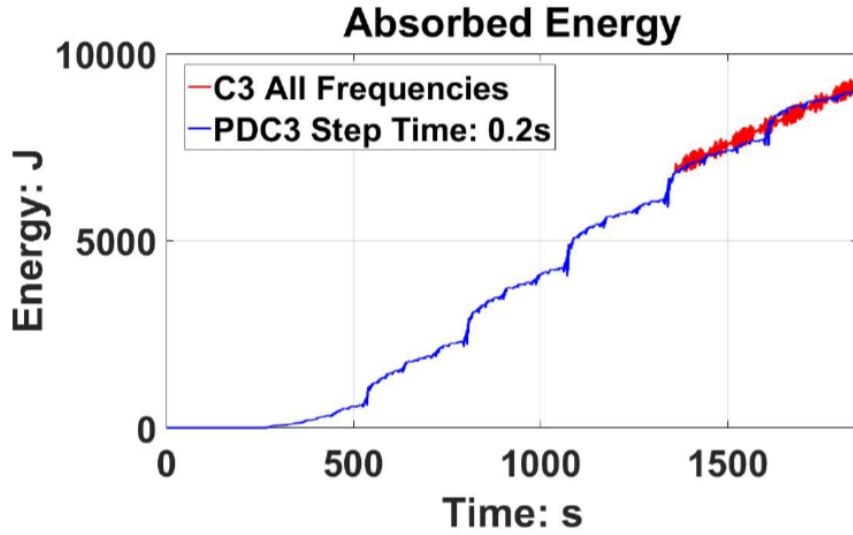
Figure 3.8: Bretshneider spectrum

computed as follows:

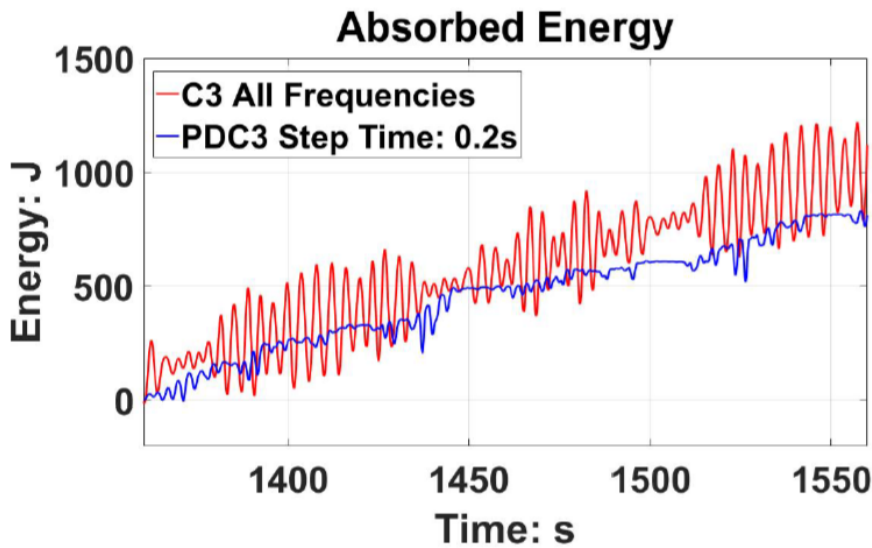
$$F_e = \sum_{i=1}^{32} \Re(f_{ei}\zeta_i e^{i\omega_i t + \phi_i}) \quad (3.28)$$

where F_e is the excitation force, f_{ei} is the excitation force coefficient for the frequency ω_i , ζ_i and ϕ_i are the amplitude and phase of frequency ω_i , respectively, and $\Re(x)$ is the real part of x . This excitation force F_e is then used to simulate the force on the buoy.

As can be seen from Figure 3.9, the PDC3 energy capture is close to that of the C3 solution. The C3 is a steady state solution, so it is implemented only starting at time 1350 seconds when the PDC3 system has become close to a steady state so that we can compare the two solutions. Also, at the time of 1350 seconds the energy absorbed of the C3 is reset to the same value as that of the PDC3, for comparison purpose. In this simulation, the control time step of the PDC3 is set to 0.2 seconds.



(a) Full history of simulation



(b) Steady state part only

Figure 3.9: Simulation of Bretshneider wave for PDC3, C3 for a 4 Dominant frequencies, C3 for All frequencies

The same device was simulated using an Ochi-Hubble wave spectrum, with a significant wave height of 0.01 m and peak period of 6.28319 seconds. The two peak

frequencies of the spectrum are at 0.78 rad/s and 1.3 rad/s. The Ochi-Hubble spectrum wave is sampled at 25 frequencies, picked in the range of 0.2 to 3 rad/s, as shown in Figure 3.10.

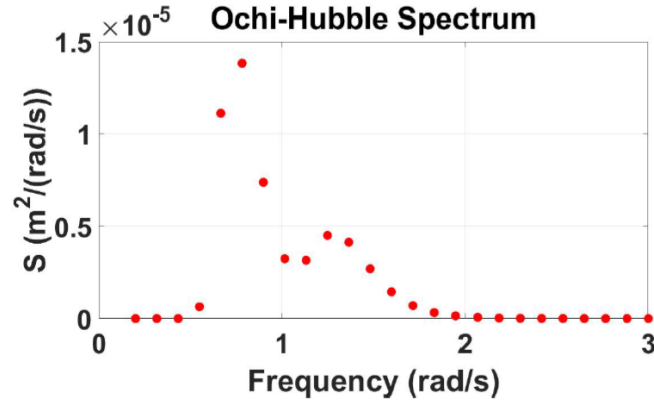
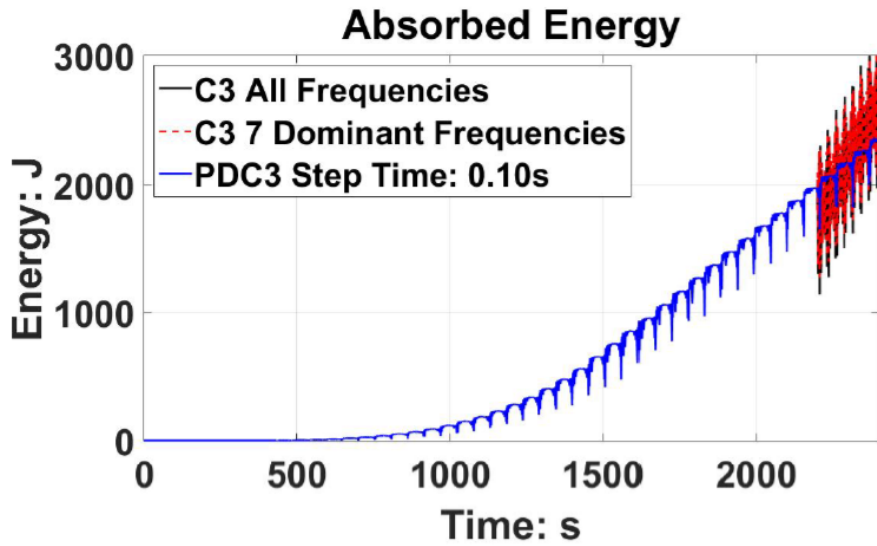
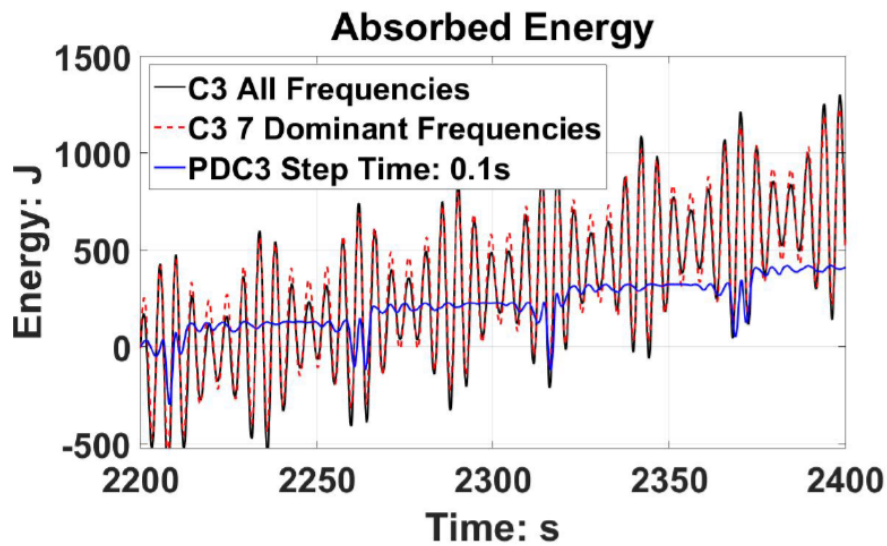


Figure 3.10: Ochi-Hubble spectrum

As can be seen from Figure 3.11, the C3 solution using all the frequencies is about the same as the C3 using only seven frequencies. The PDC3 energy capture is close to that of the C3 solution. The C3 is a steady state solution, so it is implemented only starting at time 2200 seconds when the PDC3 system has become close to a steady state so that we can compare the two solutions. Also, at the time of 2200 seconds the energy absorbed of the C3 is reset to the same value as that of the PDC3, for comparison purpose. In this simulation, the control time step of the PDC3 is set to 0.1 seconds.



(a) Full history of simulation



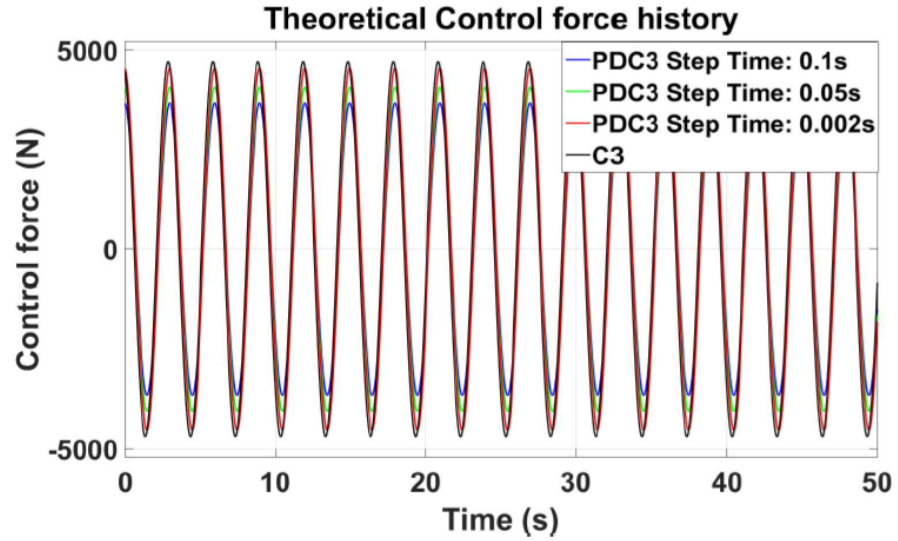
(b) Steady state part only

Figure 3.11: Simulation of Ochi-Hubble wave for PDC3, C3 for a 7 Dominant frequencies, C3 for All frequencies

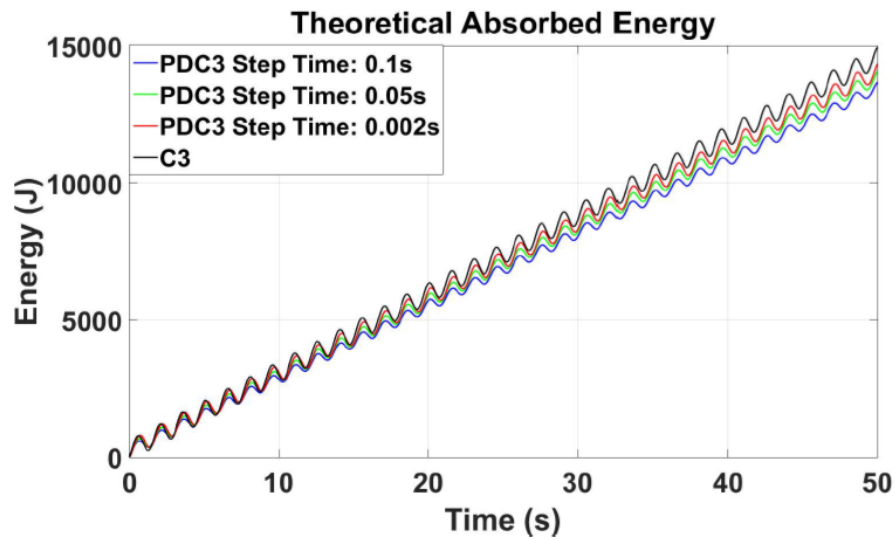
3.6 Discussion

The proposed multi-resonant control strategy in this chapter can be thought of as a way to approach complex conjugate control using feedback only; up to the accuracy of extracting the frequencies, amplitudes, and phases from the output. One main difference is that the complex conjugate control is a steady state solution while the proposed PDC3 works for both steady state and transient response. For the regular wave, the slight difference in energy extraction between the PDC3 and the C3 can be attributed to numerical errors. Specifically, the PDC3 (and PDC3 Theoretical) is a feedback control where the buoy height and velocity are numerically simulated and used for feedback. Any error in the numerical integration of the differential equations would affect the control and hence the propagation of the states; as a result this numerical error gradually accumulates over time. This type of numerical error does not affect the C3 since it is not a feedback control; hence the control is computed as a function of time, independent from the state propagation and hence it is free of propagation numerical errors. The analytic PDC3 also does not have numerical integration for the equation of motion. Also, the way the coefficients c_i are computed are via interpolation from a table at the different frequencies that are extracted from the FFT. So, any error due to resolution error in the FFT or in the interpolation will reflect on the corresponding c_i value which directly impacts the k_{di} controller gain in the PDC3 and PDC3 Theoretical. Since the control is

used to propagate the states numerically in the PDC3 and PDC3 Theoretical, these errors accumulate in time domain; whereas in the C3 the control does not need the numerical propagation of the states. This explains why the difference between the C3 and the PDC3 increases over time. To further show this effect, figures 3.12 and 3.13 compare the PDC3 and the C3 for three different integration time steps of the PDC3. As can be seen from figures 3.12 and 3.13, as the time step gets smaller the difference between the PDC3 and the C3 gets smaller as well. In the test case when a Bretschneider wave is used, there is another reason which can cause a difference between the PDC3 and C3 solutions. The C3 is a steady state solution which means that if the system is not in a steady state the energy absorption estimated by the C3 is not accurate. In the Bretschneider wave case, the frequencies change and the controller tracks these changing frequencies and hence the steady state is likely to be disturbed on a continuous basis. For panchromatic waves, T is the significant peak period. The spectral envelope is assumed stationary in this section. At the time the control is applied, the controller gains are computed based on data collected over a period of $6T - 8T$ that ends at the current time. The data is used to get an estimate for the excitation force frequencies at the current time only. If the buoy motion frequencies do not change over the $8T$ period, then the PDC3 is expected to match the C3 solution. When the frequencies change during the $8T$ period, however, there will be a difference between the PDC3 and the C3; there is two aspects about this case. First, when the frequencies change over the $8T$ period, the FFT tool may



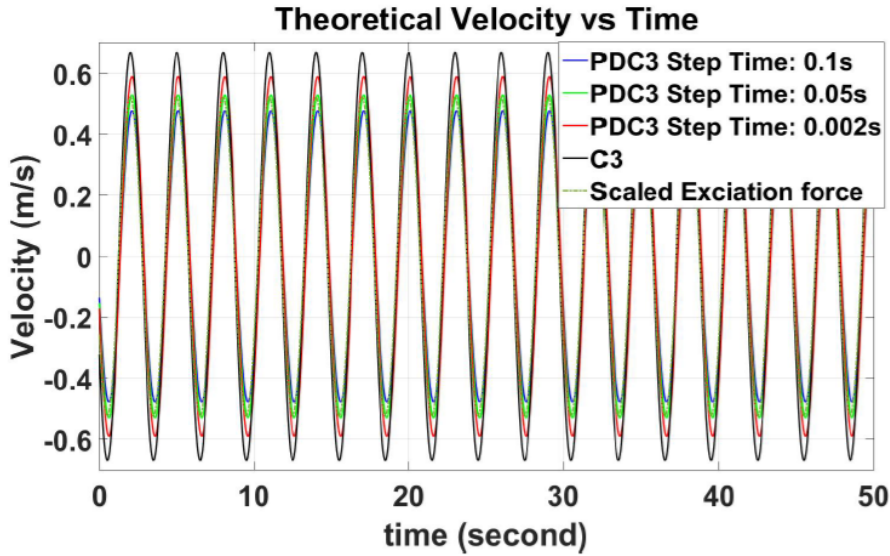
(a) Control Force



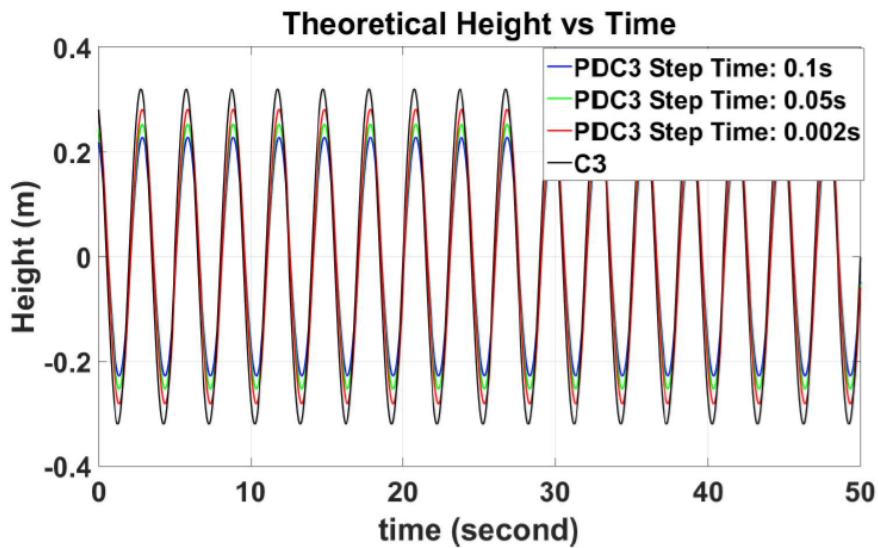
(b) Extracted Energy

Figure 3.12: Control and Energy: as the time step gets smaller the difference between the PDC3 and the C3 gets smaller

not capture accurate frequencies that match that of the excitation force, due to the picket fence effect; and hence this is a source of error. Second, as mentioned above, the C3 solution is a steady state solution which means that when the frequencies change



(a) Velocity of The Buoy



(b) Position of The Buoy

Figure 3.13: Position and Velocity: as the time step gets smaller the difference between the PDC3 and the C3 gets smaller

during the $8T$ period, a transient response is expected and the C3 calculations are not applicable in this case. The PDC3 tries to minimize the impact of this rapid frequency change on the system performance through the square error minimization

step. The simulations presented in this section highlights that there is always a difference between the PDC3 and C3; and one reason for this difference is the rapid frequency change. Again the C3 solution is not correct in that case. The fact that the C3 strategy is a steady state solution is the reason Figures 3.7 has presented the comparison between the C3 and the PDC3 only during the steady state part. As shown in Figures 3.7, the PDC3 still works in the transient part and its performance is not very different from its performance in the steady state; yet it is not possible to compare it to C3. As discussed in Section 3.3, a time window of $6T$ to $8T$ is allowed before applying the control; this is shown in Figure 3.7(a). During a WEC operation the frequencies change over time; when this change happens the FFT will be in a transient phase and the PDC3 is expected not to generate the same amount of energy as in the steady state mode. However when this change in frequency occurs, the buoy runs into a transient phase in which the C3 method also is not guaranteed to be optimal. In such a real seaway this frequency change is occurring constantly and the rate and amount of change are unknown at any given time unless time-series prediction or deterministic prediction are used [45, 46]. The PDC3 still poses a good performance during transient response periods using only a feedback control strategy.

The PDC3 control is equivalent to the C3 in terms of the required reactive power. This can be attributed to the fact that both controls are designed to resonate the system with the excitation force. The PDC3 has two components: a proportional (stiffness) control and a derivative (damping) control. The stiffness part of the control

generates the reactive power. This stiffness part is designed to resonate the velocity with the excitation force; which is the same criterion used in designing the C3 control. Figure 3.14 shows the power in the PDC3 due to the stiffness control only and the C3 reactive power; the reactive powers in both controllers are essentially the same given the numerical error in the PDC3. This conclusion can also be confirmed analytically if we compare the reactive power terms in both the u_{c3} and the u_{PDC3} . The cosine terms in equation 3.17 and 3.18 are the reactive power terms of the u_{c3} and the u_{PDC3} , respectively, and both terms are equal.

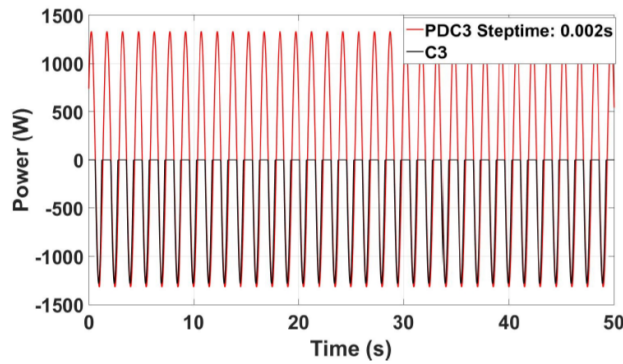


Figure 3.14: Reactive power for both the C3 and the PDC3

The PDC3 control strategy is a feedback control strategy that requires measuring the buoy position and velocity. So, sensors for both position measurement and velocity measurement are needed for implementing this control strategy. No prediction for the wave or excitation force is needed in the PDC3; yet the extracted energy is very close to that of the C3 in the numerical test cases presented in this chapter. The key is that the FFT (or any other filter) should be able to accurately identify the

frequencies in the measured signal of the buoy position, as well as their amplitudes and phases. The number of extracted frequencies N dictates the optimality of the obtained solution.

The computational cost of the PDC3 algorithm is mainly due to the signal processing part since the control itself is a simple feedback logic. The signal processing part is conducted in this chapter using FFT; the FFT might not be the most computationally efficient method to extract the frequencies but it is used in this chapter to introduce the concept of PDC3 as a new control logic for WECs. Future work will investigate the most computationally efficient way of carrying out the signal processing part. For comparison, consider the recent WEC real-time controllers presented in [44] and [30]. In [44] the controller tunes the oscillation of the system such that it is always in phase with the wave excitation. The controller is tuned based on a harmonic approximation of the wave excitation force that is function of a single instantaneous frequency, amplitude, and phase. Specifically, the approach consists of the generation of a reference velocity, from knowledge of the current wave excitation force acting on the system, and then imposition of such velocity through a feedback control. Reference [44] did not discuss the computational cost of their method but it is clear that it also consists of two parts; the first part is the estimation of the excitation force in which an extended Kalman filter is used. The main advantage of the single instantaneous frequency approach presented in [44], however, is that the excitation force is assumed to have only one time-varying frequency. Reference [30] presents a procedure for the

optimization of the control using a model-predictive control approach. It repeatedly solves the optimization problem online in order to compute the optimal control on a receding horizon. The wave excitation force is predicted by use of an augmented Kalman filter based on a damped harmonic oscillator model of the wave process. Reference [30] did not discuss the computational cost of this method; but it is clear that it has two relatively computationally intense steps: the online optimization in the model predictive control calculations and the augmented Kalman filter step.

The size of the FFT depends on the complexity of the case study. For the Bretschneider case with 257 frequencies, the FFT size is 120; that is FFT is set to capture 120 frequencies. The FFT spectrum is discrete, it estimates the spectral level at specific frequencies, which are determined independently from the signal. As a result, peaks in the true spectrum may lie between the FFT frequencies. This is known as the Picket Fence Effect (PFE). Some references in the literature show how to eliminate the PFE using windowing such as reference [86] in which formulae are derived that compute the tones frequencies and amplitudes. Also reference [90] shows how to use windowing to reduce the PFE and presents strategies for selecting the windowing type depending on the signal content. For instance for a signal content that has sine wave or a combination of sine waves, Hanning windowing is recommended, which is adopted in this chapter. In this chapter, to reduce the error due to the PFE, an optimization step is carried out after extracting the frequencies, amplitudes, and phases, as detailed in Section 3.3. It is also noted that using a high sampling rate

reduces the PFE. This chapter has implemented the FFT approach to extract the frequencies and their amplitudes from the measured signal, but FFT is not the only way to carry out this signal processing task. In future work, this PDC3 approach will be extended to multi-degrees-of-freedom WECs and other signal processing methods will be investigated.

Finally, the C3 may result in a motion that exceeds the limits on displacement. There are several techniques in the literature that address the problem of constrained control such that the buoy remains within an acceptable range of displacement all of the time. This chapter does not address this issue. The focus is on proving the concept of PDC3 and comparing it with the C3; for comparison with C3 all constraints had to be removed. It is to be noted here that in the simulations conducted in this chapter, the wave conditions we studied were deliberately chosen such that the body remains within a reasonable range of displacement, as shown in Figures 3.6(a) and 3.13(b).

Chapter 4

Hydrodynamic Design and Near-Optimal Control of a Small Wave Energy Converter for Ocean Measurement Applications

This chapter utilizes wave predictions based on incident up-wave measurements to compute the feed-forward actuation force; which is shown to achieve near-optimal relative heave oscillation. Performance of the system is tested through simulations in a range of wave climates. Wave statistics for this purpose are obtained from the site of a deployment for the instrument that forms the target application for

the present design. Section 4.1 following this introduction briefly summarizes the wave prediction approach used here. Section 4.2 discusses the present approach to geometry optimization based on force compensation and effective radiation damping maximization. Section 4.3 outlines the dynamic model for the buoy-submerged body system, and evaluates the feed-forward control force. The calculations carried out here are summarized in section 4.4. Principal results are discussed in section 4.5. The chapter ends with a brief section stating the main conclusions from this study (section 4.6).

4.1 Deterministic Wave Prediction

The approach used here is based on the formulation described in [91], [92], and developed further in [46]. Here the dynamics of wind-wave interactions over the free-surface are ignored over the distance and time scales of interest. Hence, a linear kinematic model relating the wave surface elevation $\eta(x; t)$ at one point (time) and the wave surface elevation at another point and another time may be sufficient. However, Fourier transform-ability requires that the wave elevation $\eta(x, t) \rightarrow 0$ as $t \rightarrow \pm\infty$ [49], [93]. In practice, this limits application of the present approach to periods of wave activity between periods when the sea is relatively calm. In [46] the distance separating the point of measurement x_A and the point of prediction x_B was on the order of 1000m, and an advancing time series of surface elevation spanning about 260s was used to

predict the wave elevation at the device centroid about 30s into the future. The prediction time was based on the heave radiation impulse response function for the device (particularly the time at which it could be truncated without serious loss of accuracy).

In deep water, for uni-directional wave propagation, a kinematic model relating the wave elevation at point x_A to that at point x_B in the frequency domain can be expressed as

$$\eta(x_B; i\omega) = e^{-ik(\omega)d} \eta(x_A; i\omega) \quad (4.1)$$

where $k(\omega)$ using the deep-water dispersion relation is

$$k(\omega) = \frac{|\omega|\omega}{g} \quad (4.2)$$

$k(\omega)$ has the same sign as ω . The wave elevation time history for predominantly uni-directional waves may be obtained by a non-directional wave rider buoy. For most realistic surface wave spectra over which a wave energy device operates, ω may be expected to be within finite approximate limits ω_l and ω_h . Because surface waves are dispersive, an impulsive excitation of the wave surface propagates over a range of

group velocities $[v_{gmn}, v_{gm_x}]$, where, for deep water,

$$v_{gmn} = \frac{1}{2} \left(\frac{g}{\omega_{mn}} \right)$$

$$v_{gm_x} = \frac{1}{2} \left(\frac{g}{\omega_{m_x}} \right) \quad (4.3)$$

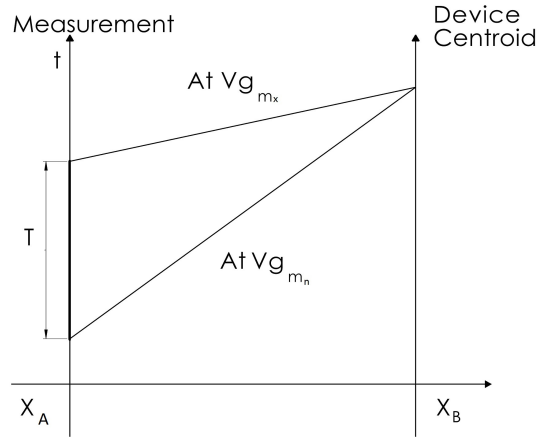


Figure 4.1: Space-time diagram for real-ocean waves. This is used along with the required prediction time to determine the distance and duration of the up-wave measurement.

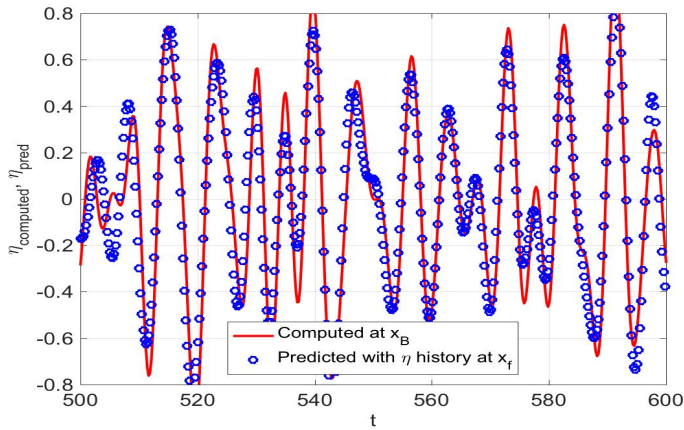


Figure 4.2: Comparison of computed wave elevation time domain history at x_B and predicted wave elevation history at x_f .

Figure 4.1 shows a space-time diagram relating the time-series length, prediction time, prediction distance, and the group velocity range considered. The prediction at x_B using a measurement at x_A can be obtained using an impulse response function $h_l(t; d)$ where

$$h_l(t; d) = \frac{1}{2\pi} \int_{-\infty}^{\infty} e^{-ik(\omega)d} e^{i\omega t} d\omega \quad (4.4)$$

$h_l(t; d)$ can be evaluated analytically as [58], [91], and [46] as

$$\begin{aligned} h_l(t; d) = & \frac{1}{4} \sqrt{\frac{2g}{\pi d}} \left[\cos\left(\frac{gt^2}{4d}\right) + \sin\left(\frac{gt^2}{4d}\right) \right] \\ & + \frac{1}{2} \sqrt{\frac{2g}{\pi d}} \left[\cos\left(\frac{gt^2}{4d}\right) C\left(t\sqrt{\frac{g}{2\pi d}}\right) \right] \\ & + \frac{1}{2} \sqrt{\frac{2g}{\pi d}} \left[\sin\left(\frac{gt^2}{4d}\right) S\left(t\sqrt{\frac{g}{2\pi d}}\right) \right] \end{aligned} \quad (4.5)$$

where C and S denote the two Fresnel integrals. Using a wave surface-elevation time-series measurement at x_A over $[t - T, t]$ seconds, the surface elevation at $x_B = x_A + d$ at time $t + t_p$ can be obtained using

$$\eta(x_B; t + t_p) = \int_0^T h_l(\tau) \eta(x_A; t - \tau) d\tau; \quad t > T$$

$$x_B - x_A = d = t_P v_{gmx}$$

$$T = \frac{d}{v_{gmn}} - \frac{d}{v_{gmx}}$$

(4.6)

4.2 Geometry Optimization

Analysis software [94] is used to calculate the hydrodynamic coefficients of the proposed wave energy converter system in heave motion. Geometry input files of the floating buoy and reaction frame are defined separately to calculate hydrodynamic interaction between two bodies. The floating buoy is defined as shown in upper part of figure 4.8. Reaction frame is defined as two discs (spheres or hemispheres) connected with a rigid rod as shown in lower parts of figures 4.3(a), 4.3(b), and 4.3(c). The design with two discs is taken to be the baseline geometry design. Although a number of geometries were examined, only the best three (in terms of the criteria below) including the baseline are discussed here.

Preliminary evaluation is focused on total and relative exciting forces F_{Total} and $F_{Relative}$ as defined in equation (4.7) and (4.8). First goal of geometry optimization is to maximize relative exciting force and to minimize total exciting force simultaneously, since high energy capture ratio and small mooring force are results of high relative exciting force and low total exciting force. Results of exciting force evaluation for three designs are shown in figures 4.4(a), 4.4(b), and 4.4(c).

$$|F_{Total}(i\omega)| = |F_{ft}(i\omega) + F_{fb}(i\omega)| \quad (4.7)$$

$$|F_{Relative}(i\omega)| = |F_{ft}(i\omega) - F_{fb}(i\omega)| \quad (4.8)$$

Another evaluation is focused on relative radiation damping R_i , defined as real part of effective impedance (equation 4.15) under no constraint. Note that the maximum energy captured is determined by the effective impedance on the relative heave motion of the system. One goal of geometry optimization is to maximize the peak value and the average value of the relative radiation damping simultaneously. A high peak value for the relative radiation damping results in high energy capture ratio at a certain frequency of the incoming wave. High average values of the relative damping result in good energy capture over the whole incoming wave spectrum.

Cylindrical, spherical and hemispherical shapes with different dimensions (e.g. radius) were evaluated. During geometry optimization, high weights were given to relative radiation damping, as R_i represents the causal resistive part of PTO control force in heave motion without constraint. High peak values of relative radiation damping and high relative exciting force are found in shape designs with the same radius as the floating buoy. High values of R_i and $F_{Relative}$ at low frequency are found concurrently in spherical and hemispherical shape designs. As shown in Figures 4.5(a), 4.5(b), and 4.5(c), although the 2-spheres design shows better relative exciting force over the frequency range of interest (Figure 4.4), the 2-hemispheres design has the highest relative radiation damping coefficient at low frequencies, and generally higher

(compared with the other two geometries) relative radiation damping over the whole frequency range.

Energy capture simulations based on realistic year-long wave data at Martha's Vineyard Coastal Observatory [1] were performed on the three proposed designs above. The 2-hemispheres design with higher relative radiation damping coefficient results in more energy capture under the same oscillation constraint conditions, (Figures 4.6, 4.7). The 2-spheres design with higher relative exciting force results in less control force under the same oscillation constraint conditions (Figure 4.6(b)).

4.3 Dynamic Model

The approach below considers an axisymmetric omni-directional wave energy converter based on relative heave oscillation of two bodies, though it should apply to other devices with appropriate modifications. Figure 4.8 shows the starting/baseline geometry for the device. The analysis below is summarized from [15], and is included for completeness. In the simulations discussed in this work, radius of the cylinder portion of the buoy $R = 1.2$ m, and the draft $D_r = 1$ m. The instrument frame is 3 m below the water surface.

For dynamic modeling purposes, it is found helpful to work in the frequency domain at first, and then to use inverse Fourier transformation of the quantities of interest at

the end. Thus,

$$\begin{aligned}
[Z_t(i\omega) + Z_L(i\omega)] v_t(i\omega) + i\omega [Z_c(i\omega) - Z_L(i\omega)] v_b(i\omega) &= F_{ft}(i\omega) \\
[Z_c(i\omega) - Z_L(i\omega)] v_t(i\omega) + [Z_b(i\omega) + Z_L(i\omega)] v_b(i\omega) &= F_{fb}(i\omega)
\end{aligned} \tag{4.9}$$

where the matrix elements are defined as,

$$\begin{aligned}
Z_t(i\omega) &= i\omega [m_t + \bar{a}_t(\infty) + a_t(\omega)] + \frac{k_t}{i\omega} + (c_{dt} + b_{dt}(\omega)) \\
Z_b(i\omega) &= i\omega [m_b + \bar{a}_b(\infty) + a_b(\omega)] + \frac{k_b}{i\omega} + (c_{db} + b_{db}(\omega)) \\
Z_c(i\omega) &= i\omega a_c(\omega) + b_c(\omega) \\
Z_L(i\omega) &= L(\omega) + \frac{N(\omega)}{i\omega}
\end{aligned} \tag{4.10}$$

Where the letter m is used to denote in-air mass, with the subscripts t and b respectively denoting the top and bottom bodies. b_{dt} and b_{db} denote the frequency-variable radiation damping for the two bodies, while $\bar{a}_t(\infty)$ and $\bar{a}_b(\infty)$ denote the infinite-frequency added masses for the two bodies and $a_t(\omega)$ and $a_b(\omega)$ represent just the frequency-dependent parts of the respective added masses. The letter k denotes stiffness (hydrostatic for the floating buoy and mooring-related for the submerged body), while c_{dt} and c_{db} represent the linearized viscous damping coefficients. a_c and b_c denote the frequency-variable added mass and radiation damping due to interaction between the two bodies. Z_L represents the load impedance applied by the power take-off on

the relative oscillation. Following the approach of Falnes [20], it is possible to express equation (4.9) as a scalar equation in terms of the relative velocity $v_r(i\omega)$,

$$v_r(i\omega) = v_t(i\omega) - v_b(i\omega) \quad (4.11)$$

by defining,

$$\bar{Z}(i\omega) = Z_t(i\omega) + Z_b(i\omega) + 2Z_c(i\omega) \quad (4.12)$$

and

$$F_e(i\omega) = \frac{F_{ft}(i\omega)(Z_b(i\omega) + Z_c(i\omega))}{\bar{Z}(i\omega)} - \frac{F_{fb}(i\omega)(Z_t(i\omega) + Z_c(i\omega))}{\bar{Z}(i\omega)} \quad (4.13)$$

It is seen that

$$v_r(i\omega) = \frac{F_e(i\omega)}{Z_i(i\omega) + Z_L(i\omega)} \quad (4.14)$$

where

$$Z_i(i\omega) = \frac{Z(i\omega)Z_s(i\omega) - Z_c^2(i\omega)}{\bar{Z}(i\omega)} \quad (4.15)$$

Details of the subsequent steps are provided in [46]. Following [20] and [46], the relative velocity is found to be at the hydrodynamic optimum (i.e. providing best power conversion) when

$$Z_{Lnu}(i\omega) = Z_{ni}^*(i\omega) \quad (4.16)$$

which leads to

$$v_{ro}(i\omega) = \frac{F_e(i\omega)}{2R_i(\omega)} \quad (4.17)$$

where

$$Z_{ni}(i\omega) = R_i(\omega) + iC_i(\omega) \quad (4.18)$$

$R_i(i\omega)$ and $C_i(i\omega)$ are the resistive and reactive parts of the effective impedance experienced by the relative velocity $v_r(i\omega)$. This can be verified by following the steps in [46]. Oscillation constraints are applied by following the approach of Evans [95] on the relative v_r . In particular, R_i in equation (4.18) is replaced by $R_i(\omega) + \Lambda_r(\omega)$

where

$$\Lambda_r(\omega) = \frac{|F_e(i\omega)|}{2\beta_r(\omega)} - R_i(\omega) \quad (4.19)$$

$Z_{ni}(i\omega)$ is then amended as,

$$Z_{ni}(i\omega) = R_i(\omega) + \Lambda_r(\omega) + iC_i(\omega) \quad (4.20)$$

The exciting forces in heave for the two bodies can be expressed in frequency domain as

$$\begin{aligned} F_{ft}(i\omega) &= H_{ft}(i\omega)\eta(x_B; i\omega) \\ F_{fb}(i\omega) &= H_{fb}(i\omega)\eta(x_B; i\omega) \end{aligned} \quad (4.21)$$

$H_{ft}(i\omega)$ and $H_{fb}(i\omega)$ are the exciting force frequency response functions for the individual bodies (evaluated for unit incident wave amplitudes at their respective centroids). $\eta(x_B; i\omega)$ denotes the incident free-surface elevation at the body centroid x_B . The effective heave force (acting on the relative oscillation v_r , [20]) $F_e(i\omega)$ can then be expressed as

$$F_e(i\omega) = H_e(i\omega)\eta(x_B; i\omega) \quad (4.22)$$

The hydrodynamically optimum velocity can then be expressed as

$$v_{ro}(i\omega) = \frac{H_e(i\omega)}{2[R_i(\omega) + \Lambda_r(\omega)]}\eta(x_B; i\omega) \quad (4.23)$$

Taking the inverse Fourier transform of equation (4.23),

$$v_{ro}(t) = \int_{-\infty}^{\infty} h_o(\tau)\eta(x_B; t - \tau)d\tau \quad (4.24)$$

where

$$h_o(t) = \frac{1}{2\pi} \int_{-\infty}^{\infty} \frac{H_e(i\omega)}{2[R_i(\omega) + \Lambda_r(\omega)]} e^{i\omega t} d\omega \quad (4.25)$$

$h_o(t)$ is non-causal for the 2-body device in Figure 4.8. However, for $t < 0$, $h_o(t)$ can be truncated as $t \rightarrow -t_T$, where in the present case $t_T \approx 30$ s, implying that $\eta(x_B; t)$ needs to be known at least 30 s ahead. With $\eta(x_B; t)$ predicted as summarized in

section 4.1, the resistive and reactive control forces can be determined as,

$$\begin{aligned}
 F_l(t) &= \int_{-\infty}^{\infty} h_{ri}(\tau)\eta(x_B; t - \tau)d\tau \\
 F_a(t) &= \int_{-\infty}^{\infty} h_{ci}(\tau)\eta(x_B; t - \tau)d\tau
 \end{aligned} \tag{4.26}$$

where

$$\begin{aligned}
 h_{ri}(t) &= \frac{1}{2\pi} \int_{-\infty}^{\infty} \frac{H_e(i\omega)}{2} e^{i\omega t} d\omega \\
 h_{ci}(t) &= \frac{1}{2\pi} \int_{-\infty}^{\infty} \frac{H_e(i\omega)C_i(\omega)}{[2R_i(\omega) + \Lambda_r(\omega)]} e^{i\omega t} d\omega
 \end{aligned} \tag{4.27}$$

To find the forces in the presence of oscillation constraints, $R_i(\omega)$ above is replaced by $R_i(\omega) + \Lambda(\omega)$. Note that these integrals in the present work are evaluated from $-t_T$ to the present time t , and $\eta(x_B; t)$ is predicted t_T beyond the present time t .

With and without the oscillation constraint present, the average power absorbed over a time period $[0, T]$ can be found using

$$P_w = \frac{1}{T} \int_0^T F_l(t)v_{ro}(t)dt \tag{4.28}$$

4.4 Calculations

The calculations were focused on a specific application where the requirement is to provide a converted power amount higher than the operation power (on the order of tens of watts) to a science instrument currently operating off Martha's Vineyard, Massachusetts, United States. The buoy was chosen to match the central surface mooring in the Pioneer Array of the Ocean Observatories Initiative [96]. The geometry optimization study of section 4.2 informed the design of the support framework for the instrument. Wave data collected by the 12m node of the Martha's Vineyard Coastal Observatory (MVCO) of the Woods Hole Oceanographic Institution was used to test the performance of the proposed designs in computer simulations[1]. Specifically, the complete year-long wave data for 2015 was reviewed, and in order to obtain reasonable performance bounds, the best and the weakest wave conditions in terms of available wave energy were chosen for the simulations. The data is available in terms of significant wave heights and dominant periods for both swell and wind-wave components, leading to a bi-modal wave spectrum overall. Waves were assumed to be largely long-crested for the site of deployment, though this assumption is not strictly necessary in view of other recent work [97]. Simulations were carried out to map the performance of the system on two time scales. First, the most energy-rich and energy-poor significant wave height – dominant period (swell and wind waves) combinations occurring each month of 2015 were chosen to sample the seasonal variations of the

available energy. Second, to sample the hourly variations of energy, the best day of the best month and the weakest day of the weakest month (in terms of energy availability) were also chosen for simulation. Using the two reported significant wave heights and two dominant periods (swells and wind seas) for each simulation test case, 10-minute long irregular wave records were generated using a standard 2-parameter bimodal spectral formulation, as follows.

$$S(\omega) = \sum_{i=1}^2 \frac{131.5H_{si}^2}{T_{ei}^4\omega^5} \exp \left[-\frac{1054}{(T_{ei}\omega)^4} \right] \quad (4.29)$$

where the contributions of swell and wind seas are added together as shown in equation (4.29).

The wave surface elevation at (x, t) can be expressed as

$$\eta(x; t) = \sum_{n=1}^N \sum_{m=1}^M \Re \{ A(\omega_n, \theta_m) \exp [-i (k(\omega_n)x - \omega_n t + \vartheta_n)] \} \quad (4.30)$$

where,

$$A(\omega_n) = \sqrt{2S(\omega_n)\Delta\omega} \quad (4.31)$$

and ϑ_n is a random phase angle $\in [0, 2\pi]$, with $S(\omega_n)$ representing the spectral density value at ω_n . $N = 512$ was used in these calculations.

The buoy dimensions and the reaction frame dimensions for these time-domain simulations are as shown in Figures 4.3(a) – 4.3(c). Recall that it is the relative heave oscillation between the two bodies that is utilized for conversion, and that the instrument is housed within the framework supporting the reaction mass. Relative oscillations are constrained to be less than the total separation between the buoy and the reaction mass. To avoid iterative calculations and use of inequalities, the constraint is specified in terms of the buoy draft (i.e. $\alpha_r = nD_r$, where $n = 1, 2, 3, \dots$) so as to ensure that, (i) the swept-volume constraint is not exceeded, and (ii) the greatest relative oscillation amplitude allowed by the constraint can be utilized for power conversion. Results discussed here include the captured power variation for the best wave conditions each month, weakest wave conditions each month, hourly wave conditions on the best day of the best month, and hourly wave conditions on the weakest day of the weakest month. As mentioned earlier, the complete year’s data for 2015 was used to arrive at the chosen wave conditions. Finally, also included are results showing the maximum control force requirement in each case above, and the maximum displacement noted (i.e. relative displacement between the buoy and the reaction frame) for each case simulated.

4.5 Discussion

As indicated in section 4.6, the results discussed here span a range of wave conditions sampled from the wave data reported at the site of deployment. Recall that these results examine the performance with wave-by-wave near-optimal control. The discussion below compares power capture performance of the three geometries for the reaction frame (see section 4.2). The 2-disc reaction frame is referred to as the baseline geometry.

Figures 4.9 and 4.10 show that, as expected, best wave conditions vary over the year. In particular, in energy rich wave conditions, the significant wave heights can sometimes exceed 3m, while in weaker wave conditions, significant wave heights can be on the order of 0.2m. Therefore, the system hardware needs to be designed for a wide range of operating conditions, to enable power conversion in the largest as well as the smallest waves. In favorable wave conditions, 10-minute averages for converted power show that over 7 kW average power can be converted by allowing the maximum relative displacement between the bodies to exceed 1.5m. Note that the maximum control forces shown in Figures 4.9(b) and 4.10(b) are just the parts of the control force that require wave prediction (which includes the resistive load for power conversion and the reactive load for cancelling the effect of the frequency-variable added masses of the two bodies). The part not requiring prediction is the reactive force required to

cancel the contributions of the rest masses and the infinite-frequency added masses of the two bodies and the hydrostatic stiffness of the buoy. The total maximum control forces can exceed 300 kN in the very large waves. Figures 4.9(a) and 4.10(a) show that even in the months with overall weaker wave climates, close to 500 W can be converted during parts of a day.

Figures 4.11 and 4.12 for the least favorable wave conditions show that the 10-minute average power conversion enabled by the wave-by-wave near-optimal control can at times drop to less than 70W (10-minute average). The relative displacement amplitudes and control force magnitudes are also considerably smaller. Therefore, the control system enabling near-optimal performance appears necessary in periods of low wave activity at the present site. Further, given the large variance between the best and the worst wave conditions, the actuator/power take-off also needs to be capable of operating efficiently over a wide range of force, stroke, and power requirements.

The set of figures 4.6–4.7 compare performance with three geometries. It is found that the reaction mass with two hemispheres provides the best performance overall in terms of greater capture, but in general also requires a greater non-causal control force. On the other hand, the 2-sphere reaction mass provides comparable or slightly less efficient power capture performance but requires a smaller non-causal control force. Given the small size of the bodies, wave diffraction effects are small, and the Froude-Krylov force component (due to incident wave potential alone) dominates. It

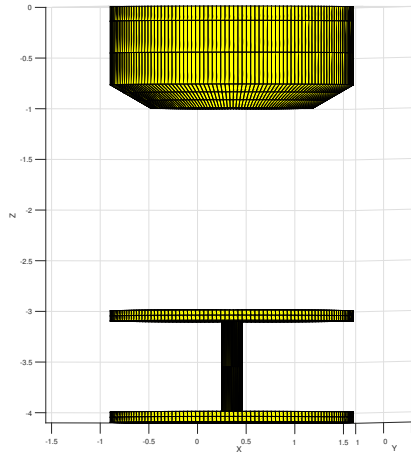
can intuitively be seen that the net downward component of the Froude-Krylov force is greater for the 2-hemisphere design (relative to the 2-disc body), thus providing better force compensation, and leading to greater effective radiation damping, which enables greater power conversion from the relative oscillation at impedance matching under oscillation constraints. The non-causal control force requirement is greater because the frequency-variable added mass is also greater. The opposite is true for the 2-sphere geometry, which is effectively situated lower than the 2-hemisphere geometry. The magnitude of the Froude-Krylov force acting on the 2-sphere body is thus somewhat smaller. In addition, the symmetry of the spheres provides no advantage relative to the 2-disc body in terms of the downward Froude-Krylov force. It is important, however, to compare the complete control forces (causal + non-causal) for a comparison with more immediate design relevance.

4.6 Conclusions

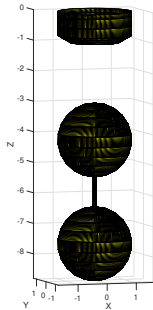
Buoys and moorings supporting ocean sensing instrumentation typically use solar, wind, or battery power despite the ready availability of a denser, more predictable energy source in the form of ocean surface waves. This is understandable, because current wave energy conversion technology is unable to meet the continuous power availability requirements of instruments through changing seasons unless the converters used are large enough. Often, this size requirement makes wave energy conversion

technology incompatible with buoy sizes common to oceanographic applications. The work discussed above investigated enhancements that may enable integration of wave power conversion hardware into ‘small’ oceanographic buoys (1.2m radius). The focus was on utilizing a 2-body axisymmetric system where the top body is the oceanographic buoy and the lower body is a framework that houses a science instrument.

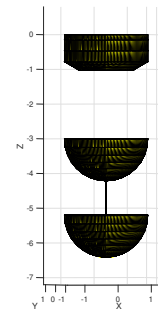
It was found that, with near-optimal wave-by-wave control, average power conversion ranged from 7kW to 70W in the best and the weakest wave conditions reported near the site of instrument deployment. Another observation that followed from the results so far was that the total energy converted from waves over the year 2015 significantly exceeded the total energy consumed by the instrument over the same period. Consequently, waves at the present site of operation alone would be sufficient as an energy source for instrument operation. However, since wave climate variability ranged from monthly to hourly time scales, it is evident that an energy storage system is required, so that a ‘guaranteed’ constant power supply can be maintained for continuous instrument operation. An added advantage of an energy storage system is expected to be an ability to enhance the overall economics of the system by optimizing the use of the large excess power generated in highly favorable wave conditions. Work on this goal is currently underway and will be reported on separately. Further, it is also important that the control as proposed be evaluated in experimental testing.



(a) A standard oceanographic buoy with original two-discs shape design of reaction frame, this figure shows input mesh file of WAMIT. A rigid connect is added between two discs to help WAMIT recognize two parts of WEC system: buoy and reaction frame. Radius of buoy and discs are $1.2m$. Thickness of discs are $0.1m$. Equivalent draft of buoy is $1m$. Spacing between bottom surface of buoy and top surface of discs is $2m$.

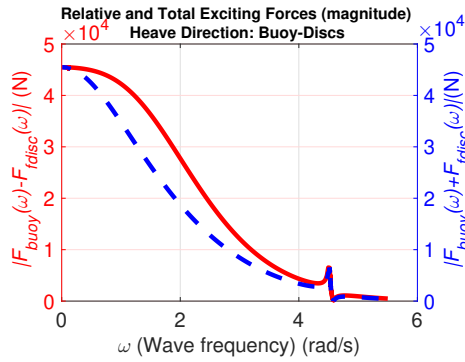


(b) Buoy with original buoy and two-spheres shape design of reaction frame, this figure shows input mesh file of WAMIT. Radius of spheres are $1.2m$. Distance between buoy and top sphere is $2m$. Distance between two spheres is $1m$.

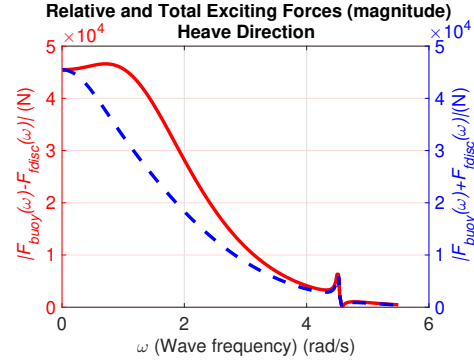


(c) Buoy with original buoy and two-hemispheres shape design of reaction frame, this figure shows input mesh file of WAMIT. Radius of hemispheres is $1.2m$, distance between top hemisphere and buoy is $2m$, distance between two hemispheres is $1m$.

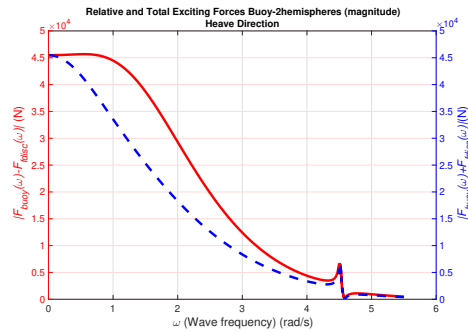
Figure 4.3



(a) Dashed line is Total exciting force, solid line is Relative exciting force. Relative exciting force larger than total exciting force leads to total movement less than relative movement.

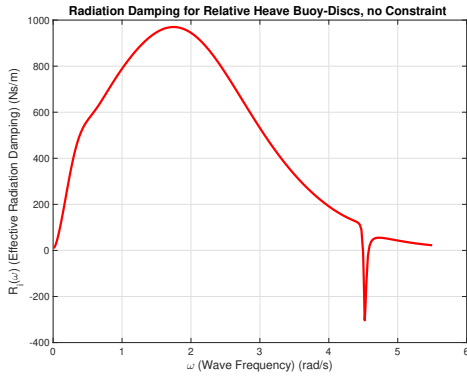


(b) Dashed line is Total exciting force, solid line is Relative exciting force. Two spheres design provide large exciting force for reaction frame. Peak of solid line means largest difference between relative and total exciting force at low frequency.

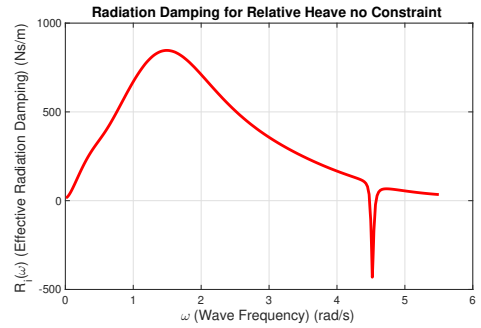


(c) Hemispheres design for reaction frame provide highest average difference between relative and total exciting force, through peak difference value is less than spheres design.

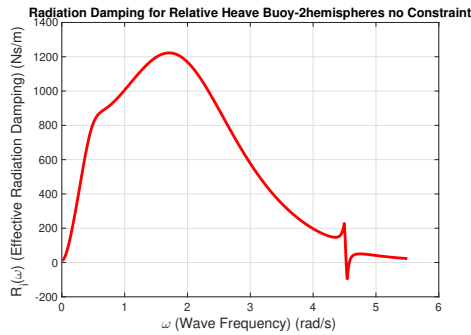
Figure 4.4



(a) Reaction frame with a flat top surface shows a second peak at low frequency.

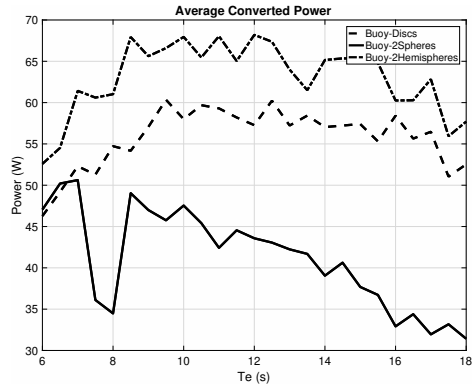


(b) Reaction Frame with deeper submerged design shows lower value in radiation damping then original design.

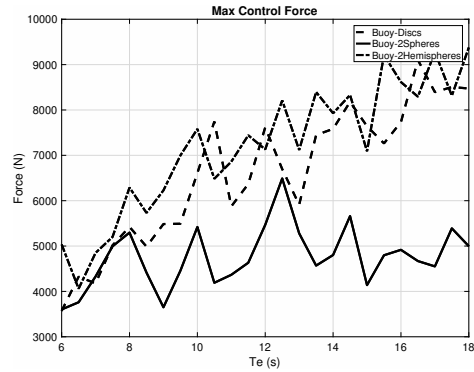


(c) Larger design of reaction frame give higher value of effective radiation damping, flat top surface of reaction frame give high second peak value at low frequency.

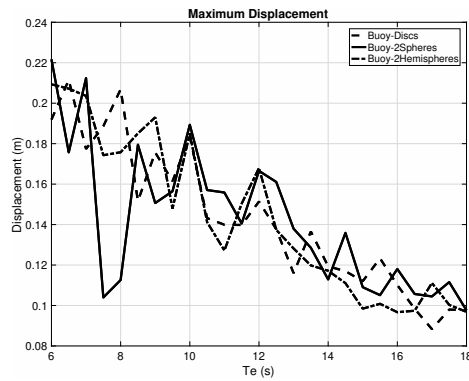
Figure 4.5: Effective Radiation Damping calculated with $H_{s1} = 0.3m$, $H_{s2} = 0.2m$, $T_{e1} = 9s$, $T_{e2} = 4.5s$, with out motion constraint.



(a)



(b)



(c)

Figure 4.6: Figure 4.6(a) shows converted power by Buoy-Discs design, Buoy-Spheres design and Buoy-Hemispheres design constraint $\alpha_r = 2.5$. Dashed line is Buoy-Discs, Solid line is Buoy-Spheres, Dash-Dot line is Buoy-Hemispheres. This figure use Significant Wave height $H_s = 0.2m$.

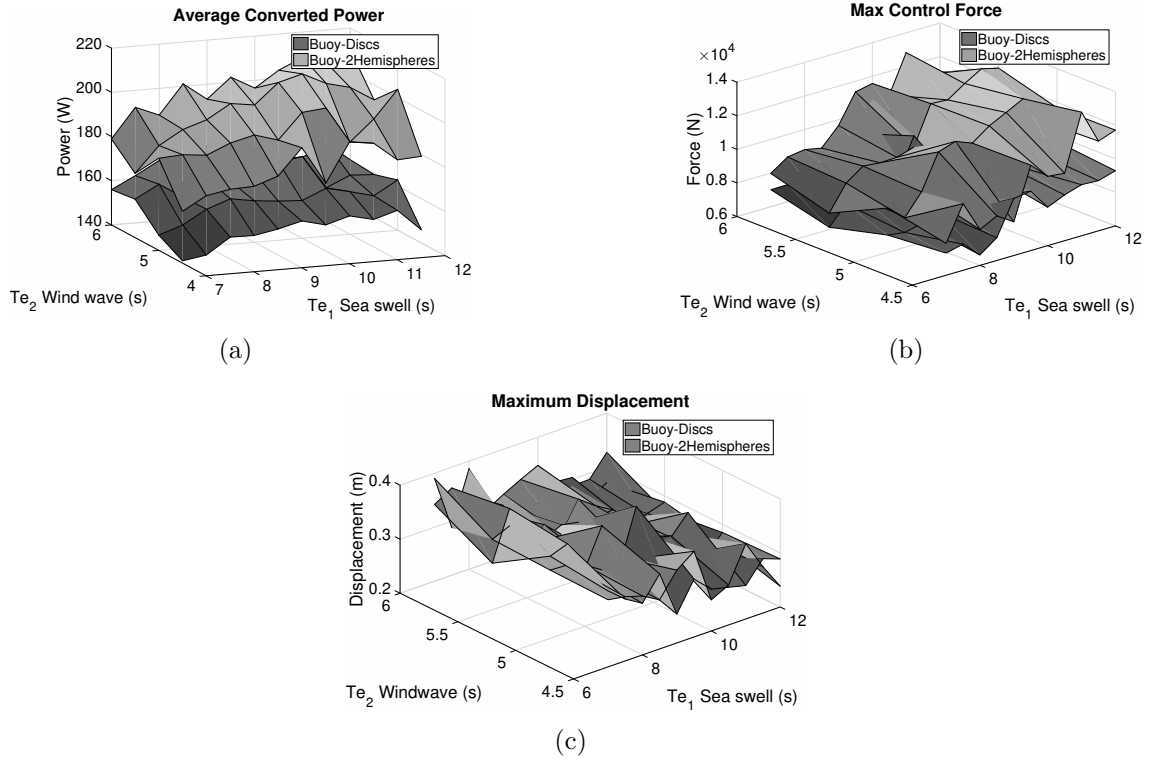


Figure 4.7: This figure shows converted power result (4.7(a)) from $H_{s1} = 0.3m, H_{s2} = 0.2m$, constraint $\alpha_r = 2.5$, Buoy-Hemispheres design have higher converted power over T_{e1}, T_{e2} spacing.

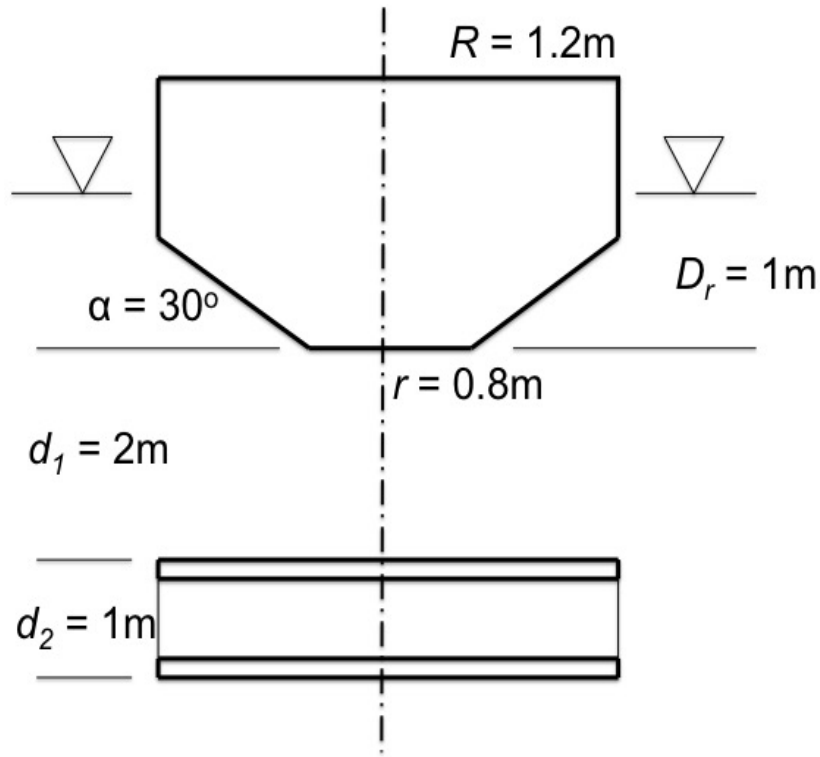
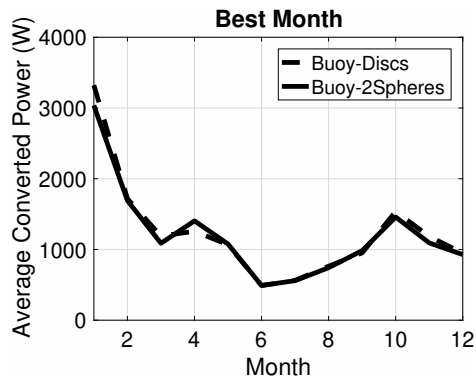
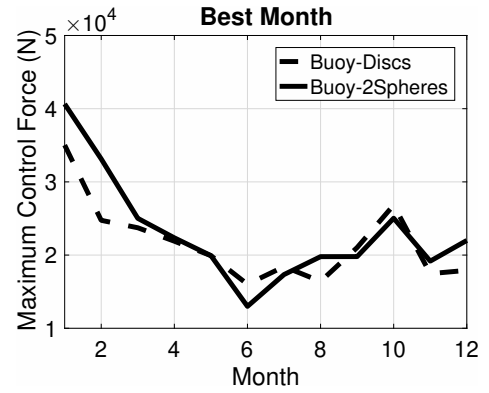


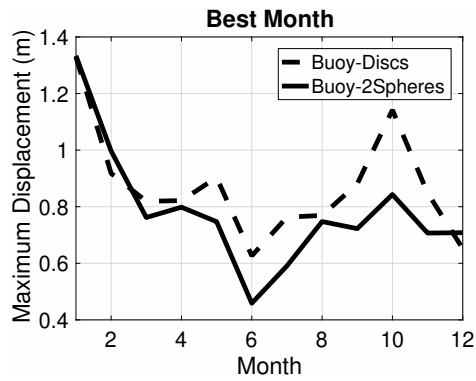
Figure 4.8: The heaving axisymmetric 2-body device used in this work. Relative oscillation is used for energy conversion using a linear generator or hydraulic cylinder type power take-off mechanism/actuator, which is assumed to be linear and ideal (i.e. lossless). The figure shows the ‘starting/baseline’ geometry for the submerged instrument frame comprised of two circular discs held together by a central strut (not shown). The power take-off also applies the required control force in this work, though in practice it may be advantageous to use two actuators, one for power take-off, and one for reactive forcing.



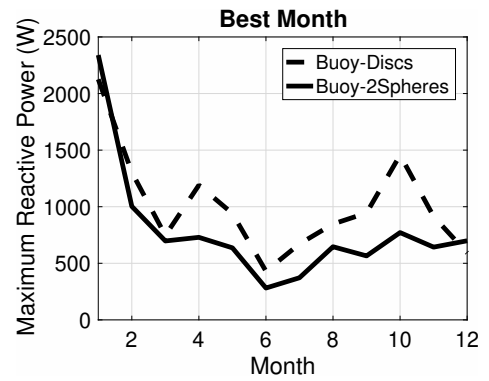
(a)



(b)



(c)



(d)

Figure 4.9: Calculation based on yearly data from [1], constraint $\alpha_r = 1$, is applied to maintain in feasible relative displacement range. Dashed line is Buoy-Discs, Solid line is Buoy-Spheres. Best wave climate data of each month is collected to run this calculation. 2-spheres design of reaction frame shows slightly smaller control force.

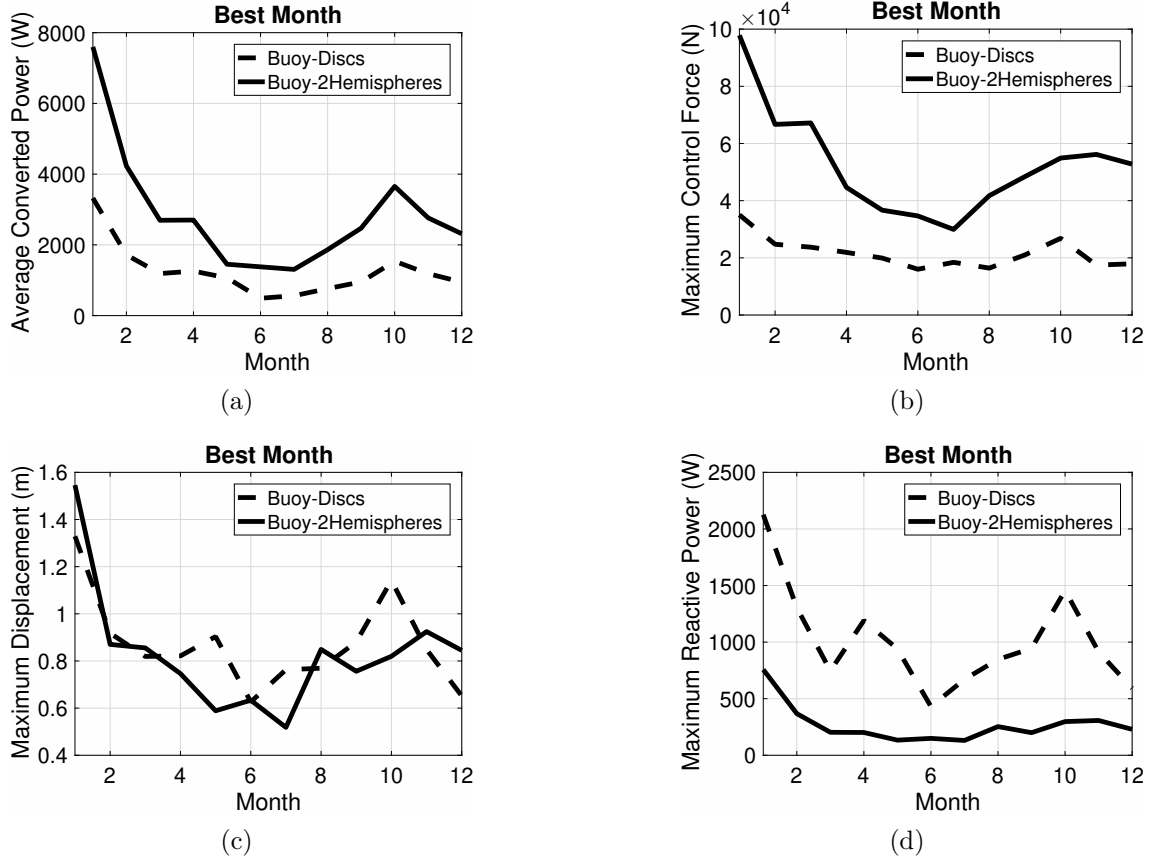


Figure 4.10: Calculation based on yearly data from [1], constraint $\alpha_r = 1$, is applied to maintain in feasible relative displacement range. Dashed line is Buoy-Discs, Solid line is Buoy-Hemispheres. Best wave climate data of each month is collected to run this calculation. 2-hemispheres design of reaction frame shows greater energy conversion, meanwhile control force increase significantly. Simulation results of Buoy-Discs design consistent with Figure 4.9.

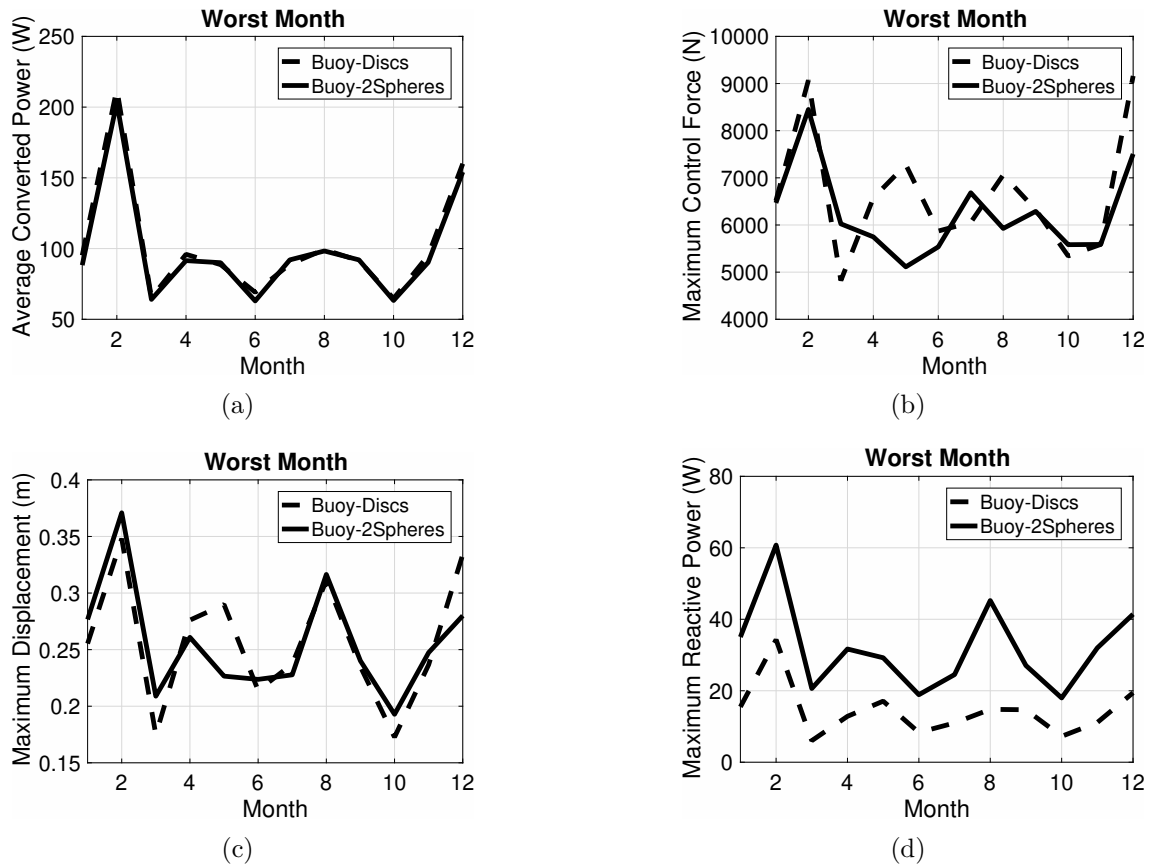


Figure 4.11: Calculation based on yearly data from [1], constraint $\alpha_r = 2.5$, is applied to keep energy capture level. Dashed line is Buoy-Discs, Solid line is Buoy-Spheres. Worst wave climate data of each month is collected to run this calculation. 2-spheres design of reaction frame shows smaller Maximum value of reactive power. Contribute to easy energy storage design.

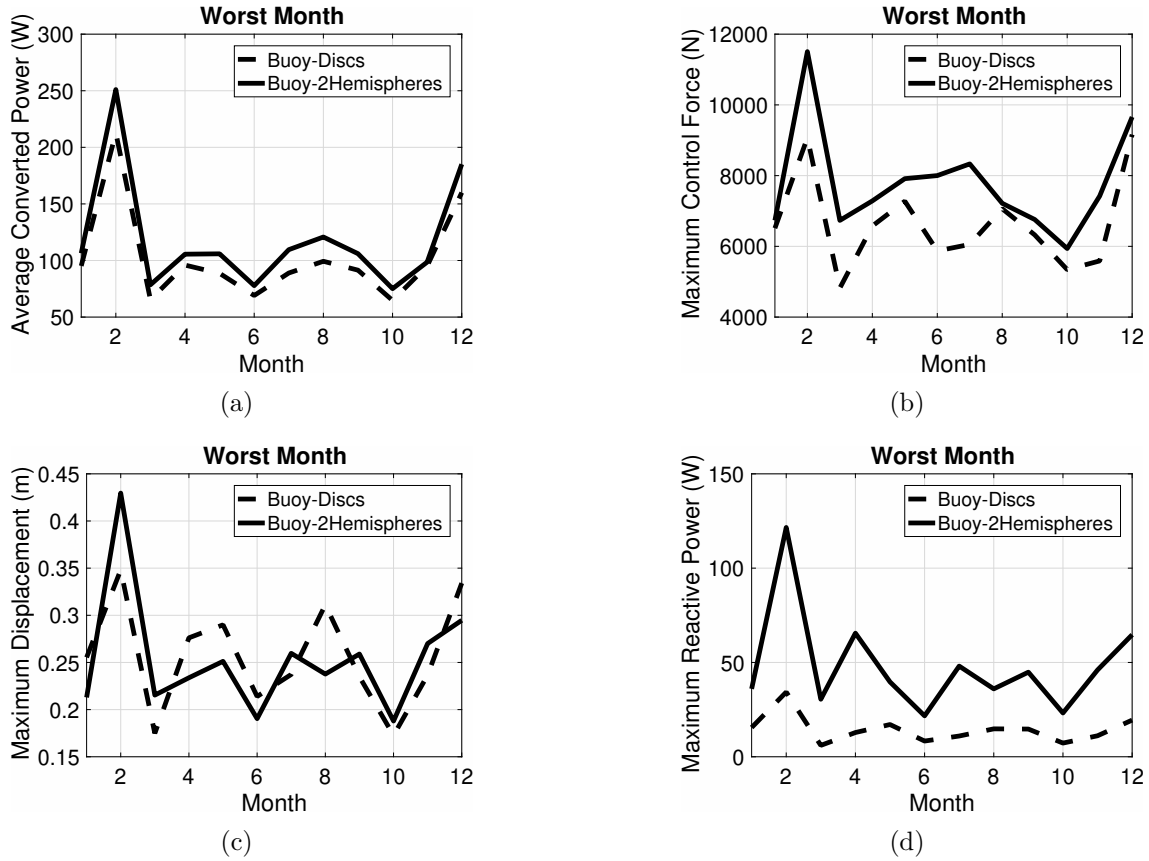


Figure 4.12: Calculation based on yearly data from [1], constraint $\alpha_r = 2.5$, is applied to maintain in feasible relative displacement range. Dashed line is Buoy-Discs, Solid line is Buoy-Hemispheres. Worst wave climate data of each month is collected to run this calculation. 2-hemispheres design of reaction frame still shows greater energy conversion, control force with smaller constraint α_r shows lower value compared to original design. Simulation results of Buoy-Discs design consistent with Figure 4.11.

Chapter 5

Optimization of Shape and Control of non-linear Wave Energy Converters Using Genetic Algorithms

This chapter presents an optimization approach to design axisymmetric wave energy converters (WECs) based on a non-linear hydrodynamic model. This chapter shows optimal non-linear shapes of buoy can be generated by combing basic shapes in an optimal sense.

This chapter presents a Genetic Algorithm optimization approach to design axisymmetric WECs based on a non-linear hydrodynamic model. The proposed optimization tool optimize the buoy shape and the control simultaneously. The complex buoy shape provides the non-linearity of the simulation results from the non-linear Froude-Krylov analytical model. The proposed optimization tool generates the optimal solution based on a cost function focus on the evaluation of the energy conversion.

5.1 Optimization of the Buoy Shape

There are several categories of energy extraction concepts utilising heave motion of a single floating body[25], based on the interaction between the ocean wave and the WEC device. The oscillating body design [98], such as point absorbers and attenuators. The oscillating water column design [12]. And the over-topping converters [47], [99].

This chapter focus on the oscillating body design, specifically, the axisymmetric heave-oscillating body design. Benefits of choosing axisymmetric body design are: only one direction of the incoming exciting wave is needed to be considered, convenience of the computation of an analytical solution for the non-linear Froude-Krylov force.

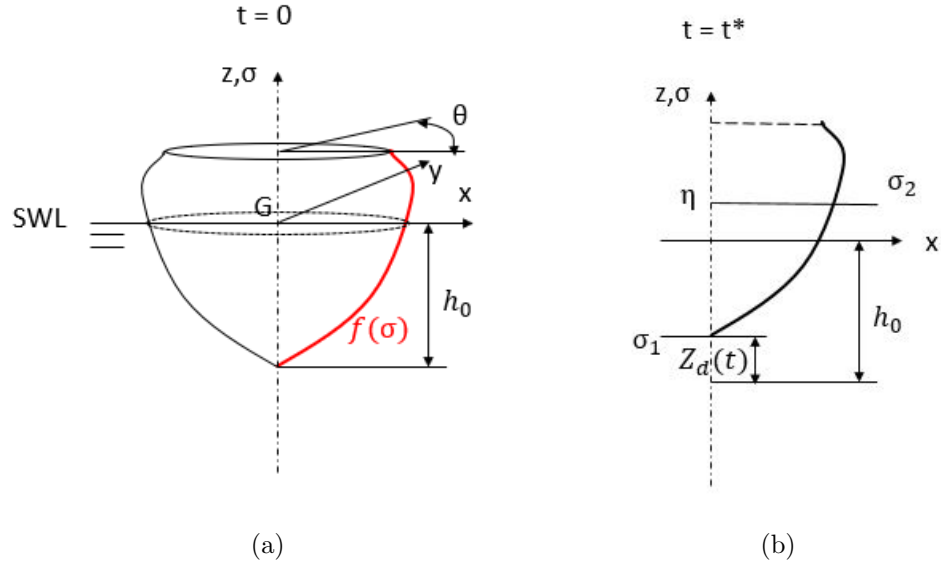


Figure 5.1: The surface of an axisymmetric heaving device with generic profile $f(\sigma)$. 2.1(a) shows the equilibrium position at the still water level (SWL) and the draft h_0 ; 2.1(b) shows the free elevation η and the device displacement z_d after a time t^* . The pressure is integrated over the wetted surface between σ_1 (the bottom point of the buoy) and σ_2 (the wave elevation at time t).

Giorgi developed a format to describe an axisymmetric geometry with a fixed vertical axis as in Eqn.(5.1) [19].

As shown in Fig.5.1, the surface of an axisymmetric body can be described in parametric cylindrical coordinates $[\sigma, \theta]$ as generic profile $f(\sigma)$, where σ is the coordinate of a point with respect to z axis, θ is the angle oriented from the positive x axis

direction to the position vector of a point:

$$\begin{aligned}
 x(\sigma, \theta) &= f(\sigma) \cos \theta \\
 y(\sigma, \theta) &= f(\sigma) \sin \theta \\
 z(\sigma, \theta) &= \sigma \\
 \theta &\in [0, 2\pi) \cap \sigma \in [\sigma_1, \sigma_2]
 \end{aligned} \tag{5.1}$$

Based on the superposition of integral, the total Froude-Krylov force on heaving axis acting on a surface S can be decomposed into smaller forces acting on corresponding areas in Eqn.(5.2).

$$\begin{aligned}
 F_{FK} &= \iint_S P \vec{n} dS \\
 &= \int_0^{2\pi} \int_{\sigma_1}^{\sigma_2} P f'(\sigma) f(\sigma) d\sigma d\theta \\
 &= \int_0^{2\pi} \left[\sum_{i=1}^{N-1} \int_{\hat{\sigma}_i}^{\hat{\sigma}_{i+1}} P f'(\sigma) f(\sigma) d\sigma \right] d\theta \\
 &= \sum_{i=1}^{N-1} \int_0^{2\pi} \int_{\hat{\sigma}_i}^{\hat{\sigma}_{i+1}} P f'(\sigma) f(\sigma) d\sigma d\theta
 \end{aligned} \tag{5.2}$$

where $\hat{\sigma}_1 = \sigma_1, \hat{\sigma}_N = \sigma_2$, P is the pressure on the wetted surface. Previously, a simplified analytical equation of the non-linear Froude-Krylov force can be implement only when the buoy shape is one of the four categories in Fig.5.2. From Eqn.(5.2), the

Froude-Krylov force of a complex buoy shape now can be computed using simplified analytical equations, if the complex buoy shape can be decomposed into sub-section shapes from the four categories in Fig.5.2.

Complex WEC shapes, which can be decomposed into several simple shape elements, were tested in the non-linear Froude-Krylov model. Decomposition of the whole shape generate several section elements, each section element S_i can be described by just two variables α_i and h_i , as shown in Fig.5.2.

The start point of the outline is designed to be the bottom center of the shape, to generate the total immersed mesh of the buoy. Two design variables α_i and h_i will define the coordinate of the end point for each section. With the end point defined and the start point inherited from the previous section, outline points of the new section can be defined corresponding to the section type.

The optimization process is conducted with Genetic Algorithm (GA)[100], to better invest the energy output of different combinations of the element shapes [101]. To lower the computational cost, the size of of design variables of each section element is reduce to 2 using the geometry define method as shown in Fig.5.2.

In standard Genetic Algorithms, the variables of the optimization problem are coded into chromosomes. Each chromosome represents a solution and consists of the variables that are coded as genes [102]. The objective of optimization determines the

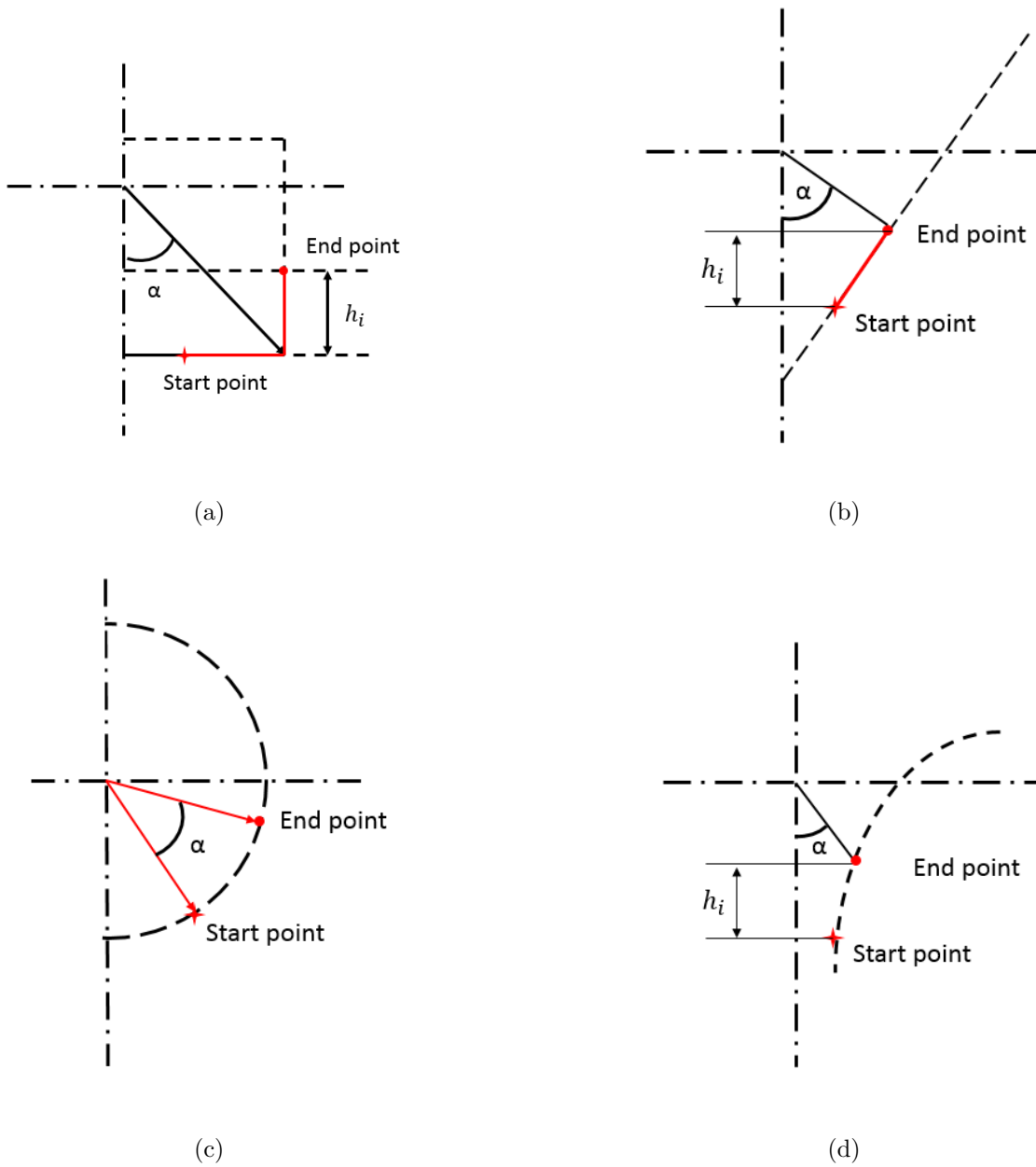


Figure 5.2: Each section i of decomposed shape can be described by two variables α_i and h_i or less.

fitness of the solution.

In this chapter, a chromosomes is defined in the following format as shown in

Eqn.(5.3):

$$X_i = [N_i, S_{ty1}, \dots, S_{tyN}, X_1(1, 2), \dots, X_N(1, 2)] \quad (5.3)$$

Definition of each element in the chromosome is: N_i , the number of active section elements. Meaning how many sections can be decomposed from the total shape. $N_i \in [1, N]$ where N is the maximum number of section elements, and N_i is an integer.

S_{tyi} is the geometry type of the i_{th} section. $S_{tyi} = 1$ is a cylindrical shape, $S_{tyi} = 2$ is an oblique line, $S_{tyi} = 3$ is an arc of circumference, and $S_{tyi} = 4$ is an exponential profile.

$X_i(1, 2)$ are the design variables of each section, $X_i(1) = \alpha_i, X_i(2) = h_i$. Where $\alpha_i \in (0, 90^\circ)$, $h_i \in (0, h_C)$ and defined in Fig.5.2. h_C is the maximum height of each shape section. Previously, the profile $f(\theta)$ of different shapes contains different size of the define variables. The cylindrical profile needed the radius, the oblique profile needed the start point coordinates and the slope etc. Using shape defining variables from previous work would require extension of the chromosome size, which leaded to non-efficient usage of gene information. This chapter proposed a compact GA chromosome design as Eqn.(5.3) to reduce the total computation time of the optimization for complex shape design and control design of a non-linear WEC device.

The manual tuning of GA population is implemented as the niching method [103]. Specifically, in the variable section size case. As the section size increase, the population size in each generation increase accordingly. Such increase in generation size leads to local optimal solutions in the GA process, which add more computation time to solve the global optimization problem of design the non-linear buoy and non-linear control. By niching method, alternatively, adding penalty weight to best solutions of each 10 generations. The computation time reduce by 10% to converge to the global optimal solution, as the result of avoiding local optimal solutions.

5.2 Optimization of the Control

Several reasons such as nonuniform buoy shapes and/or complex input wave frequencies will contribute to the non-linearity of the hydrodynamic model. The non-linear effects also arise from wave-buoy interactions and non-linear incoming waves. A non-linear control algorithm is needed for such non-linear WEC designs to optimize the energy conversion [104].

Abdelkhalik and Darani [100] in Michigan Technological University (MTU) developed a non-linear controller to improve energy extraction in non-linear wave environment.

Control force was constructed as Eqn.(5.4):

$$F_{PTO} = \sum_{i=1}^N a_i Z_i + \sum_{j=1}^M b_j |\dot{Z}^j| \text{sign}(\dot{Z}) \quad (5.4)$$

Where F_{PTO} is the non-linear control force, a_i and b_j are the constant control coefficients, N and M are the number of terms contributing towards the total non-linear control force. This control algorithm shows improvement in the energy extraction compared to the traditional linear resistive loading control method [105].

5.3 Numerical results

Optimization of non-linear buoy shape and non-linear control were conducted. Optimal solution of buoy shape designs and controls are show below. The hydrodynamic coefficients of the non-linear shape and of the baseline cylinder buoy were computed using boundary element solver Nemoh. The input wave profile is selected from a Bertschneider spectrum with a significant wave height of $H_s = 0.8$ m and peak period of $T_p = 8$ seconds. Total of 34 frequencies were used to construct the complex input wave profile, as shown in Fig 5.3. The mass difference between the non-linear optimal solution and the baseline cylindrical buoy is less then 1 %. And the shape of the baseline case is optimized to achieve optimal energy extraction under resistive linear control, motion constraint is not considered in the baseline cylindrical simulation.

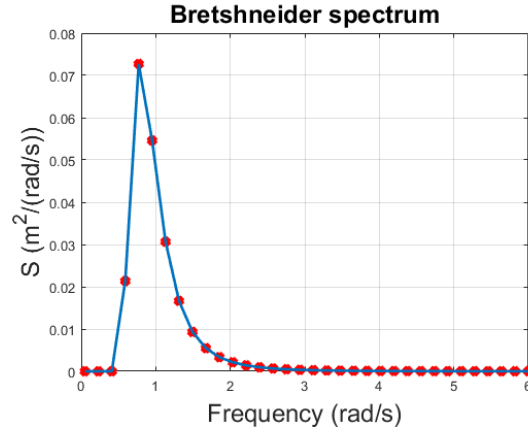


Figure 5.3: Bretshneider spectrum used in the time domain simulation. The spectrum is with $H_s = 0.8m$ and $T_p = 10s$.

A simple format of non-linear control is select from Eqn.(5.4). Assuming $N = 0$, $M = 3$ and $b_1 = a, b_2 = 0, b_3 = b$, to generate the resistive control force, as Eqn.(5.5).

$$F_{PTO} = a(\dot{z}) + b(\dot{z})^3 \quad (5.5)$$

5.3.1 Test Case Without Control Force Constraint

For this test, the size of section elements is constrained to be a integer between 3&5. A range of mass from 380kg to 500kg was selected to show case the ability of GA to generate stochastic solutions. The shape and control coefficients were optimized to maximize the ratio of the steady state power over the mass of the buoy. Alternatively, to maximize the steady state power per unit mass. Material cost was not considered

here, as leveled cost function would be more efficient to investigate construction costs in the future. The optimization problem can be expressed as follows:

$$\begin{aligned} \text{Maximize : } F_{cost}(X, a, b) &= p_{average}/m \\ &= \left[\int_{T_{steady}}^{T_{final}} p(t) dt \right] / (mT) \end{aligned} \quad (5.6)$$

Where, X is the chromosome in Eqn.(5.3), a and b are control coefficients in Eqn.(5.5), $p(t) = -F_{PTO}(t)\dot{Z}(t)$ is the power at time t . $T = T_{final} - T_{steady}$ is the time window of energy extraction performance evaluation, $p_{average}$ is the average power in the evaluation time window.

Simulation results shown as Fig.5.4, Fig.5.5, Fig.5.6, Fig.5.7 and Fig.5.8. This chapter focus on axisymmetric heaving buoy design, as shown in Fig.5.4(a). With a multi-frequency wave profile input, the non-linear shape using non-linear control shows better energy extraction result. Position response and velocity response of the non-linear shape design show more frequency response components. The large control is the result of the non-linear term $b(\dot{z})^3$ in Eqn.5.5, as the linear damping term a in Eqn.5.5 is comparable to the resistive control coefficient of the baseline case.

The new shape has a mass of $401kg$, similar to the $399kg$ baseline cylindrical buoy. The energy ratio of the new shape in steady state was $18W/kg$. However, the power quality was not good as the ratio between the mean and maximum power was smaller than the baseline design. As a result of the large resistive control force, as shown in

Fig.5.7, the oscillating motion of the buoy was damped with respect to the baseline cylindrical buoy. The results show that the non-linear shape design requires longer time to reach optimal operation condition.

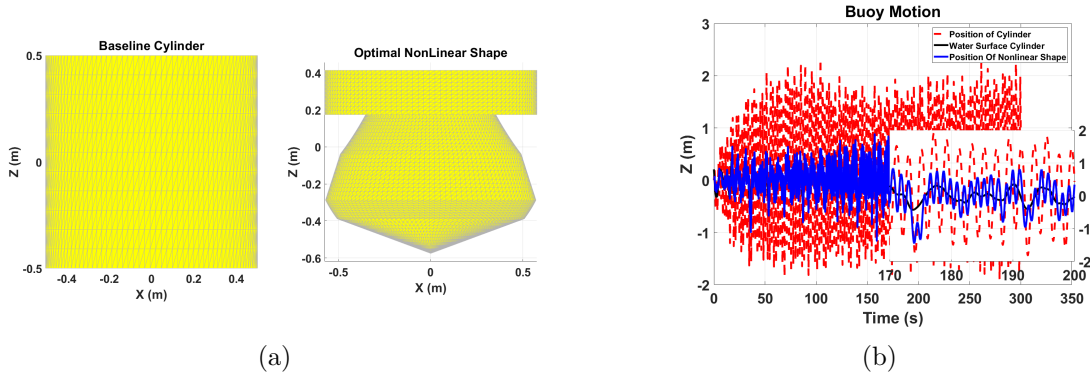


Figure 5.4: Shape comparison between the optimal solution without control constraint and the baseline cylindrical WEC. And motion comparison between both cases in time domain simulation.

5.3.2 Test Case With Control Force Constraint

For this test, initial setting keep constant with respect to the previous test case. Additional penalty term was added to the cost function, allowing soft-constraint in the control force. The optimization problem can be expressed as follows:

$$\begin{aligned}
 \text{Maximize : } F_{cost}(X, a, b) &= p_{average}/m - S_c F_{PTO_{max}} \\
 &= \left[\int_{T_{steady}}^{T_{final}} p(t) dt \right] / (mT) - S_c F_{PTO_{max}}
 \end{aligned} \tag{5.7}$$

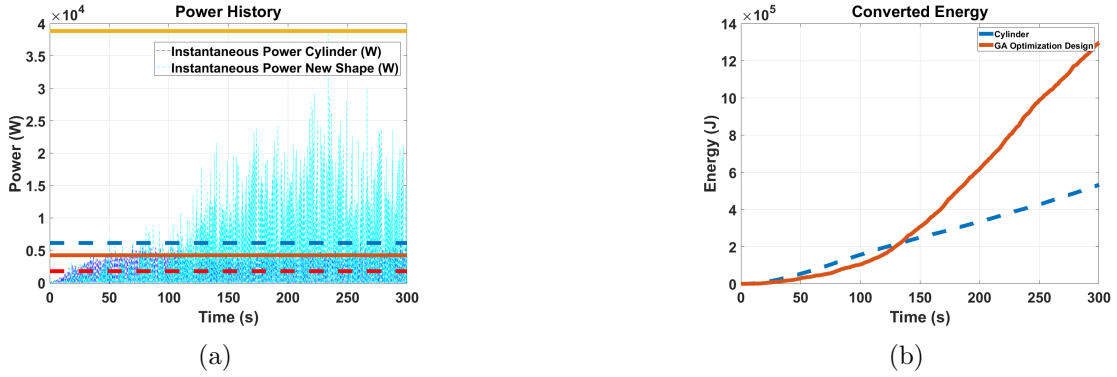


Figure 5.5: Time domain simulation results of the optimal solution without control constraint and the baseline cylindrical WEC using the complex wave profile as input, in terms of instantaneous power, mean power, maximum power, and total converted energy. Solid horizontal lines in Fig.5.5(a) represent the maximum power and the average power of the optimal non-linear shape design, dashed horizontal lines in Fig.5.5(a) represent the maximum power and the average power of the baseline shape.

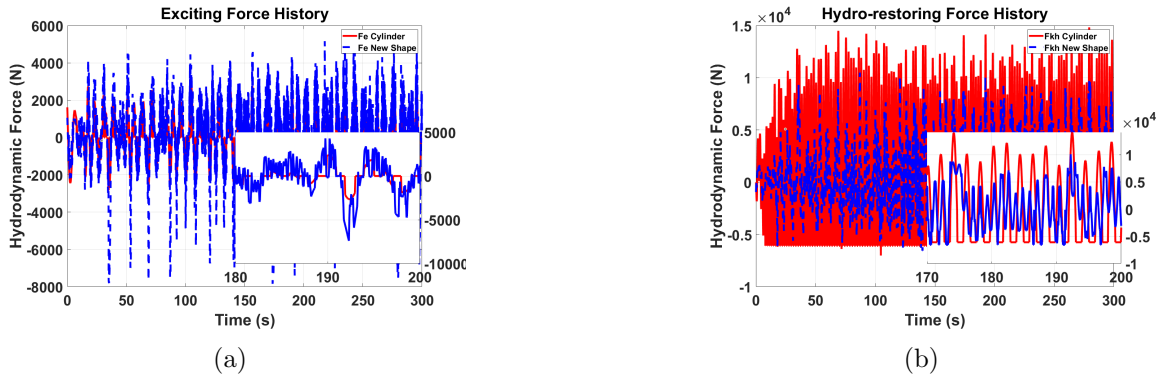


Figure 5.6: Different hydrodynamic force history for the optimal solution without control constraint and the baseline WEC in the time domain simulation.

Where, S_c is the penalty weight factor, which has $W/(kgN)$ as unit. $F_{PTO_{max}}$ is the maximum absolute value of the force in the evaluation time window. Increase S_c will leads to higher constraint on the control force.

Simulation results shown as Fig.5.9, Fig.5.10, Fig.5.11, Fig.5.12 and Fig.5.13. The

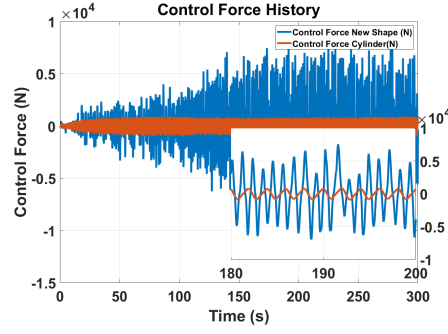


Figure 5.7: Different control force history for the optimal solution without control constraint and the baseline WEC in the time domain simulation.

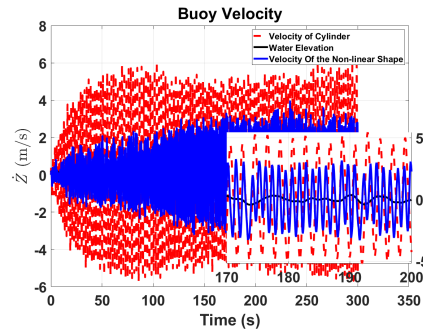


Figure 5.8: Different velocity history for the optimal solution without control constraint and the baseline WEC in the time domain simulation.

new shape has a mass of $397kg$, similar to the $399kg$ baseline cylindrical buoy. The energy ratio of the new shape in steady state was $5.94W/kg$. Compare the power results of the constrained control force case and the non-constrained control force case, the ration between maximum and mean power is lower in the constrained control force case.

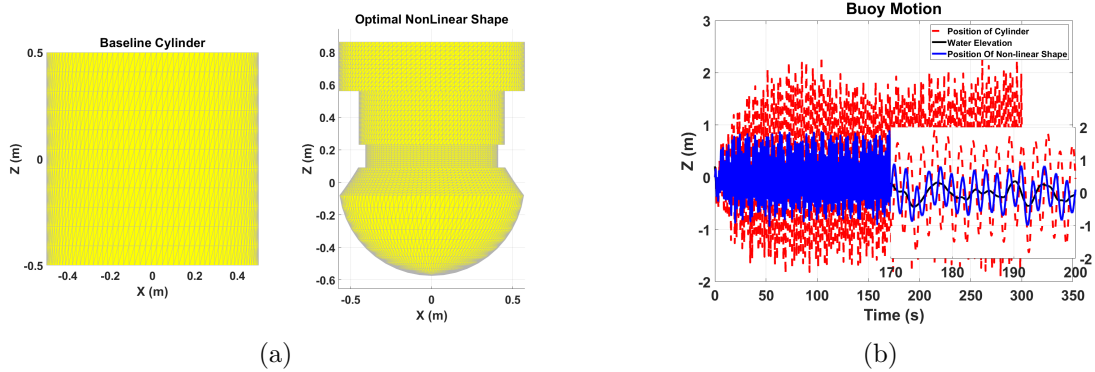


Figure 5.9: Shape comparison between the optimal solution with control constraint and the baseline cylindrical WEC. And motion comparison between both cases in time domain simulation.

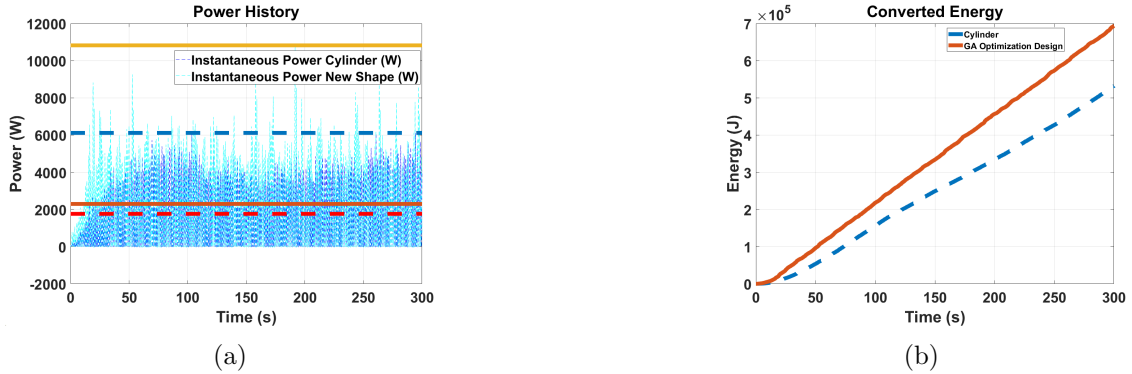


Figure 5.10: Time domain simulation results of the optimal solution with control constraint and the baseline cylindrical WEC using the complex wave profile as input, in terms of instantaneous power, mean power, maximum power, and total converted energy. Solid horizontal lines in Fig.5.5(a) represent the maximum power and the average power of the optimal non-linear shape design, dashed horizontal lines in Fig.5.5(a) represent the maximum power and the average power of the baseline shape.

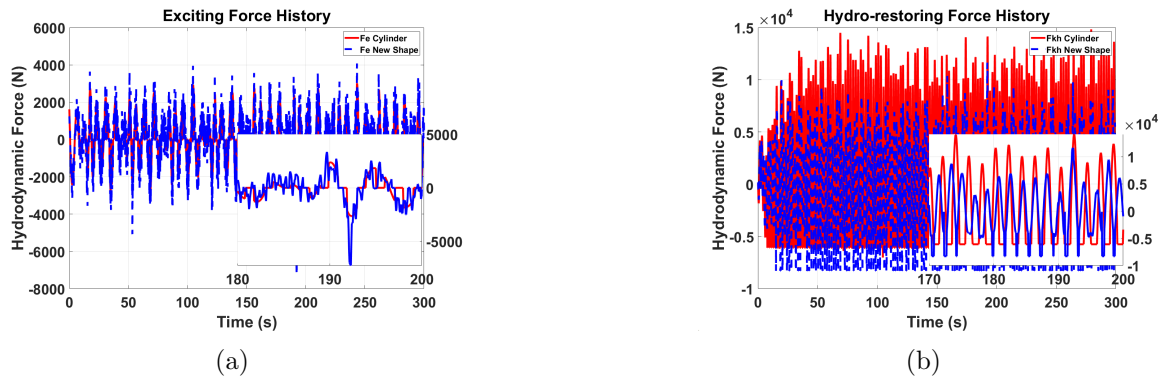


Figure 5.11: Different hydrodynamic force history for the optimal solution with control constraint and the baseline WEC in the time domain simulation.

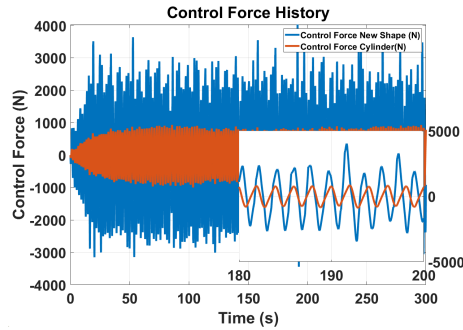


Figure 5.12: Different control force history for the optimal solution with control constraint and the baseline WEC in the time domain simulation.

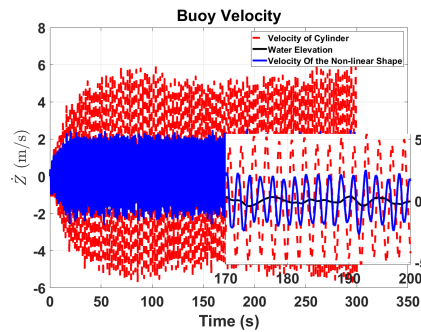


Figure 5.13: Different velocity history for the optimal solution with control constraint and the baseline WEC in the time domain simulation.

Chapter 6

Conclusion

Three objectives are completed in this thesis. A multi-resonant wide band controller that decomposes the WEC problem into sub-problems; for each sub-problem an independent single-frequency controller is designed. Different shape designs of ‘small’ 2-body WEC (1.2 radius) were investigated, showing enhancements in wave energy conversion. A genetic algorithm optimization tool is developed to simultaneously optimize the shape and control of a non-linear single body point absorber.

In chapter 3, a multi-resonant wide band controller was presented. One advantage of this approach is the possibility to optimize each sub-problem controller independently. The proposed feedback control demonstrated actual time-domain realization of the

multi-frequency complex conjugate control design. The proposed control is a feedback strategy that requires only measurements of the buoy position and velocity. No knowledge of excitation force, wave measurements, nor wave prediction is needed. The feedback signal processing is carried out in section 3.3 using Fast Fourier Transform with Hanning windows and optimization of amplitudes and phases. Numerical simulation for a sphere buoy shows that the proposed time-domain Proportional Derivative feedback control generates the frequency-domain complex conjugate control solution. Given that the output signal is decomposed into very simple yet generates energy similar to the complex conjugate control. One limitation of this method is not including constraints on the motion amplitude; hence the method is applicable only to cases of small excitation force.

Chapter 4 investigated enhancements that may enable integration of wave power conversion hardware into ‘small’ oceanographic buoys (1.2m radius). The focus was on utilizing a 2-body axisymmetric system where the top body is the oceanographic buoy and the lower body is a framework that houses a science instrument. It was found that, with near-optimal wave-by-wave control, average power conversion ranged from 7kW to 70W in the best and the weakest wave conditions reported near the site of instrument deployment. Another observation that followed from the results so far was that the total energy converted from waves over the year 2015 significantly exceeded the total energy consumed by the instrument over the same period. Consequently, waves at the present site of operation alone would be sufficient as an energy source for

instrument operation. However, since wave climate variability ranged from monthly to hourly time scales, it is evident that an energy storage system is required, so that a ‘guaranteed’ constant power supply can be maintained for continuous instrument operation. An added advantage of an energy storage system is expected to be an ability to enhance the overall economics of the system by optimizing the use of the large excess power generated in highly favorable wave conditions.

In chapter 5, optimization of the buoy shape of non-linear axisymmetric WECs along with the non-linear control were conducted using a GA optimization tool. Complex shape designs of non-linear Froude-Krylov model can be decomposed into basic shape elements, the total Froude-Krylov force acting on the complex buoy can be computed in terms of the pressure integration over all shape elements. The optimization tool is tested using a Bretschneider spectrum wave input. The main findings of chapter 5 are: First, a new tool is developed to optimize the buoy shapes of WECs under a non-linear hydrodynamic model. Second, WECs with non-linear buoy shapes can be more efficient in energy extraction than that with traditional linear buoy shapes. Third, the non-linear Froude-Krylov force of a complex WEC buoy can be evaluated analytically. Finally, it is noted that the objective function in the optimization tool can be modified to achieve designs that are suitable for other objectives.

References

- [1] MVCO, 2017, martha’s Vineyard Coastal Observatory; www.whoi.edu/mvco.

- [2] J. Song, O. Abdelkhalik, R. Robinett, G. Bacelli, D. Wilson, and U. Korde, “Multi-resonant feedback control of heave wave energy converters,” Ocean Engineering, vol. 127, pp. 269 – 278, 2016. [Online]. Available: <http://www.sciencedirect.com/science/article/pii/S0029801816304346>

- [3] U. A. Korde, J. Song, R. D. Robinett, and O. O. Abdelkhalik, “Hydrodynamic considerations in near-optimal control of a small wave energy converter for ocean measurement applications,” Marine Technology Society Journal, vol. 51, no. 6, pp. 44–57, 2017.

- [4] O. Abdelkhalik, J. Song, R. Robinett, G. Bacelli, D. Wilson, and U. Korde, “Feedback control of wave energy converters,” in Asian Wave and Tidal Energy Conference (AWTEC 2016), Marina Bay Sands, Singabore, 2016, pp. 258–261.

- [5] J. Song, O. O. Abdelkhalik, and S. Darani, “Optimization of shape and control

- of nonlinear wave energy converters,” in the 13th European Wave and Tidal Energy Conference, Naples, Italy, 2019, pp. 1700–1–6.
- [6] H. Titah-Benbouzid and M. Benbouzid, “Ocean wave energy extraction: Up-to-date technologies review and evaluation,” in 2014 International Power Electronics and Application Conference and Exposition, Nov 2014, pp. 338–342.
- [7] e. a. Janet L. Sawin, in REN21 Annual Report 2017, Sep 2017. [Online]. Available: <http://www.ren21.net/about-ren21/annual-reports/>
- [8] H. Polinder and M. Scuotto, “Wave energy converters and their impact on power systems,” in 2005 International Conference on Future Power Systems, Nov 2005, pp. 9 pp.–9.
- [9] H. Eidsmoen, “On theory and simulation of heaving-buoy wave energy converters with control,” Ph.D. dissertation, Norwegian University of Science and Technology, Trondheim, Norway, 1996.
- [10] B. M. Count, “Wave power – a problem searching for a solution,” in Power from Sea Waves, B. M. Count, Ed. Academic Press, London, 1980, pp. 11–27.
- [11] C. J. Garrison, “Hydrodynamic interaction of waves with a large displacement floating body,” Naval Postgraduate School, Monterey, CA, Tech. Rep., August 1977, nPS–69GM77091.

- [12] M. Hsieh, I. . Lin, D. G. Dorrell, M. Hsieh, and C. Lin, “Development of a wave energy converter using a two chamber oscillating water column,” IEEE Transactions on Sustainable Energy, vol. 3, no. 3, pp. 482–497, July 2012.
- [13] M. E. McCormick, Ocean Wave Energy Conversion. John Wiley and Sons, NY, 1981, reissued with revisions, 2007, Dover, NY.
- [14] T. Bjarte-Larsson and J. Falnes, “Laboratory experiment on heaving body with hydraulic power take off and latching control,” Ocean Engineering, vol. 33, pp. 847–877, 2006.
- [15] U. A. Korde, “Performance of two 2-body heaving axisymmetric wave energy converters under control in irregular waves,” in Proc. 11th European Wave and Tidal Energy Conference (EWTEC), September 2015.
- [16] U. A. Korde, “Development of a reactive control apparatus for a fixed two-dimensional oscillating water column wave energy device,” Ocean Engineering, vol. 18, no. 5, pp. 465–483, 1991.
- [17] U. A. Korde and R. C. Ertekin, “An open water submerged device for wave energy focusing and conversion,” in Proc. 10th European Wave and Tidal Energy Conference (EWTEC 2013), 2013, Aalborg, Denmark.
- [18] D. Evans, D. Jeffrey, S. Salter, and J. Taylor, “Submerged cylinder wave energy device: theory and experiment,” Applied Ocean Research, vol. 1, no. 1,

- pp. 3 – 12, 1979. [Online]. Available: <http://www.sciencedirect.com/science/article/pii/0141118779900038>
- [19] G. Giorgi and J. V. Ringwood, “Analytical formulation of nonlinear froude-kylov forces for surging-heaving-pitching point absorbers,” in ASME 2018 37th International Conference on Ocean, Offshore and Arctic Engineering. American Society of Mechanical Engineers, 2018, pp. V010T09A036–V010T09A036.
- [20] J. Falnes, “Wave-energy conversion through relative motion between two single-mode oscillating bodies,” in Proc. ASME Offshore Mechanics and Arctic Engineering Conference, July 1998, Lisbon, Portugal.
- [21] C. Mei, “Hydrodynamic principles of wave power extraction,” Philosophical Transactions of the Royal Society A, vol. 370, pp. 208–234, 2012.
- [22] J. Taylor, “High pressure hydraulics,” in Ocean Wave Energy: Current Status and Future Perspectives, J. Cruz, Ed. Springer, Berlin, 2008, pp. 189–285.
- [23] U. A. Korde and J. V. Ringwood, Hydrodynamic Control of Wave Energy Devices. Cambridge University Press, 2016.
- [24] C. Villegas and H. der Schaaf, “Implementation of pitch stability control for a wave energy converter,” in Proc. 9th European Wave and Tidal Energy Conference, 2011, southampton, UK.

- [25] J. Falnes, Ocean Waves and Oscillating Systems: Linear Interactions Including Wave-Energy Extraction. Cambridge University Press, 2002.
- [26] S. Naito and S. Nakamura, “Wave energy absorption in irregular waves by feed-forward control system,” in Hydrodynamics of ocean wave-energy utilization. Springer, 1986, pp. 269–280.
- [27] U. A. Korde, “Phase control of floating bodies from an on-board reference,” Applied Ocean Research, vol. 23, pp. 251–262, 2001.
- [28] U. Korde, “Efficient primary energy conversion in irregular waves,” Ocean Engineering, vol. 26, no. 7, pp. 625 – 651, 1999. [Online]. Available: <http://www.sciencedirect.com/science/article/pii/S0029801898000171>
- [29] A. Babarit and A. H. Clement, Applied Ocean Research, vol. 28, no. 2, pp. 77–91, 2006.
- [30] J. Hals, J. Falnes, and T. Moan, “Constrained optimal control of a heaving buoy wave-energy converter,” Journal of Offshore Mechanics and Arctic Engineering, vol. 133, no. 1, 2011.
- [31] F. Fusco and J. V. Ringwood, “A study of the prediction requirements in real-time control of wave energy converters,” IEEE Transactions on Sustainable Energy, vol. 3, no. 1, pp. 176–184, 2012.

- [32] B. Teillant, J.-C. Gilloteaux, and J. Ringwood, “Optimal damping profile for a heaving buoy wave energy converter,” IFAC Proceedings Volumes, vol. 43, no. 20, pp. 360–365, 2010.
- [33] A. Babarit, M. Guglielmi, and A. H. Clément, “Declutching control of a wave energy converter,” Ocean Engineering, vol. 36, no. 12-13, pp. 1015–1024, 2009.
- [34] A. Clément and A. Babarit, “Discrete control of resonant wave energy devices,” Philosophical Transactions of the Royal Society A: Mathematical, Physical and Engineering Sciences, vol. 370, no. 1959, pp. 288–314, 2012.
- [35] J. T. Allison, A. Kaitharath, and D. R. Herber, “Wave energy extraction maximization using direct transcription,” in ASME 2012 International Mechanical Engineering Congress and Exposition. American Society of Mechanical Engineers Digital Collection, 2012, pp. 485–495.
- [36] P. Kracht, S. Perez-Becker, J. B. Richard, and B. Fischer, “First results from wave tank testing of different control strategies for a point absorber wave energy converter,” in 2014 Ninth international conference on ecological vehicles and renewable energies (EVER). IEEE, 2014, pp. 1–8.
- [37] P. Beirao, D. Valério, and J. S. da Costa, “Identification and phase and amplitude control of the archimedes wave swing using a pid and imc,” in Second International Conference on Electrical Engineering, Coimbra, ISEC, 2007.

- [38] S. R. Nielsen, Q. Zhou, M. M. Kramer, B. Basu, and Z. Zhang, “Optimal control of nonlinear wave energy point converters,” Ocean engineering, vol. 72, pp. 176–187, 2013.
- [39] J. T. Scruggs, S. M. Lattanzio, A. A. Taflanidis, and I. I. Cassidy, “Optimal causal control of a wave energy converter in a random sea,” Applied Ocean Research, vol. 42, pp. 1–15, 2013.
- [40] G. Li, G. Weiss, M. Mueller, S. Townley, and M. R. Belmont, “Wave energy converter control by wave prediction and dynamic programming,” Renewable Energy, vol. 48, pp. 392–403, 2012.
- [41] G. Bacelli, J. V. Ringwood, and J.-C. Gilloteaux, “A control system for a self-reacting point absorber wave energy converter subject to constraints,” IFAC Proceedings Volumes, vol. 44, no. 1, pp. 11 387–11 392, 2011.
- [42] O. O. Abdelkhalik, R. R. III, G. Bacelli, R. Coe, D. Bull, D. Wilson, and U. Korde, “Control optimization of wave energy converters using a shape-based approach,” in ASME Power & Energy 2015. San Diego, CA: ASME, June 2015.
- [43] O. Abdelkhalik, R. Robinett, S. Zou, G. Bacelli, R. Coe, D. Bull, D. Wilson, and U. Korde, “On the control design of wave energy converters with wave prediction,” Journal of Ocean Engineering and Marine Energy, vol. 2, no. 4, pp. 473–483, 2016.

- [44] F. Fusco and J. Ringwood, "A simple and effective real-time controller for wave energy converters," IEEE Transactions on Sustainable Energy, vol. 4, no. 1, pp. 21–30, 2013.
- [45] U. A. Korde, R. D. Robinett, and D. G. Wilson, "Approaching maximum power conversion with exergy-based adaptive wave-by-wave control of a wave energy converter," in OCEANS 2015 - MTS/IEEE Washington, Oct 2015, pp. 1–5.
- [46] U. Korde, "Near-optimal control of a wave energy device in irregular waves with deterministic-model driven incident wave prediction," Applied Ocean Research, vol. 53, pp. 31–45, 2015.
- [47] A. F. de O. Falcão, "Wave energy utilization: A review of the technologies," Renewable and Sustainable Energy Reviews, vol. 14, no. 3, pp. 899 – 918, 2010. [Online]. Available: <http://www.sciencedirect.com/science/article/pii/S1364032109002652>
- [48] B. M. Count, "On the hydrodynamic behavior of the OWC device," Proc. Royal Soc. Lond. A, vol. 363, pp. 559–578, 1978.
- [49] J. N. NEWMAN, Marine hydrodynamics. MIT Press, 1977. [Online]. Available: <http://search.ebscohost.com/login.aspx?direct=true&scope=site&db=nlebk&db=nlabk&AN=48612>.
- [50] S. Salter, "Development of the duck concept," in Proc. Wave Energy Conference, 1978, Heathrow, U.K.

- [51] K. Budal and J. Falnes, “Optimum operation of improved wave power converter,” Marine Science Communication, vol. 3, pp. 133–150, 1977.
- [52] J. V. Ringwood, G. Bacelli, and F. Fusco, “Energy-maximizing control of wave-energy converters,” IEEE Control Systems Magazine, pp. 30–55, October 2014.
- [53] P. Nebel, “Maximizing the efficiency of wave-energy plants using complex conjugate control,” Proc. IMechE Part I - Journal of Systems and Control Engineering, vol. 206, no. 4, pp. 225–236, 1992.
- [54] R. Hansen and M. Kramer, “Modeling and control of the wave star prototype,” in Proc. 9th European Wave and Tidal Energy Conference, 2011, Southampton, UK, paper 163.
- [55] K. Budal and J. Falnes, “Interacting point absorbers with controlled motion,” in Power from Sea Waves, B. Count, Ed. Academic Press, London, 1980, pp. 381–399.
- [56] R. E. Hoskin, B. M. Count, N. Nichols, and D. A. C. Nicol, “Phase control for the oscillating water column,” in Proc. IUTAM Symp. Hydrodynamics of Wave Energy Utilization, D. V. Evans and A. F. O. Falcao, Eds. Springer Verlag, Berlin, 1985, pp. 257–268.
- [57] S. Naito and S. Nakamura, “Wave energy absorption in irregular waves by feedforward control system,” in Proc. IUTAM Symp. Hydrodynamics of Wave

- Energy Utilization, D. V. Evans and A. F. O. Falcao, Eds. Springer Verlag, Berlin, 1985, pp. 269–280.
- [58] J. Falnes, “On non-causal impulse response functions related to propagating water waves,” Applied Ocean Research, vol. 17, no. 6, pp. 379–389, 1995.
- [59] J. Falnes and J. Hals, “Heaving buoys, point absorbers and arrays,” Phil. Trans. Royal Society A, vol. 370, pp. 246–277, 2012.
- [60] J. H. Todalshaug, “Practical limits to the power that can be captured from ocean waves by oscillating bodies,” International Journal of Marine Energy, vol. 3–4, pp. e70 – e81, 2013, special Issue – Selected Papers - {EWTEC2013}. [Online]. Available: <http://www.sciencedirect.com/science/article/pii/S2214166913000386>
- [61] M. Penalba Retes, G. Giorgi, and J. Ringwood, “A review of non-linear approaches for wave energy converter modelling,” in Proceedings of the 11th European Wave and Tidal Energy Conference. European Wave and Tidal Energy Conference 2015, 2015.
- [62] M. Penalba, G. Giorgi, and J. Ringwood, “Mathematical modelling of wave energy converters: A review of nonlinear approaches,” Renewable and Sustainable Energy Reviews, vol. 78, pp. 1188–1207, 2017, cited By 16. [Online]. Available: <https://www.scopus.com/inward/record.uri?eid=>

2-s2.0-85019239868&doi=10.1016%2fj.rser.2016.11.137&partnerID=40&md5=898954ae6f79f77e5a45a5212e7821bd

- [63] M. Penalba, J. Davidson, C. Windt, and J. V. Ringwood, “A high-fidelity wave-to-wire simulation platform for wave energy converters: Coupled numerical wave tank and power take-off models,” Applied Energy, vol. 226, pp. 655 – 669, 2018. [Online]. Available: <http://www.sciencedirect.com/science/article/pii/S0306261918308754>
- [64] G. Giorgi and J. V. Ringwood, “Nonlinear froude-krylov and viscous drag representations for wave energy converters in the computation/fidelity continuum,” Ocean Engineering, vol. 141, pp. 164 – 175, 2017. [Online]. Available: <http://www.sciencedirect.com/science/article/pii/S0029801817303256>
- [65] —, “Computationally efficient nonlinear froude-krylov force calculations for heaving axisymmetric wave energy point absorbers,” Journal of Ocean Engineering and Marine Energy, vol. 3, no. 1, pp. 21–33, 2017.
- [66] A. Clement and P. Ferrant, “Superharmonic waves generated by the large amplitude heaving motion of a submerged body,” in Nonlinear Water Waves, K. Horikawa and H. Maruo, Eds. Berlin, Heidelberg: Springer Berlin Heidelberg, 1988, pp. 423–433.
- [67] M. Penalba, A. Merigaud, J.-c. Gilloteaux, and J. Ringwood, “Influence of

- nonlinear froude–krylov forces on the performance of two wave energy points absorbers,” Journal of Ocean Engineering and Marine Energy, 06 2017.
- [68] J.-C. Gilloteaux, “Large amplitude motions of floating bodies in potential theory. Application to wave energy conversion,” Theses, Ecole Centrale de Nantes (ECN) ; Université de Nantes, May 2007. [Online]. Available: <https://tel.archives-ouvertes.fr/tel-00521689>
- [69] G. Giorgi, M. Penalba Retes, and J. Ringwood, “Nonlinear hydrodynamic models for heaving buoy wave energy converters,” in Asian Wave and Tidal Energy Conference, 2016, pp. 1–10. [Online]. Available: <http://mural.maynoothuniversity.ie/9418/>
- [70] U. A. Korde and J. Ringwood, Hydrodynamic Control of Wave Energy Devices. Cambridge University Press, 2016.
- [71] W. Cummins, “The impulse response function and ship motions,” Schiff-stechnik, 1962.
- [72] T. Perez and T. I. Fossen, “A matlab toolbox for parametric identification of radiation-force models of ships and offshore structures,” 2009.
- [73] S. Naito and S. Nakamura, “Wave energy absorption in irregular waves by feed-forward control system,” in Hydrodynamics of Ocean Wave-Energy Utilization, D. V. Evans and A. F. O. de Falcão, Eds. Berlin, Heidelberg: Springer Berlin Heidelberg, 1986, pp. 269–280.

- [74] G. Giorgi and J. Ringwood, “Comparing nonlinear hydrodynamic forces in heaving point absorbers and oscillating wave surge converters,” Journal of Ocean Engineering and Marine Energy, vol. 4, no. 1, pp. 25–35, 2018, cited By 2. [Online]. Available: <https://www.scopus.com/inward/record.uri?eid=2-s2.0-85028763761&doi=10.1007%2fs40722-017-0098-2&partnerID=40&md5=c67dcde1659df6841a33ae27a8970dc8>
- [75] G. Giorgi, M. Penalba, and J. Ringwood, “Nonlinear froude–krylov force representations for heaving buoy wave energy converters,” in Submitted to the 3rd Asian wave and tidal energy conference, Singapore, 2016.
- [76] W. Cummins, “The impulse response function and ship motions,” David Taylor Model Basin Washington DC, Tech. Rep., 1962.
- [77] R. N. Bracewell and R. N. Bracewell, The Fourier transform and its applications. McGraw-Hill New York, 1986, vol. 31999.
- [78] D. Wilson and R. Robinett, “Pd version complex conjugate control for optimal wec performance,” in Technical Advance, SD# 13535. Sandia National Laboratories, 2015.
- [79] D. Valerio, P. Beirao, M. J. Mendes, and J. S. da Costa, “Comparison of control strategies performance for a wave energy converter,” in 2008 16th Mediterranean Conference on Control and Automation. IEEE, 2008, pp. 773–778.

- [80] G. Bacelli, “Optimal control of wave energy converters,” Ph.D. dissertation, National University of Ireland Maynooth, 2014.
- [81] K. Ogata, “Modern control engineering,” Book Reviews, vol. 35, no. 1181, p. 1184, 1999.
- [82] O. M. Solomon, “The use of dft windows in signal-to-noise ratio and harmonic distortion computations,” in 1993 IEEE Instrumentation and Measurement Technology Conference. IEEE, 1993, pp. 103–108.
- [83] G. Andria, M. Savino, and A. Trotta, “Fft-based algorithms oriented to measurements on multifrequency signals,” Measurement, vol. 12, no. 1, pp. 25–42, 1993.
- [84] S. R. Chintakindi, O. Varaprasad, and D. S. Sarma, “Improved hanning window based interpolated fft for power harmonic analysis,” in TENCON 2015-2015 IEEE Region 10 Conference. IEEE, 2015, pp. 1–5.
- [85] T. R. Mendonça, C. H. Martins, M. F. Pinto, and C. A. Duque, “Variable window length applied to a modified hanning filter for optimal amplitude estimation of power systems signals,” in 2015 IEEE Power & Energy Society General Meeting. IEEE, 2015, pp. 1–5.
- [86] Y. F. Li and K. F. Chen, “Eliminating the picket fence effect of the fast fourier transform,” Computer Physics Communications, vol. 178, no. 7, pp. 486–491, 2008.

- [87] B. A. Ling and B. A. Batten, “Real time estimation and prediction of wave excitation forces on a heaving body,” in ASME 2015 34th international conference on ocean, offshore and arctic engineering. American Society of Mechanical Engineers Digital Collection, 2015.
- [88] A. Babarit and G. Delhommeau, “Theoretical and numerical aspects of the open source bem solver nemoh,” 2015.
- [89] P. Schmitt, C. Windt, J. Nicholson, and B. Elsässer, “Development and validation of a procedure for numerical vibration analysis of an oscillating wave surge converter,” European Journal of Mechanics-B/Fluids, vol. 58, pp. 9–19, 2016.
- [90] N. Instruments, “The fundamentals of fft-based signal analysis and measurement in labview and labwindows/cvi,” 2009.
- [91] M. Belmont, J. Horwood, R. Thurley, and J. Baker, “Filters for linear sea-wave prediction,” Ocean Engineering, vol. 33, no. 17–18, pp. 2332–2351, 2006.
- [92] K. Budal and J. Falnes, “Wave power conversion by point absorbers,” Norwegian Maritime Research, vol. 6, no. 4, pp. 2–11, 1978.
- [93] M. Schetzen, The Volterra and Wiener Theories of Nonlinear Systems. John Wiley & Sons, NY, 1980, a Wiley-Interscience publication.
- [94] Wamit, WAMIT 7.0 User manual, The Massachusetts Institute of Technology, 2012.

- [95] D. Evans, “Power from water waves,” Annual Review of Fluid Mechanics, vol. 13, pp. 157–187, 1981.
- [96] OOI Pioneer Array, 2017, <https://ooinet.oceanobservatories.org/>.
- [97] U. A. Korde, R. D. Robinett, D. G. Wilson, G. Bacelli, and O. O. Abdelkhalik, “Wave-by-wave control of a wave energy converter with deterministic wave prediction,” in European Wave and Tidal Energy Conference, 2017, submitted, April 2017.
- [98] A. Sproul and N. Weise, “Analysis of a wave front parallel wec prototype,” IEEE Transactions on Sustainable Energy, vol. 6, no. 4, pp. 1183–1189, Oct 2015.
- [99] M. Buccino, D. Banfi, D. Vicinanza, M. Calabrese, G. Giudice, and A. Carravetta, “Non breaking wave forces at the front face of seawave slotcone generators,” Energies, vol. 5, no. 11, pp. 4779–4803, nov 2012. [Online]. Available: <https://doi.org/10.3390%2Fen5114779>
- [100] O. Abdelkhalik and S. Darani, “Optimization of nonlinear wave energy converters,” Ocean Engineering, vol. 162, pp. 187–195, 2018.
- [101] P. B. Garcia-Rosa and J. V. Ringwood, “On the sensitivity of optimal wave energy device geometry to the energy maximizing control system,” IEEE Transactions on Sustainable Energy, vol. 7, no. 1, pp. 419–426, Jan 2016.

- [102] A. Garcia-Teruel and D. Forehand, “Optimal wave energy converter geometry for different modes of motion,” in Proceedings of the 3rd International Conference on Renewable Energies Offshore. RENEW 2018, 2018, pp. 299–305.
- [103] O. M. Shir, Niching in Evolutionary Algorithms. Berlin, Heidelberg: Springer Berlin Heidelberg, 2012, pp. 1035–1069. [Online]. Available: https://doi.org/10.1007/978-3-540-92910-9_32
- [104] E. Rusu and F. Onea, “A review of the technologies for wave energy extraction,” Clean Energy, 2018.
- [105] J. Falnes and J. Lovseth, “Ocean wave energy,” Energy Policy, vol. 19, no. 8, pp. 768–775, 1991.
- [106] A. Babarit, J. Hals, M. J. Muliawan, A. Kurniawan, T. Moan, and J. Krokstad, “Numerical benchmarking study of a selection of wave energy converters,” Renewable Energy, vol. 41, pp. 44–63, 2012. [Online]. Available: <http://www.sciencedirect.com/science/article/pii/S0960148111005672>
- [107] E. M. Evans, “Tidal stream energy,” Ph.D. dissertation, Plymouth Polytechnic, 1987.
- [108] I. P. Castro, “Wake characteristics of two-dimensional perforated plates normal to an air-stream,” Journal of Fluid Mechanics, vol. 46, no. 3, pp. 599—609, 1971.

- [109] G. I. Taylor, “Tidal Oscillations in gulfs and rectangular basins,” Proceedings of the London Mathematical Society, vol. 20, pp. 148–181, 1919.
- [110] M. Penalba Retes, A. Mérigaud, J.-C. Gilloteaux, and J. Ringwood, “Nonlinear froude-krylov force modelling for two heaving wave energy point absorbers,” in Proceedings of the 11th European Wave and Tidal Energy Conference. European Wave and Tidal Energy Conference 2015, 2015.
- [111] C. O. AB, <http://www.corpowerocean.com/>.
- [112] AeroVironment, https://www.avinc.com/engineering/marine_energy.
- [113] G. Bacelli, “Optimal control of wave energy converters,” PhD, National University of Ireland, Maynooth, Maynooth, Ireland, 2014.
- [114] EMEC, “List of wave energy developers,” May 2015, <http://www.emec.org.uk/marine-energy/wave-developers/>. [Online]. Available: <http://www.emec.org.uk/marine-energy/wave-developers/>
- [115] D. Evans, “Power from water waves,” Annual Review of Fluid Mechanics, vol. 13, pp. 157–187, 1981.
- [116] J. Falnes, Ocean Waves and Oscillating Systems: Linear interactions including wave energy extraction. Cambridge University Press, Cambridge, UK, 2002.

- [117] U. Korde, R. R. III, D. Wilson, N. M. O. Abdelkhalik, and G. Bacelli, “Obtaining a 10-fold increase in wave energy conversion by small buoys for underwater micro grids,” presentation at personal meeting in Arlington, VA, May 2015.
- [118] P. Kracht, S. Perez-Becker, J. Richard, and B. Fischer, “First results from wave tank testing of different control strategies for a point absorber wave energy converter,” in Ecological Vehicles and Renewable Energies (EVER), 2014 Ninth International Conference on, March 2014, pp. 1–8.
- [119] M. Longuet-Higgins, “Statistical properties of wave groups in a random sea state,” Philosophical Transactions of the Royal Society of London, Series A, vol. 312, no. 1521, pp. 219–250, 1984.
- [120] C. Mei, The Applied Dynamics of Ocean Surface Waves. World Scientific, Singapore, 1992, chapter 7.
- [121] A. Shagalov, J. Rasmussen, and V. Naulin, “Phase-locking phenomena and excitation of damped and driven nonlinear oscillators,” Journal of Physics A: Mathematical and Theoretical, vol. 42, no. 045502, p. 14p, 2009.
- [122] WaveNET, <http://albatern.co.uk/wavenet/wavenet/>.
- [123] D. Wilson and R. R. III, “PD version of complex-conjugate controller for optimal wec performance,” Sandia National Laboratories, Tech. Rep., March 2015, sD # 13535.

- [124] G. Wu, “Direct simulation and deterministic prediction of large-scale nonlinear wave field,” Ph.D. dissertation, Massachusetts Institute of Technology, 2004, cambridge, MA.
- [125] W. Xiao, “Study of directional ocean wavefield evolution and rogue wave occurrence using large-scale phase-resolved nonlinear simulations,” Ph.D. dissertation, Massachusetts Institute of Technology, 2013, cambridge, MA.
- [126] D. Yue and Y. Liu, “High-resolution measurement-based phase-resolved prediction of ocean wave-fields,” Massachusetts Institute of Technology, Tech. Rep., 2013, final report, Office of Naval Research (ONR).
- [127] J. Dannenberg, P. Naaijen, K. Hessner, H. den Boom, and K. Reichert, “The on board wave and motion estimator OWME,” in Proc. Int. Soc. Offshore and Polar Engr. Conf., 2010, beijing, China.
- [128] U. Korde and R. R. III, “On integrating object detection capability into a coastal energy conversion system,” white paper submitted to the Office of Naval Research, June 2015.
- [129] —, “On integrating object detection capability into a coastal energy conversion system: free-floating wave energy converters,” supplementary note on free-floating energy-converting sensor arrays, July 2015.
- [130] M. B. A. R. Institute, <http://www.mbari.org/news/homepage/2012/powerbuoy/powerbuoy.html>.

- [131] O. P. Technologies., <http://www.oceanpowertechnologies.com/pb40>.
- [132] J. Eder, J. Bretl, and K. Edwards, “Empirical demonstration of acausal control strategies for wave energy converters,” in Proc. 32nd Ocean, Offshore, and Arctic Engineering Conference, 2013, nantes, France.
- [133] J. P. Den Hartog, Mechanical vibrations. Courier Corporation, 1985.
- [134] J. Wehausen, “Motion of floating bodies,” Annual Review of Fluid Mechanics, vol. 3, pp. 237–268, 1971.
- [135] U. Korde, R. R. III, and D. Wilson, “Approaching maximum power conversion with exergy based adaptive wave-by-wave control of a wave energy converter,” in Proc. MTS/IEEE Oceans 2015 Conference, 2015, washington, DC, October 2015.
- [136] U. Korde and R. R. III, “Modeling of relevant nonlinearities for wave energy devices,” in Proc. Wave Energy Workshop, 2015, maynooth University, Maynooth, Ireland, January 2015.
- [137] L. de recherche en Hydrodynamique, 2015, ecole de Nantes, Nantes, France, <http://lheea.ec-nantes.fr/cgi-bin/hgweb.cgi/nemoh/>.
- [138] Datawell BV, “Datawell waverider reference manual,” Datawell BV Oceanographic Instruments, Tech. Rep., 2009, the Netherlands.

- [139] Furuno USA, “Operator’s manual: Marine radar,” Furuno Electric Co. Ltd., Tech. Rep., 2011, japan.
- [140] O. O. Initiative, <http://oceanobservatories.org/technical-data-package/>, December 2015.
- [141] R. Olson and H. Sosik, “A submersible imaging-in-flow instrument to analyze nano and microplankton: Imaging FlowCytobot,” Limnology and Oceanography: Methods, vol. 5, pp. 193–203, 2007.
- [142] G. Payne, J. Taylor, and D. Ingram, “Best practice guidelines for tank testing of wave energy converters,” The Journal of Ocean Technology–Renewable Ocean Energy, vol. 4, no. 4, pp. 39–70, 2009.
- [143] S. Salter, “Ring cam pumps for flood prevention,” personal communication, January 2016.
- [144] O. Technology and I. C. Program, http://www.nsf.gov/funding/pgm_summ.jsp?pims_id=12724&org=OCE&from=home, National Science Foundation, January 2016.
- [145] O. Abdelkhalik, R. R. III, G. Bacelli, R. Coe, D. Bull, D. Wilson, and U. Korde, “A dynamic programming approach for control optimization of wave energy converters,” Ocean Engineering, Elsevier, 2015, in review.

- [146] R. Waters, A. Stålberg, O. Danielsson, O. Svensson, S. Gustafsoon, E. Stroömstedt, M. Eriksson, J. Sundberg, and M. Leijon, “Experimental results from sea trials of an offshore wave energy system,” Applied Physics Letters, vol. 90, no. 034105, pp. 1–3, 2007.
- [147] D. Quick, “Autonomous wave energy powerbuoy device commences sea trial,” 2011.
- [148] P. W. Power, “Pelamis: P-750 wave energy converter,” 2009, <http://www.pelamiswave.com>.
- [149] NDBC, “Station 51207–Kaneohe Bay, HI (198),” 2016, <http://www.ndbc.noaa.gov>, June 2016.
- [150] S. H. Salter, “Changing the 1981 spine-based ducks,” in Proc. 1st European Wave Energy Conf., 1993, edinburgh, Scotland.
- [151] J. Falnes, “Optimum control of oscillation of wave energy converters,” Int. J. Offshore and Polar Engineering, vol. 12, no. 2, pp. 147–155, 2002.
- [152] D. Skyner, “Solo duck linear analysis,” University of Edinburgh, Tech. Rep., 1987, technical Report.
- [153] U. A. Korde, M. P. Schoen, and F. Lin, “Strategies for time-domain control of wave energy devices in irregular waves,” in Proc. 11th Int. Soc. Offshore and Polar Engr. (ISOPE) Conference, 2002, stavanger, Norway.

- [154] U. A. Korde, “A power take-off mechanism for maximizing the performance of an oscillating water column wave energy device,” Applied Ocean Research, vol. 13, no. 2, pp. 75–81, 1991.
- [155] J. N. B. A. Perdigao and A. J. N. A. Sarmiento, “A phase control strategy for OWC devices in irregular waves,” in Proc. 4th Int. Workshop on Water Waves and Floating Bodies, J. Grue, Ed., 1989, pp. 205–209.
- [156] A. F. O. Falcão and P. A. P. Justino, “OWC wave energy devices with air flow control,” Ocean Engineering, pp. 1275–1295, 1999.
- [157] U. A. Korde, “On using up-wave surface elevation for efficient wave energy conversion in irregular waves,” Applied Ocean Research, 2014, in press.
- [158] —, “Up-wave surface elvation for smooth hydrodynamic control of wave energy conversion in irregular waves,” in Proc. MTS/IEEE Oceans 2013, Sept. 2013, san Diego, CA.
- [159] A. F. O. Falcão, “Phase control through load control of oscillating body wave energy converters with hydraulic PTO system,” Ocean Engineering, vol. 35, pp. 358–366, 2008.
- [160] M. F. P. Lopes, J. Hals, R. P. F. Gomes, T. Moan, L. M. C. Gato, and A. F. O. Falcão, “Experimental and numerical investigation of non-predictive phase control strategies for a point absorbing wave energy converter,” Ocean Engineering, vol. 36, pp. 386–402, 2009.

- [161] M. P. Schoen, J. Hals, and T. Moan, “Wave prediction and robust control of heaving wave energy devices for irregular waves,” IEEE Trans. Energy Conversion, vol. 26, no. 2, pp. 627–638, 2011.
- [162] J. Cretel, G. Lightbody, G. Thomas, and A. Lewis, “Maximization of energy capture by a wave-energy point absorber using Model Predictive Control,” in Proc. 18th IFAC World Congress, 2011, Milano, Italy, September 2011, preprint.
- [163] F. Fusco and J. Ringwood, “A hierarchical robust control of oscillating wave energy converters with uncertain dynamics,” IEEE Transactions on Sustainable Energy, vol. 5, no. 3, pp. 958–966, 2014.
- [164] J. Hals, J. Falnes, and T. Moan, “Constrained optimal control of a heaving buoy wave energy converter,” J. Offshore Mechanics and Arctic Engineering, vol. 133, no. 1, pp. 1–15, 2011.
- [165] —, “A comparison of selected strategies for adaptive control of wave energy converters,” J. Offshore Mechanics and Arctic Engineering, vol. 133, no. 3, pp. 1–12, 2011.
- [166] S. H. Salter, “Use of gyros as a reference frame for wave energy converters,” in Proc. 2nd Symp. on Wave Energy Utilization, 1982, trondheim, Norway.
- [167] M. J. French and R. Bracewell, “Heaving point absorbers reacting against an internal mass,” in Proc. IUTAM Symp. Hydrodynamics of Wave Energy

- Utilization, D. V. Evans and A. F. de O. Falcão, Eds. Springer Verlag, Berlin, 1985, pp. 2547–255.
- [168] D. J. Pizer and U. A. Korde, “Recent studies on mighty whale hydrodynamics,” in Proc. 3rd European Wave Energy Conference, 1998, patras, Greece.
- [169] U. A. Korde, “Study of a wave energy device for possible application in communication and spacecraft propulsion,” Ocean Engineering, vol. 17, no. 6, pp. 587–599, 1990.
- [170] R. Carter, R. C. Ertekin, and P. Lin, “On the reverse flow beneath a submerged plate due to wave action,” in Proc. 25th Int. Conference on Offshore Mechanics and Arctic Engineering, 2006, aSME, OMAE2006–92623.
- [171] P. Lin and H.-W. Liu, “Scattering and trapping of wave energy by a submerged paraboloidal shoal,” J. Waterway, Port, Coastal, and Ocean Engineering, vol. 133, no. 2, pp. 94–103, 2007.
- [172] X. Yu and A. Chwang, “Analysis of wave scattering by submerged circular disk,” J. Engineering Mechanics, vol. 119, no. 9, pp. 1804–1817, 1993.
- [173] S. Zhang and A. N. Williams, “Wave scattering by submerged elliptical disk,” J. Waterway, Port, Coastal, and Ocean Engineering, vol. 122, no. 1, pp. 38–45, 1996.

- [174] P. McIver and M. McIver, “Trapped modes in an axi-symmetric water-wave problem,” Quarterly J. Mechanics and Applied Mathematics, vol. 50, pp. 165–178, 1997.
- [175] D. V. Evans and R. Porter, “Examples of motion trapped modes in two and three dimensions,” in Proc. 22 nd Int. Workshop on Water Waves and Floating Bodies, 2007, pp. 81–84, plitvice, Croatia.
- [176] R. Porter, “Trapping of water waves by pairs of submerged cylinders,” Proc. Royal Society A, vol. 458, pp. 607–624, 2002.
- [177] P. A. Martin and L. Farina, “Radiation of water waves by a heaving submerged horizontal disc,” J. Fluid Mechanics, vol. 337, pp. 365–379, 1997.
- [178] U. A. Korde, “On a submerged device with controlled dynamics for efficient wave energy conversion,” GREEN–An international journal for sustainable energy conversion and storage, vol. 2, pp. 87–95, 2012.
- [179] U. Korde, R. Robinett, and D. Wilson, “Hydrodynamic modeling and control of buoy oscillations for efficient use of wave power in ocean sensing,” in Proc. ONR/MTS Buoy Workshop 2016, 2016, Woods Hole, MA.
- [180] J. Lighthill, “Mathematical analysis related to the vickers project–general background and results of two-dimensional analysis,” in Power from Sea Waves, B. M. Count, Ed. Academic Press, London, 1980, pp. 345–355.

- [181] M. J. Simon, “Mathematical analysis related to the vickers project—calculations relating to a submerged circular duct,” in Power from Sea Waves, B. Count, Ed. Academic Press, London, 1980, pp. 356–379.
- [182] J. Falnes and P. McIver, “Surface wave interactions with systems of oscillating bodies and pressure distributions,” Applied Ocean Research, vol. 7, no. 4, pp. 225–234, 1985.
- [183] G. A. Buck, “Added mass and radiation damping of a submerged circular disc by solving integral equation,” March 2012, based on Martin and Farina (1997), Personal Communication.
- [184] F. Fusco, J.-C. Gilloteaux, and J. Ringwood, “A study on the prediction requirements in time domain control of wave energy converters,” in Proc. Control Applications in Marine Systems, Germany, 2010.
- [185] F. Fusco and J. V. Ringwood, “Short-term wave forecasting for real-time control of wave energy converters,” IEEE Trans. on Sustainable Energy, vol. 1, no. 2, pp. 99–106, 2010.
- [186] G. Bacelli and J. V. Ringwood, “A geometric tool for analysis of position and force constraints in wave energy converters,” Ocean Engineering, vol. 65, pp. 10–18, 2013.
- [187] M. R. Belmont, J. M. K. Horwood, R. W. F. Thurley, and J. Baker, “Shallow

- angle wave profiling lidar,” J. Atmospheric and Oceanic Technology, vol. 24, no. 6, pp. 1150–1156, 2007.
- [188] J. V. Wehausen, “Causality and the radiation condition,” J. Engineering Mathematics, vol. 26, pp. 153–158, 1992.
- [189] U. A. Korde and R. C. Ertekin, “On wave energy focusing and conversion in open water,” Renewable Energy - an international journal, vol. 62, pp. 84–99, 2014.
- [190] C. Garrison, Hydrodynamic Loading of Large Offshore Structures: Three-dimensional Source Distribution Methods, ser. Eds. O. C. Zienkiewicz and R. W. Lewis and K. G. Stagg, in Numerical Methods in Offshore Engineering. New York: John Wiley & Sons, 1978, call No. (TC 1650.N 85), xii + 582 pp.
- [191] J. V. Wehausen and E. V. Laitone, Surface Waves, ser. in Handbuch der Physik, Ed. S. Flugge. Berlin: Springer-Verlag, 1960, vol. Vol. 9, call No. (QC 21.H191), pp. 446-778.
- [192] O. M. Faltinsen and F. C. Michelsen, “Motions of large structures in waves at zero froude number,” in Int. Symp. on the Dynamics of Marine Vehicles and Structures in Waves, 1974, pp. 91–106, university College, London.
- [193] J. N. Newman, “Algorithms for the free-surface green function,” J. Engineering Math, vol. 19, pp. 57–67, 1985.

- [194] R. W. Yeung, “A singularity distribution method for free surface flow problems,” Dept. of Naval Architecture, Univ. of California, Berkeley, Tech. Rep., 1973, nA-73-6.
- [195] HYDRAN, “A computer program for the hydroelastic response analysis of ocean structures,” Offcoast Inc., Kailua, HI, Tech. Rep., September 2012, ver. 5.1.7.
- [196] D. Wang, H. R. Riggs, and R. C. Ertekin, “Simulation of wave power devices,” Int. J. Offshore and Polar Engineering, vol. 1, no. 4, pp. 307–316, 1991.
- [197] R. C. Ertekin, H. R. Riggs, X. L. Che, and S. X. Du, “Efficient methods for hydroelastic analysis of very large floating structures,” J. Ship Research, vol. 37, no. 1, pp. 58–76, 1993.
- [198] H. R. Riggs, R. C. Ertekin, and T. Mills, “Impact of stiffness on the response of a multi-module mobile offshore base,” Int. J. Offshore and Polar Eng., vol. 9, no. 2, pp. 126–133, 1999.
- [199] H. R. Riggs, H. Suzuki, R. C. Ertekin, J. W. Kim, and K. Iijimae, “Comparison of hydroelastic computer codes based on the issc vlfs benchmark,” Ocean Engineering, vol. 35, no. 7, pp. 589–597, 2008.
- [200] E. R. Jeffreys, “Simulation of wave power devices,” Applied Ocean Research, vol. 6, no. 1, pp. 31–39, 1984.

- [201] R. D. Robinett, C. R. Dohrmann, G. R. Eisler, J. T. Feddema, G. G. Parker, D. G. Wilson, and D. Stokes, Flexible Robot Dynamics and Controls. Springer, London, 2002.
- [202] R. D. Robinett and D. G. Wilson, Nonlinear Power Flow Control Design: Utilizing Exergy, Entropy, Static and Dynamic Stability, and Lyapunov Analysis. Springer, London, 2011.
- [203] J.-J. E. Slotine and W. Li, Applied Nonlinear Control. Prentice-Hall, NJ, 1991.
- [204] A. E. Bryson and Y.-C. Ho, Applied Optimal Control—Optimization, Estimation, and Control. Hemisphere Publishing Corporation, 1975.
- [205] R. D. Robinett and D. G. Wilson, “Exergy and irreversible entropy production:thermodynamic concepts for nonlinear control design,” International Journal of Exergy, vol. 6, no. 3, pp. 357–387, 2009.
- [206] —, “Hamiltonian surface shaping with information theory and exergy/entropy control for collective plume tracing,” International Journal of Systems, Control and Communications, vol. 2, no. 1/2/3, pp. 144–169, 2010, invited paper, special issue on Information Processing and Decision Making in Control Systems.
- [207] R. Robinett and D. Wilson, “Collective systems: Physical and information exergies,” Sandia National Laboratories, Tech. Rep., 2007, SAND2007–2327.

- [208] —, “Nonlinear slewing spacecraft control based on exergy, power flow, and static and dynamic stability,” The Journal of the Astronautical Sciences, vol. 57, no. 4, pp. 717–741, 2010.
- [209] A. F. O. Falcao, “Phase control through load control of oscillating body wave energy converters with hydraulic pto system,” Ocean Engineering, vol. 35, pp. 358–366, 2008.
- [210] U. Korde and R. Ertekin, “Wave energy conversion by controlled floating and submerged cylindrical buoys,” Journal of Ocean Engineering and Marine Energy, vol. 1, no. 3, pp. 255–272, 2015.
- [211] U. A. Korde, “On a near-optimal control approach for a wave energy converter in irregular waves,” Applied Ocean Research, vol. 46, pp. 79–93, 2014.
- [212] S. A. Mavrakos and P. McIver, “Comparison of methods for calculation of hydrodynamic characteristics of arrays of wave power devices,” Applied Ocean Research, vol. 19, no. 5, 6, pp. 283–291, 1997.
- [213] I. Gradshteyn and I. Ryzhik, Table of Integrals, Series, and Products, 5th ed. Academic Press, San Diego, CA, 1994, Alan Jeffrey (ed.).
- [214] J. Nolte, R. C. Ertekin, and E. P. Davis, “In-ocean experiments of a wave energy conversion device moored to an anchor and to a drogue,” J. Ocean Technology, vol. 8, no. 1, pp. 72–85, March 2013.

- [215] J. Nolte and R. C. Ertekin, “Wave power calculations for a wave energy conversion device connected to a drogue,” J. of Renewable and Sustainable Energy (AIP), vol. 6, no. 1, pp. 013 117–1–013 117–21, 2014, DOI: 10.1063/1.4862785.
- [216] P. O’Neill, Advanced Engineering Mathematics, 7th ed. Cengage Learning, CT, 2012.
- [217] D. V. Evans, “A theory for wave power absorption by oscillating bodies,” J. Fluid Mechanics, vol. 77, no. 1, pp. 1–25, 1976.
- [218] H. Lamb, Hydrodynamics. Cambridge University Press, UK, 1932, 6th ed. reissued by Dover, NY, 1945.
- [219] G. Whitham, Linear and Nonlinear Waves. John Wiley & Sons, NY, 1973, a Wiley-Interscience Publication.
- [220] S. Salter, “Wave power,” Nature, pp. 720–724, June 1974.
- [221] S. Salter, J. Taylor, and N. Caldwell, “Power conversion mechanisms for wave energy,” Proc. Institution of Mechanical Engineers, Part M—Journal of Engineering for the Maritime Environment, vol. 216, pp. 1–27, 2002.
- [222] D. Valerio, P. Berraio, and J. da Costa, “Optimization of wave energy extraction with the archimedes wave swing,” Ocean Engineering, vol. 34, pp. 2330–2344, 2007.

- [223] P. Frigaard and M. Brorsen, “A time-domain method for separating incident and reflected irregular waves,” Aalborg: Hydraulics and Coastal Engineering Laboratory, Department of Civil Engineering, Aalborg University, Tech. Rep., 1993, technical report.
- [224] A. Babarit, M. Guglielmi, and A. Clement, “Declutching control of a wave energy converter,” Ocean Engineering, vol. 36, pp. 1015–1024, 2009.
- [225] G. Li and M. Belmont, “Model predictive control of a sea-wave energy converter—part i: a convex approach for the case of a single device,” Renewable Energy, vol. 69, pp. 453–463, 2014.
- [226] J. V. Wehausen and E. V. Laitone, Surface Waves, ser. in Handbuch der Physik, Ed. S. Flugge. Berlin: Springer-Verlag, 1960, vol. Vol. 9, call No. (QC 21.H191), pp. 446-778.
- [227] R. W. Yeung, A. Peiffer, N. Tom, and T. Matlock, “Design, analysis, and evaluation of the uc-berkeley wave energy extractor,” J. Offshore Mechanics and Arctic Engineering, vol. 134, 2012, 021902, 8 pp.
- [228] D. Y. Wang, H. R. Riggs, and R. C. Ertekin, “Three-dimensional hydroelastic response of a very large floating structure,” Int. J. Offshore and Polar Engineering, vol. 1, no. 4, pp. 307–316, 1991.
- [229] U. A. Korde and R. C. Ertekin, “On wave energy conversion and focusing in open water,” Renewable Energy, vol. 62, pp. 84–99, 2014.

- [230] D. L. Bull, M. E. Ochs, D. L. Laird, B. Boren, and R. A. Jepsen, “Technological cost-reduction pathways for point absorber wave energy converters in the marine hydrokinetic environment,” Sandia National Laboratories, Tech. Rep., October 2013, SAND2013–7204.
- [231] U. A. Korde and R. C. Ertekin, “An active-controlled submerged wave energy device with energy focusing,” in Proc. 4th Int. Conference on Ocean Energy, 2012, dublin, Ireland.
- [232] J. L. Forsberg, “On-line identification and prediction of incident waves,” in Proc. IUTAM Symp. Hydrodynamics of Wave Energy Utilization, D. Evans and A. de O. Falcão, Eds. Springer Verlag, Berlin, 1985, pp. 185–193.
- [233] S. H. Salter, “Wave energy: nostalgic ramblings, future hopes, and heretical suggestions,” J. Ocean Engineering and Marine Energy, vol. 2, no. 4, pp. 399–428, 2016.
- [234] U. A. Korde, R. D. Robinett, and D. G. Wilson, “Wave-by-wave control in irregular waves for a wave energy device with approximate parameters,” J. Ocean Engineering and Marine Energy, vol. 2, no. 4, pp. 509–519, 2016.
- [235] U. A. Korde, “Hydrodynamic modeling and control of buoy oscillations for efficient conversion of wave power in ocean sensing,” in Proc. ONR/MTS Buoy Workshop 2016, April 2016, woods Hole, MA.

- [236] NDBC, “Station 46006: Southeast Papa,” 2017, <http://www.ndbc.noaa.gov>, April 16, 2017.
- [237] K. Budal, “Floating structure with heave motion reduced by force compensation,” in Proc. ASME Offshore Mechanics and Arctic Engineering Conference, vol. 1, 1985, pp. 92–101.
- [238] O. Abdelkhalik, S. Zou, R. R. III, G. Bacelli, D. Wilson, R. Coe, and U. A. Korde, “Multi resonant feedback control of three-degree-of-freedom wave energy converters,” IEEE Transactions on Sustainable Energy, vol. PP, no. 99, pp. 1–1, 2017.
- [239] J. Falnes and A. Kurniawan, “Fundamental formulae for wave-energy conversion,” Royal Society Open Science, vol. 2, no. 3, 2015. [Online]. Available: <http://rsos.royalsocietypublishing.org/content/2/3/140305>
- [240] S. Salter, A. Dixon, and C. Greated, “Wave forces on partially submerged cylinders,” Journal of Waterway, Port, Coastal and Ocean Engineering, vol. 105, pp. 421–438, 1979.
- [241] K. Budal, “Floating structure with heave motion reduced by force compensation,” in Proc. ASME Offshore Mechanics and Arctic Engineering Conference, vol. 1, 1985, pp. 92–101.
- [242] Ocean Observatories Initiative, 2017, <http://oceanobservatories.org/technical-data-package/>.

- [243] O. Abdelkhalik, R. Robinett, G. Bacelli, R. Coe, D. Bull, D. Wilson, and U. Korde, “Control optimization of wave energy converters using a shape-based approach,” in Proc. ASME Power Energy, 2015.
- [244] S. Zou, “Optimal control of wave energy converters,” Ph.D. dissertation, Michigan Technological University, 2018.
- [245] J. Lyu, “Optimization and control of an array of wave energy converters,” Ph.D. dissertation, Michigan Technological University, 2018.
- [246] J. Falnes, Ocean waves and oscillating systems: linear interactions including wave-energy extraction. Cambridge university press, 2002.
- [247] J. Hals, J. Falnes, and T. Moan, “A comparison of selected strategies for adaptive control of wave energy converters,” Journal of Offshore Mechanics and Arctic Engineering, vol. 133, no. 3, 2011.
- [248] U. Korde, M. Schoen, F. Lin et al., “Time domain control of a single mode wave energy device,” in The Eleventh International Offshore and Polar Engineering Conference. International Society of Offshore and Polar Engineers, 2001.
- [249] U. Korde, “Efficient primary energy conversion in irregular waves,” Ocean engineering, vol. 26, no. 7, pp. 625–651, 1999.
- [250] C. Maisondieu and A. Clement, “A realizable force feedback-feedforward control loop for a piston wave absorber,” in Proceedings of the 8th Int. Workshop on

Water Waves and Floating bodies, St Johns Newfoundland, Canada, 1993, pp. 79–82.


- [251] J. Scruggs, S. Lattanzio, A. Taflanidis, and I. Cassidy, “Optimal causal control of a wave energy converter in a random sea,” Applied Ocean Research, vol. 42, pp. 1–15, 2013.

Appendix A

Letters of Permission

In this chapter, the permission letters from the journals for approving the reuse of the materials in the papers are listed.

1. The permission letter is shown in Figure A.1 for using the paper from the Journal of Ocean Engineering, Elsevier.
2. The permission letter is shown in Figure A.2 for using the paper from the Marine Technology Society Journal, Marine Technology Society.



Multi-resonant feedback control of heave wave energy converters

Author: Jiajun Song, Ossama Abdelkhalik, Rush Robinett, Giorgio Bacelli, David Wilson, Umesh Korde

Publication: Ocean Engineering

Publisher: Elsevier

Date: 15 November 2016

© 2016 Elsevier Ltd. All rights reserved.

Please note that, as the author of this Elsevier article, you retain the right to include it in a thesis or dissertation, provided it is not published commercially. Permission is not required, but please ensure that you reference the journal as the original source. For more information on this and on your other retained rights, please visit: <https://www.elsevier.com/about/our-business/policies/copyright#Author-rights>

BACK CLOSE WINDOW

© 2020 Copyright - All Rights Reserved | [Copyright Clearance Center, Inc.](#) | [Privacy statement](#) | [Terms and Conditions](#)
 Comments? We would like to hear from you. E-mail us at customer-care@copyright.com

Figure A.1: The permission letter of reusing the paper [2]

Permission for reusing a paper. » Inboxed

Jiajun Song <jiajuns@mtu.edu> to: most@mtu.edu 12:29 AM (10 hours ago)

Dear All,

I'm writing my Ph.D dissertation and I have decided to put a great portion of the paper listed below in my dissertation. I was the second author of this paper and I'm wondering if I need permission from Marine Technology Society to reuse those materials. If so, I would appreciate if you could provide me with a letter of permission.

Korde, Umesh A; Song, Jiajun; Robinett, Rush D; Abdelkhalik, Ossama O.
 "Hydrodynamic Considerations in Near-Optimal Control of a Small Wave Energy Converter for Ocean Measurement Applications"
 Marine Technology Society Journal, Volume 51, Number 6, November/December 2017, pp. 44-57(14)

Thank you so much! And stay healthy!
 JJ Song

—
 Jiajun Song
 Ph.D Candidate
jiajuns@mtu.edu
 1- (906) -201-6236
 DEEL 400, ROOM 1020
 Mechanical Engineering Graduate
 Michigan Technological University

Monica Ostrander <most@mtu.edu> to: me 9:51 AM (1 hour ago)

Hi,

You may use the paper as long as you cite it in your work.

Best Regards,
 Monica

Monica Ostrander, PMP | Director of Programs | Marine Technology Society
 1100 H St., NW, Suite LL-100 | Washington, DC 20005 | Email: most@mtu.edu | Phone: +1 202 827 7174

Figure A.2: The permission letter of reusing the paper [3]